TẠP CHÍ KHOA HỌC
TRƯỜNG ĐẠI HỌC QUY NHƠN

Tính ổn định của ánh xạ đa trị chính quy* Milyutin bởi nhiễu Lipschitz

Đào Ngọc Hân*

Khoa Giáo dục Tiểu học và Mầm non, Trường Đại học Quy Nhơn, Việt Nam

Ngày nhận bài: 24/01/2024; Ngày sửa bài: 20/04/2024
Ngày nhận đăng: 24/04/2024; Ngày xuất bản: 28/06/2024

TÓM TẮT

Bài báo nghiên cứu tính ổn định của ánh xạ đa trị chính quy* Milyutin bị nhiễu bởi một ánh xạ Lipschitz trong ngữ cảnh các khái niệm chính quy Milyutin và chính quy* Milyutin được phỏng lại cho phù hợp với một số tình huống trong thực tiễn.

Từ khóa: *Tính chính quy mêtric, tính chính quy* mêtric, độ dốc mạnh, tính ổn định nhiễu, tính pseudo-Lipschitz**.*

**Tác giả liên hệ chính.*
Email: daongochan@qnu.edu.vn

https://doi.org/10.52111/qnjs.2024.18306

QUY NHON UNIVERSITY
JOURNAL OF SCIENCE

The stability of star Milyutin regularity multifunctions under Lipschitz perturbation

Dao Ngoc Han*

Department of Primary Education and Preschool, Quy Nhon University, Vietnam

Received: 24/01/2024; Revised: 20/04/2024
Accepted: 24/04/2024; Published: 28/06/2024

ABSTRACT

The paper investigates the stability of a star Milyutin regular set-valued mapping perturbed by a Lipschitz mapping in the context of the concepts of Milyutin regularity and star Milyutin regularity that have been adapted to be suitable for some practical situations.

Keywords: *Metric regularity, star metric regularity, strong slope, perturbation stability, star pseudo-Lipschitz.*

1. INTRODUCTION

First discovered from classical results: Lyusternik-Graves Theorem, which is formed from two independent results by L. A. Lyusternik and L. M. Graves, Open Mapping Theorem by Rudin, and Implicit Function Theorem by Cauchy, Dini,... until now, the local metric regularity for single-valued mappings has been studied and expanded by many mathematicians such as: Borwein, Ioffe, Penot, Frankowska, Aubin,... to set-valued mappings in nonlinear case of high order or in non-local forms in works by Arutyunov,[1] Gfrerer,[2] Frankowska and Quicampoix,[3] Mordukhovich and Ouyang,[4] Penot,[5] Ioffe,[6,7] Ngai, Tron, and Théra,[8] Ivanov and Zlateva,[9] etc. In the most recent paper by Tron, Han, and Ngai,[10] models of nonlocal metric regularity of multivalued mappings are considered on an arbitrary subset of product metric space. And then, the infinitesimal characterization for these models as well as the stability of Milyutin regular under perturbation are also established.

Besides, in the process of expansion of Aubin property to the fixed set situation, Ioffe[6] led to a weak version of metric regularity which is called *star metric regularity*. Recall that star metric regularity of a set-valued mapping on fixed subsets of the form $\mathcal{U} \times \mathcal{V}$ is the metric regularity of the mapping whose images are the ones of the original set-valued mapping truncated by $\mathcal{V}$, i.e., a set-valued mapping T between metric spaces is said to be star metric regularity on $\mathcal{U} \times \mathcal{V}$ if there exists $\tau > 0$ such that

$$d(u, T^{-1}(v)) \leq \tau d(v, T(u) \cap \mathcal{V}),$$

for all $(u, v) \in \mathcal{U} \times \mathcal{V}$ and $0 < \tau d(v, T(u) \cap \mathcal{V}) \leq \delta(u)$, where δ is a gauge function that takes positive values on $\mathcal{U}$. In the researching,[6] Ioffe has shown that there exist set-valued mappings that satisfy star metric regularity but are not metric regularity. And so, star metric regularity is claimed to be weaker than metric regularity. Then, for the such mappings, the use of the Milyutin perturbation theorems as mentioned in[10] with the metric regularity assumption of the original set-valued mapping may not useful. Con-

*Corresponding author.
Email: daongochan@qnu.edu.vn

https://doi.org/10.52111/qnjs.2024.18306

sequently, the purpose of this article is to consider the stability of Milyutin regular when the initial mapping just satisfies star Milyutin regularity.

The paper is organized as follows. In Section 2 we introduce some basic notations and preliminaries. Further we recall the related results by Tron, Han and Ngai.[10] In Section 3 we prove stability theorems of perturbed star Milyutin regularity set-valued mappings.

2. PRELIMINARIES

Throughout the article, we shall mainly be working in the setting of a metric space X, endowded with a metric d. For $u \in X$, we denote by $d(u, A)$ the distance from u to $A \subseteq X$, $d(u, A) := \inf\{d(u, t) \mid t \in A\}$. By $B(C, \rho), \overline{B}(C, \rho)$ we denote respectively an open and a closed neighborhood of C with radius $\rho \in (0, +\infty)$. *A set-valued mapping (or a multifunction) between metric spaces* X, Y denoted by $T : X \rightrightarrows Y$ is a correspondence which associates every u a set $T(u)$, possibly empty. For every set-valued mapping $T : X \rightrightarrows Y$, we associate two sets, the graph of T and the domain of T, are defined by $\operatorname{Graph} T := \{(u, v) \in X \times Y \mid v \in F(u)\}$ and $\operatorname{Dom} T := \{u \in X \mid T(u) \neq \emptyset\}$. The inverse of T is the mapping $T^{-1} : Y \rightrightarrows X$ defined by $T^{-1}(v) = \{u \in X \mid v \in F(u)\}$. Then,

$$(u, v) \in \operatorname{Graph} T \Longleftrightarrow (v, u) \in \operatorname{Graph} T^{-1}.$$

2.1. Some basic notations and notions

In view of variational analysis, stability theory is closely related to the basic notion of metric regularity. The versions of this key property are recalled below, and for more details and further references, readers refer to the works.[11,12]

Let X, Y be metric spaces, $T : X \rightrightarrows Y$ be a multifunction, $(\bar{u}, \bar{v}) \in \operatorname{Graph} T$.

Definition 1. [11,12] *A multifunction T is called metrically regular around $(\bar{u}, \bar{v}) \in \operatorname{Graph} T$ with modulus $\kappa > 0$ if there exists a neighborhood $U \times V$ of $(\bar{u}, \bar{v})$ such that*

$$d(u, T^{-1}(v)) \leq \kappa d(v, T(u)), \text{ for all } (u, v) \in U \times V.$$

We denoted by $\operatorname{reg} T(\bar{u}, \bar{v})$ *the infimum of all modulus κ above.*

Ioffe[11,6] suggested a nonlocal regularity model of set-valued mapping $T : X \rightrightarrows Y$ associated to a gauge function γ as follows. Let $\mathcal{U} \subset X, \mathcal{V} \subset Y$ and $\gamma : X \to \mathbb{R} \cup \{+\infty\}$ be positive on $\mathcal{U}$.

Definition 2. [6,12] *A multifunction $T : X \rightrightarrows Y$ is called γ-metrically regular on $\mathcal{U} \times \mathcal{V}$ if there is a real number $\kappa > 0$ such that*

$$d(u, T^{-1}(v)) \leq \kappa d(v, T(u)), \tag{2.1}$$

provided that $u \in \mathcal{U}$, $v \in \mathcal{V}$, and $0 < \kappa d(v, T(u)) < \gamma(u)$. Denote by $\operatorname{reg}_\gamma T(\mathcal{U}|\mathcal{V})$ the lower bound of the κ satisfying (2.1). If no such κ exists, set $\operatorname{reg}_\gamma T(\mathcal{U}|\mathcal{V}) = \infty$.

Furthermore, in the work[10] by Tron, Han and Ngai, a different version of γ-metric regularity which is extended to an arbitrary set $\mathcal{W} \subset X \times Y$ suggested as follows.

Definition 3. [10] *Let $T : X \rightrightarrows Y$ be a multifunction and W be a subset of $X \times Y$. T is called γ-metrically regular on $\mathcal{W}$ with constant κ if there is a real number $r > 0$ such that*

$$d(u, T^{-1}(v)) \leq \kappa d(v, T(u)), \tag{2.2}$$

for all $(u, v) \in \mathcal{W}$ with $0 < rd(v, T(u)) < \gamma(u)$. The lower bound $\operatorname{reg}_\gamma T(\mathcal{W})$ of κ in (2.3) is the modulus of γ-metric regularity of T on $\mathcal{W}$. If no such κ exists, set $\operatorname{reg}_\gamma T(\mathcal{W}) = \infty$.

The above definition covers the case where the parameters κ and r coincide, which is known as the concept of γ-metric regularity *in the sense of Ioffe*, as shown in the following definition.

Definition 4. [10] *Let X, Y be metric spaces, W be a subset of $X \times Y$ and let $T : X \rightrightarrows Y$ be a set-valued mapping. T is called γ-metrically regular on W if there is $\kappa > 0$ such that*

$$d(u, T^{-1}(v)) \leq \kappa d(v, T(u))$$

for all $(u, v) \in W$ with $0 < \kappa d(v, T(u)) < \gamma(u)$.

Next, we recall a weaker version of metric regularity, star metric regularity, introduced by Ioffe in also.[6]

Definition 5. [6] *Set $T_{\mathcal{V}}(u) = T(u) \cap \mathcal{V}$. A multifunction T is said to be γ-regular* (or star γ-regular) on $\mathcal{U} \times \mathcal{V}$ if $T_{\mathcal{V}}$ is γ-regular on $\mathcal{U} \times \mathcal{V}$. Specifically, T is called γ-regular* on $\mathcal{U} \times \mathcal{V}$ if there is a $\kappa > 0$ such that*

$$d(u, T^{-1}(v)) \leq \kappa d(v, T(u) \cap \mathcal{V})$$

for all $u \in \mathcal{U}$, $v \in \mathcal{V}$ and $0 < \kappa d(v, T(u) \cap \mathcal{V}) < \gamma(u)$.

In order to be convenient in some applications, in this paper, we propose an improved version of the above definition in which the parameters "κ" in the regularity inequality and the gauge condition could be distinguished.

Definition 6. *A multifunction $T : X \rightrightarrows Y$ is called γ-metrically regular* on $\mathcal{U} \times \mathcal{V} \subset X \times Y$ with constant κ if there is a real number $r > 0$ such that*

$$d(u, T^{-1}(v)) \leq \kappa d(v, T(u) \cap \mathcal{V}), \tag{2.3}$$

for all $(u, v) \in \mathcal{U} \times \mathcal{V}$ with $0 < rd(v, T(u) \cap \mathcal{V}) < \gamma(u)$. The lower bound $\operatorname{reg}^*_\gamma T(\mathcal{U}|\mathcal{V})$ of κ in (2.3) is the modulus of γ-metric regularity of T on $\mathcal{U} \times \mathcal{V}$. If no such κ exists, set $\operatorname{reg}^*_\gamma T(\mathcal{U}|\mathcal{V}) = \infty$.*

Remark 7. *In case of $r = \kappa$, Definition 6 leads to the version of γ-metric regularity* on $\mathcal{U} \times \mathcal{V}$ in the sense of Ioffe as in Definition 5.*

γ-openness* and γ-pseudo-Lipschitz* of set-valued mappings are equivalent properties of the regularity* stated as follows.

Definition 8. *A multifunction $T : X \rightrightarrows Y$ is γ-open* on $\mathcal{U} \times \mathcal{V}$ with constant κ if there is a real number $\rho > 0$ such that*

$$B(T(u) \cap \mathcal{V}, \rho t) \cap \mathcal{V} \subset T(B(u, \kappa^{-1}\rho t)), \tag{2.4}$$

whenever $u \in \mathcal{U}$, $0 < t < \gamma(u)$. The upper bound $\operatorname{sur}^*_\gamma T(\mathcal{U}|\mathcal{V})$ of κ in (2.4) is the modulus of γ-surjection of T on $\mathcal{U} \times \mathcal{V}$. If no such κ exists, set $\operatorname{sur}^*_\gamma T(\mathcal{U}|\mathcal{V}) = 0$.*

Definition 9. *A multifunction $T^{-1} : Y \rightrightarrows X$ is γ-pseudo-Lipschitz* on $\mathcal{V} \times \mathcal{U}$ with constant κ if there is a real number $\rho > 0$ such that*

$$d(u, T^{-1}(v)) \leq \kappa d(v, w), \tag{2.5}$$

provided that $u \in T^{-1}(w) \cap \mathcal{U}$, $v, w \in \mathcal{V}$ and $0 < \rho d(v, w) < \gamma(x)$. The lower bound $\operatorname{lip}^*_\gamma T^{-1}(\mathcal{U}|\mathcal{V})$ of κ in (2.5) is the γ-pseudo-Lipschitz modulus of T^{-1} on $\mathcal{V} \times \mathcal{U}$. If no such κ exists, set $\operatorname{lip}^*_\gamma T^{-1}(\mathcal{U} \times \mathcal{V}) = \infty$.*

The following propositon shows the equivalence of the above three star regular concepts.

Proposition 10. *Let $T : X \rightrightarrows Y$ be set-valued mapping and $\mathcal{U} \subset X$, $\mathcal{V} \subset Y$. The following statements are equivalent:*

(i) T is γ-open on $\mathcal{U} \times \mathcal{V}$ with modulus not smaller than κ^{-1};*

(ii) T is γ-regular on $\mathcal{U} \times \mathcal{V}$ with modulus not greater than κ;*

(iii) T^{-1} is γ-pseudo-Lipschitz on $\mathcal{V} \times \mathcal{U}$ with modulus not greater than κ.*

Proof. To show $(i) \Rightarrow (ii)$, let $(u, v) \in \mathcal{U} \times \mathcal{V}$ be with $0 < \rho d(v, T(u) \cap \mathcal{V}) < \gamma(u)$. Then, for all $\epsilon > 0$, take $\tau = \rho(d(v, T(u) \cap \mathcal{V}) + \epsilon)$ such that $0 < \rho d(v, T(u) \cap \mathcal{V}) < \tau < \gamma(u)$. Then, $u \in \mathcal{U}, 0 < \tau < \gamma(u)$ and $v \in B(T(u) \cap \mathcal{V}, \rho^{-1}\tau) \cap \mathcal{V}$. By (i), $v \in T(B(u, \kappa\rho^{-1}\tau))$. So, there exists $z \in B(u, \kappa\rho^{-1}\tau)$ such that $v \in T(z)$. It follows that $d(u, T^{-1}(v)) \leq d(u, z) \leq \kappa\rho^{-1}\tau = \kappa(d(v, T(u) \cap \mathcal{V}) + \epsilon)$. Let $\epsilon \downarrow 0$, one gets $d(u, T^{-1}(v)) \leq \kappa d(v, T(u) \cap \mathcal{V})$.

The implication $(ii) \Rightarrow (iii)$ is obvious. For $(iii) \Rightarrow (i)$. Let $u \in \mathcal{U}$, $0 < \tau < \gamma(u)$, and let $v \in B(T(u) \cap \mathcal{V}, \rho^{-1}\tau) \cap \mathcal{V}$. Then $u \in U$ and there exists $w \in T(u) \cap \mathcal{V}$ such that $0 < d(v, w) < \rho^{-1}\tau$. It follows $u \in T^{-1}(w) \cap \mathcal{U}$, $v, w \in \mathcal{V}$ and $0 < \rho d(v, w) < \tau < \gamma(u)$. By (iii), $d(u, T^{-1}(v)) \leq \kappa d(v, w) < \kappa\rho^{-1}\tau$. This means that there is $z \in T^{-1}(v)$ such that $d(u, z) < \kappa\rho^{-1}\tau$, that is $v \in T(B(u, \kappa\rho^{-1}\tau))$. So,

$$B(T(u) \cap \mathcal{V}, \rho^{-1}\tau) \cap V \subset T(B(u, \kappa\rho^{-1}\tau)).$$

The proof is complete.

2.2. Auxiliary results

Now, we recall the concept of (strong) slope which is considered as an infinitesimal tool in metric spaces, first introduced in 1980 by De Giorgi, Marino, and Tosques.[13]

Definition 11. [13,14] *Let X be a metric space and $f : X \to \mathbb{R} \cup \{+\infty\}$ be a given function. The symbol $[f(x)]_+$ stands for $\max(f(x), 0)$ and $\operatorname{Dom} f := \{x \in X \mid f(x) < +\infty\}$ denotes the domain of f.*

https://doi.org/10.52111/qnjs.2024.18306

(i) The quantity defined by $|\nabla f|(x) = 0$ *if* x *is a local minimum of* f*; otherwise*

$$|\nabla f|(x) = \limsup_{u\to x, u\neq x} \frac{f(x)-f(u)}{d(x,u)}.$$

is called the local slope of the function f *at* $x \in \text{Dom } f$.

(ii) The quantity

$$|\Gamma f|(x) := \sup_{u\neq x} \frac{[f(x)-f(u)]_+}{d(x,u)}$$

is called the nonlocal slope of the function f *at* $x \in \text{Dom } f$.

For $x \notin \text{Dom } f$*, we set* $|\nabla f|(x) = |\Gamma f|(x) = +\infty$. *Obviously,* $|\nabla f|(x) \leq |\Gamma f|(x)$ *for all* $x \in X$.

In case of X being a normed space and f being Fréchet differentiable function at x then the slope of f coincides with the norm of the derivative ∇f at the point. For a fuller treatment of strong slope, we refer the reader to the researches.[13,15-18]

To establish infinitesimal characterizations for regularity, an effective tool that has been used is the lower semicontinuous envelop of the distance function associated to a set-valued mapping $T : X \rightrightarrows Y$ defined by

$$\varphi_y^T(x) := \liminf_{(u,v)\to(x,y)} d(v,T(u)) := \liminf_{u\to x} d(y,T(u)).$$

The following theorem established by Tron, Han, Ngai[10] gives the necessary/ sufficient conditions for the metric regularity via nonlocal slope of the function φ_y^T. Now, let be given a subset W of $X \times Y$, we associate every $v \in Y$ to set $W_v = \{u \in X : (u,v) \in W\}$, and every $u \in X$ to set $W_u = \{v \in Y : (u,v) \in W\}$. Then, denoted by $P_X W := \cup_{v\in Y} W_v$, and $P_Y W := \cup_{u\in X} W_u$. In particular, in the case where the form of W is a box $U \times V$, the sets W_v (with $v \in V$), $P_X W$ are identical to U and the sets W_u (with $u \in U$), $P_Y W$ are identical to V.

Theorem 12. *(Tron-Han-Ngai[10]) Given* X *is a complete metric space,* Y *is a metric space and* $\mathcal{W} \subset X \times Y$ *is a nonempty subset. Let* $T : X \rightrightarrows Y$ *be a closed set-valued mapping and* $\gamma : X \to \mathbb{R}_+ \cup \{+\infty\}$ *be a gauge function. Then,*

(i) Suppose that γ *is lower semicontinuous. If* $\mathcal{W}$ *is open and* T *is* γ*-metrically regular on* $\mathcal{W}$ *with constant* κ*, i.e., there exists a real* $r > 0$ *such that for every* $(x,y) \in \mathcal{W}$*, with* $0 < rd(y,T(x)) < \gamma(x)$*,*

$$d(x,T^{-1}(y)) \leq \kappa d(y,T(x)),$$

then for each $(x,y) \in \mathcal{W}$*, with* $0 < r\varphi_y^T(x) < \gamma(x)$*, one has*

$$|\Gamma\varphi_y^T|(x) \geq \kappa^{-1}$$

(ii) Conversely, assume further that $\gamma : X \to \mathbb{R}_+$ *is a Lipschitz continuous function with constant* 1*. If there are a positive real* κ *such that*

$$\liminf_{\delta\downarrow 0}\{|\Gamma\varphi_y^T|(x) : d(x,\mathcal{W}_y) < \delta\gamma(x),\ y \in P_Y\mathcal{W},\ 0 < \varphi_y^T(x) < \delta\gamma(x)\} > \kappa^{-1}.$$

then T *is* γ*-metrically regular on* $\mathcal{W}$ *with constant* κ.

Regarding Definition 4, the theorem below in the work by Tron, Han, Ngai[10] gives a suficient condition for the γ-metric regularity via the nonlocal slope.

Theorem 13. *(Tron-Han-Ngai[10]) Let* X *be a complete metric space and* Y *be a metric space,* $\mathcal{W} \subset X \times Y$ *be a nonempty subset. Let* $T : X \rightrightarrows Y$ *be a closed set-valued mapping. Suppose that* $\gamma : X \to \mathbb{R}_+$ *is a Lipschitz function with constant* 1*. If there exists* $\kappa > 0$ *such that*

$$|\Gamma\varphi_y^T|(x) \geq \kappa^{-1},$$

$\forall x \in (\mathcal{W}_y)_\gamma, y \in P_y\mathcal{W}, 0 < \kappa\varphi_y^T(x) < \gamma(x)$*, where* $(\mathcal{W}_y)_\gamma = \cup_{x\in\mathcal{W}_y} B(x,\gamma(x))$*, then one has*

$$d(x,T^{-1}(y)) \leq \kappa d(y,T(x)),$$

for all $(x,y) \in \mathcal{W}$ *with* $0 < \kappa d(y,T(x)) < \gamma(x)$.

3. PERTURBATION STABILITY OF STAR MILYUTIN REGULARITY MULTIFUNCTIONS

Let X, Y be metric spaces and $\mathcal{W}$ be a nonempty subset of $X \times Y$. Firstly, we recall the defintiton of Milyutin regular on $\mathcal{W}$ given by Tron, Han and Ngai in the research.[10]

Definition 14. *(Tron-Han-Ngai[10]) A multifunction $T : X \rightrightarrows Y$ is called Milyutin regular on $\mathcal{W}$ with constant κ if there is a real number $r > 0$ such that*

$$d(T^{-1}(y)) \leq \kappa d(y, T(x)),$$

for all $(x, y) \in \mathcal{W}$ with $0 < rd(y, T(x)) < m_{P_X\mathcal{W}}(x)$. The infimum of all above κ denoted by $\operatorname{reg}_m T(\mathcal{W})$.

Next, we consider the definitions of Milyutin regular* associated to the gauge function $\gamma \equiv m_{P_X\mathcal{W}} : X \to \mathbb{R}_+$ defined by $m_{P_X\mathcal{W}}(x) := d(x, X \backslash P_X\mathcal{W})$.

Definition 15. *A multifunction $T : X \rightrightarrows Y$ is called Milyutin regular* on $\mathcal{W}$ with constant κ if there is a real number $r > 0$ such that*

$$d(T^{-1}(y)) \leq \kappa d(y, T(x) \cap P_X\mathcal{W}),$$

for all $(x, y) \in \mathcal{W}$ with $0 < rd(y, T(x) \cap P_X\mathcal{W}) < m_{P_X\mathcal{W}}(x)$. The infimum of all above κ denoted by $\operatorname{reg}^*_m T(\mathcal{W})$ is the modulus of Milyutin regular of T on $\mathcal{W}$. If the above constant κ does not exists, set $\operatorname{reg}^*_m T(\mathcal{W}) = \infty$.*

Remark 16. *In the above definition, taking $r = \kappa$ one obtains the definition of Milyutin regular* on $\mathcal{W}$ in the sense of Ioffe.*

It is easily seen that $m_{P_X\mathcal{W}}(x)$ is positive on $P_X\mathcal{W}$ if and only if $P_X\mathcal{W}$ is an open set, which follows from $\mathcal{W}$ is open. And then, the results of Theorem 12 and Theorem 13 are also applied to the function $m_{P_X\mathcal{W}}$ due to Lipschitz property with constant 1 of this one.

In this part, we shall investigate the stability of Milyutin regular under perturbation by single-valued mappings and the original set-valued mapping is assumed to be Milyutin regular*.

Theorem 17. *Let X be a complete metric space and Y be a Banach space. Let $\mathcal{U} \subset X$, $\mathcal{V} \subset Y$ be open sets. Let a closed set-valued mapping $T : X \rightrightarrows Y$ and a single-valued mapping $h : X \to Y$ be Lipschitz on $\mathcal{U}$ with constant $\lambda \in (0, \kappa^{-1})$. If T is Milyutin regular* on $\mathcal{U} \times \mathcal{V}$ with constant κ, i.e, there exists $r > 0$ such that for all $(x, y) \in \mathcal{U} \times \mathcal{V}$ with $0 < rd(y, T(x) \cap \mathcal{V}) < m_{\mathcal{U}}(x)$,*

$$d(x, T^{-1}(y)) \leq \kappa d(y, T(x) \cap \mathcal{V}).$$

Then, for every $\eta > 0$, $T + h$ is Milyutin regular on $\mathcal{W}^{\lambda\eta}$ with $\operatorname{reg}_m(T + h)(\mathcal{W}^{\lambda\eta}) \leq (\kappa^{-1} - \lambda)^{-1}$, where

$$\mathcal{W}^{\lambda\eta} = \{(x, y) \in X \times Y \mid x \in \mathcal{U}, B(y - h(x), \lambda\eta m_{\mathcal{U}(x)}) \subset \mathcal{V}\}.$$

Proof. Let $\eta > 0$ be given. According to Theorem 12, we only need to prove that

$$\lim_{\delta \downarrow 0} \inf\{|\Gamma\varphi_y^{T+h}|(x) : d(x, \mathcal{W}_y^{\lambda\eta}) < \delta m_{P_X\mathcal{W}^{\lambda\eta}}(x), y \in P_Y\mathcal{W}^{\lambda\eta}, 0 < \varphi_y^{T+h}(x) < \delta m_{P_X\mathcal{W}^{\lambda\eta}}(x)\} > \kappa^{-1} - \lambda. \tag{3.1}$$

Indeed, choose δ such that $\frac{\delta}{1-\delta} < \min\{1, \eta\}$, $0 < r\delta < 1$, $\frac{(\lambda+1)\delta}{1-\delta} < \lambda\eta$.

Let $(x, y) \in X \times Y$ such that $d(x, \mathcal{W}_y^{\lambda\eta}) < \delta m_{P_X\mathcal{W}^{\lambda\eta}}(x)$, $y \in P_X\mathcal{W}^{\lambda\eta}$ and $0 < \varphi_y^{T+h}(x) < \delta m_{P_X\mathcal{W}^{\lambda\eta}}(x)$. Then there exists $u \in \mathcal{W}^{\lambda\eta}$ such that

$$d(x, u) < \delta m_{P_X\mathcal{W}^{\lambda\eta}}(x) \leq \delta m_{\mathcal{U}}(x).$$

So, $u \in \mathcal{U}, B(y - h(u), \lambda\eta m_{\mathcal{U}}(x)) \subset \mathcal{V}$, and since $m\mathcal{U}$ is Lipschitz with constant 1, it follows that

$$d(x, u) < \delta m_{\mathcal{U}}(u) + \delta d(x, u).$$

By the choice of δ, one has

$$d(x, u) < \frac{\delta}{1-\delta} m_{\mathcal{U}}(u) < m_{\mathcal{U}}(u) \tag{3.2}$$

which gives $x \in \mathcal{U}$.

Let now $\{u_n\} \subset X$ be such that $u_n \to x$ and

$$d(y, (T + h)(u_n)) \to \varphi_y^{T+h}(x) \text{ as } n \to \infty.$$

Thus, there exists $n_0 \in \mathbb{N}$ such that for all $n \geq n_0$,

$$0 < d(y, (T + h)(u_n)) < \delta m_{\mathcal{U}}(u_n) \tag{3.3}$$

and, as $u_n \to x \in \mathcal{U}$, we have $u_n \in \mathcal{U}$ due to the openness of $\mathcal{U}$. And then, by the choice of δ when n is sufficiently large, we have

$$0 < d(y, (T + h)(u_n)) < r^{-1} m_{\mathcal{U}}(u_n). \tag{3.4}$$

Furthermore, for n large enough, we find that $d(y_n, T(u_n)) = d(y_n, T(u_n) \cap \mathcal{V})$. Indeed, fixing $n \in \mathbb{N}^*$, we take a sequence $\{a_k\} \subset T(u_n)$ such that

$$d(y - h(u_n), a_k) \to d(y - h(u_n), T(u_n)),\ k \to \infty.$$

https://doi.org/10.52111/qnjs.2024.18306

By (3.2), (3.3) and the continuity of distance function, we conclude that

$$\begin{aligned} d(y-h(u_n),a_k) &< \delta m_{\mathcal{U}}(u_n) \\ &\le \delta m_{\mathcal{U}}(u) + \delta d(u_n,u) \\ &\le \delta m_{\mathcal{U}}(u) + \frac{\delta^2}{1-\delta} m_{\mathcal{U}}(u) \\ &= \frac{\delta}{1-\delta} m_{\mathcal{U}}(u). \end{aligned} \tag{3.5}$$

From (3.2), (3.5) and the choice of δ, it follows that for $n \ge n_0$,

$$\begin{aligned} d(a_k, y-h(u)) &\le d(a_k, y-h(u_n)) \\ &\quad + d(y-h(u_n), y-h(u)) \\ &\le \frac{\delta}{1-\delta} m_{\mathcal{U}}(u) + \lambda d(u_n,u) \\ &\le \frac{\delta}{1-\delta} m_{\mathcal{U}}(u) + \lambda \frac{\delta}{1-\delta} m_{\mathcal{U}}(u) \\ &= \frac{(\lambda+1)\delta}{1-\delta} m_{\mathcal{U}}(u) \le \lambda\eta m_{\mathcal{U}}(u) \end{aligned}$$

which gives $a_k \in B(y-h(u), \lambda\eta m_{\mathcal{U}}(u)) \subset \mathcal{V}$, and thus $a_k \in T(u_n) \cap \mathcal{V}$. Consequently, $d(y-h(u_n), a_k) \ge d(y-h(u_n), T(u_n)\cap\mathcal{V})$, So, $d(y-h(u_n), T(u_n)) \le d(y-h(u_n), T(u_n)\cap\mathcal{V})$. And then, $d(y-h(u_n), T(u_n)) = d(y-h(u_n), T(u_n)\cap\mathcal{V})$ when n is sufficiently large.

Then from (3.4), we see that

$$\begin{aligned} 0 < d(y-h(u), T(u_n)\cap\mathcal{V}) &= d(y-h(u), T(u_n)) \\ &< r^{-1} m_{\mathcal{U}}(u_n). \end{aligned}$$

Moreover, by (3.2), for n is large enough, we conclude from the continuity of distance function that

$$\begin{aligned} d(y-h(u_n), y-h(u)) &< \lambda d(u_n,u) \le \lambda d(x,u) \\ &\le \lambda \frac{\delta}{1-\delta} m_{\mathcal{U}}(u) \\ &\le \lambda\eta m_{\mathcal{U}}(u), \end{aligned}$$

where the last inequality is followed from the choice of δ. Consequently,

$$y - h(u_n) \in B(y-h(u), \lambda\eta m_{\mathcal{U}}(u)) \subset \mathcal{V}.$$

Then from the fact that T is Milyutin regular* on $\mathcal{U}\times\mathcal{V}$ with constant κ, we obtain

$$\begin{aligned} d(u_n, T^{-1}(y-h(u_n))) &\le \kappa d(y-h(u_n), T(u_n)\cap\mathcal{V}) \\ &= d(y-h(u_n), T(u_n)),\ \forall n \ge n_0. \end{aligned}$$

Now we choose some $z_n \in T^{-1}(y-h(u_n))$ (i.e., $y-h(u_n) \in T(z_n)$) such that

$$d(u_n, z_n) \le (\kappa + n^{-1}) d(y-h(u_n), T(u_n)). \tag{3.6}$$

From (3.3) and the choice of δ, for all $n \ge n_0$, one has

$$d(u_{n,z_n}) < (\kappa + n^{-1})\delta m_{\mathcal{U}}(u_n) < m_{\mathcal{U}}(u_n).$$

This yields $z_n \in \mathcal{U}$, and thus from the Lipschitz property of h on $\mathcal{U}$, we have

$$d(h(u_n), h(z_n)) \le \lambda d(u_n, z_n). \tag{3.7}$$

Since $\varphi_y^{T+h}(x) > 0$, the closeness of T, and $\lim_{n\to\infty} u_n = x$, we see that $\liminf_{n\to\infty} d(u_n, z_n) > 0$. Note that $d(y-h(u_n), T(z_n)) = 0$ since $y-h(u_n) \in T(z_n)$, and from (3.6), (3.7), we conclude that

$$\begin{aligned} |\Gamma\varphi_y^{T+h}|(x) &\ge \limsup_{n\to\infty} \frac{\varphi_y^{T+h}(x) - \varphi_y^{T+h}(z_n)}{d(x,z_n)} \\ &\ge \limsup_{n\to\infty} \frac{d(y,(T+h)(u_n)) - d(y,(T+h)(z_n))}{d(u_n,z_n)} \\ &= \limsup_{n\to\infty} \frac{d(y-h(u_n), T(u_n)) - d(y-h(z_n), T(z_n))}{d(u_n,z_n)} \\ &\ge \limsup_{n\to\infty} \frac{d(y-h(u_n), T(u_n))}{d(u_n,z_n)} - \lambda \\ &\ge \limsup_{n\to\infty} \frac{1}{\kappa+n^{-1}} - \lambda = \kappa^{-1} - \lambda. \end{aligned}$$

This finishes the proof.

The next theorem is a version of the above one in which the definition of Milyutin regular* is replaced by the definition of Milyutin regular* in the sense of Ioffe.

Theorem 18. *Given X is a complete metric space, Y is a Banach space and $\mathcal{U} \subset X$, $\mathcal{V} \subset Y$ are open sets. Let a closed set-valued mapping $T : X \rightrightarrows Y$ and a single-valued mapping $h : X \to Y$ be Lipschitz on $\mathcal{U}$ with constant $\lambda \in (0, \kappa^{-1})$. If T is Milyutin regular* on $\mathcal{U}\times\mathcal{V}$ with constant κ, i.e, for all $(x,y) \in \mathcal{U}\times\mathcal{V}$ with $0 < \kappa d(y, T(x)\cap\mathcal{V}) < m_{\mathcal{U}}(x)$,*

$$d(x, T^{-1}(y)) \le \kappa d(y, T(x)\cap\mathcal{V}).$$

Then, $T+h$ is Milyutin regular on $\mathcal{W}$ with $\mathrm{reg}_m(T+h)(\mathcal{W}) \le (\kappa^{-1}-\lambda)^{-1}$, where

$$\begin{aligned} \mathcal{W} = \{(x,y) \in X\times Y \mid\ & x \in \mathcal{U}, \\ & B(y-h(x), (2\kappa^{-1}-\lambda) m_{\mathcal{U}}(x)) \subset \mathcal{V}\}. \end{aligned}$$

Proof. Set $(\mathcal{W}_y)_m := \cup_{u\in\mathcal{W}_y} B(u, m_{P_X\mathcal{W}}(u))$. According to Theorem 13, now we shall show that for any $x \in (\mathcal{W}_y)_m$, $y \in P_Y\mathcal{W}$ with $0 < (\kappa^{-1} - \lambda)^{-1}\varphi_y^{T+h}(x) < m_{P_X\mathcal{W}}(x)$,

$$| \Gamma\varphi_y^{T+h} | (x) \geq \kappa^{-1} - \lambda.$$

Indeed, take $(x, y) \in X \times Y$ such that $x \in (\mathcal{W}_y)_m$, $y \in P_Y\mathcal{W}$ with $0 < (\kappa^{-1}-\lambda)^{-1}\varphi_y^{T+h}(x) < m_{P_X\mathcal{U}}(x)$. Then, there is $u \in \mathcal{W}_y$ such that

$$d(x, u) < m_{P_X\mathcal{W}}(u) \leq m_{\mathcal{U}}(u). \tag{3.8}$$

So, $u \in U, B(y - h(u), \lambda m_{\mathcal{U}}(u)) \subset \mathcal{V}$, and $x \in \mathcal{U}$.

Now, we take $\{u_n\} \subset X$ such that $u_n \to x$ and $d(y, (T+h)(u_n)) \to \varphi_y^{T+h}(x)$ as $n \to \infty$. Thus, there exists $n_0 \in \mathbb{N}$ such that for all $n \geq n_0$,

$$\begin{aligned} 0 < d(y, (T + h)(u_n)) &\leq (\kappa^{-1} - \lambda)m_{P_X\mathcal{W}}(x) \\ &\leq (\kappa^{-1} - \lambda)m_{\mathcal{U}}(x) \\ &\leq (\kappa^{-1} - \lambda)m_{\mathcal{U}}(u_n) \quad (3.9) \\ &< \kappa^{-1}m_{\mathcal{U}}(u_n), \quad (3.10) \end{aligned}$$

and that $u_n \in \mathcal{U}$ follows from the openness of $\mathcal{U}$ and $u_n \to x \in \mathcal{U}$.

Furthermore, $d(y - h(u_n), T(u_n)) = d(y - h(u_n), T(u_n) \cap \mathcal{V})$ for n large enough. Indeed, fixing $n \in \mathbb{N}^*$, we choose a sequence $\{a_k\} \subset T(u_n)$ such that $d(y-h(u_n), a_k) \to d(y-h(u_n), T(u_n))$, $k \to \infty$. By (3.8), (3.9), and the continuity of the distance function, we conclude that

$$\begin{aligned} d(y - h(u_n), a_k) &< (\kappa^{-1} - \lambda)m_{\mathcal{U}}(u_n) \\ &\leq (\kappa^{-1} - \lambda)m_{\mathcal{U}}(u) + (\kappa^{-1} - \lambda)d(u_n, u)) \\ &\leq (2\kappa^{-1} - \lambda)m_{\mathcal{U}}(u), \end{aligned} \tag{3.11}$$

which yields $a_k \in B(y - h(u_n), (2\kappa^{-1} - \lambda)m_{\mathcal{U}}(u)) \subset \mathcal{V}$, and thus $a_k \in T(u_n) \cap \mathcal{V}$. Consequently, $d(y - h(u_n), a_k) \geq d(y - h(u_n), T(u_n) \cap \mathcal{V})$. So, $d(y - h(u_n), T(u_n)) \geq d(y - h(u_n), T(u_n) \cap \mathcal{V})$.

This gives $d(y - h(u_n), T(u_n)) = d(y - h(u_n), T(u_n) \cap \mathcal{V})$ when n is sufficiently large.

Then from (3.10), we see that

$$\begin{aligned} 0 < d(y - h(u_n), T(u_n) \cap \mathcal{V}) &= d(y - h(u_n), T(u_n)) \\ &< \kappa^{-1}m_{\mathcal{U}}(u_n). \end{aligned}$$

Otherwise, by (3.8) and for n large enough, one also have

$$\begin{aligned} d(y - h(u_n), y - h(u)) &\leq \lambda d(u_n, u) \\ &\leq \lambda d(u_n, x) + \lambda d(x, u) \\ &\leq \lambda m_{\mathcal{U}}(u) \\ &\leq (2\kappa^{-1} - \lambda)m_{\mathcal{U}}(u) \end{aligned}$$

which leads to $y-h(u_n) \in B(y-h(u), \lambda m_{\mathcal{U}}(u)) \subset \mathcal{V}$.

So, due to the Milyutin regularity* of T on $\mathcal{U}\times\mathcal{V}$ with constant κ, one obtains

$$d(u_n, T^{-1}(y - h(u_n))) \leq \kappa d(y - h(u_n), T(u_n) \cap \mathcal{V})$$

We now choose $z_n \in T^{-1}(y-h(u_n))$ (i.e., $y-h(u_n) \in T(z_n)$) such that

$$\begin{aligned} d(u_n, z_n) &\leq (\kappa + n^{-1})d(y - h(u_n), T(u_n) \cap \mathcal{V}) \\ &= (\kappa + n^{-1})d(y - h(u_n), T(u_n)) \quad (3.12) \\ &\leq (\kappa + n^{-1})\kappa^{-1}m_{\mathcal{U}}(u_n) \\ &< m_{\mathcal{U}}(u_n), \end{aligned}$$

where the last inequality is obtained when n is large enough. It follows that $z_n \in \mathcal{U}$, and thus from the Lipschitz property of h on $\mathcal{U}$, we have

$$d(y - h(u_n), y - h(z_n)) \leq \lambda d(u_n, z_n). \tag{3.13}$$

Since $\varphi_y^{T+h}(x) > 0$, the closeness of T, and $\lim_{n\to\infty} u_n = x$, we have $\liminf_{n\to\infty} d(u_n, z_n) > 0$. From (3.12), (3.13), and note that $y-h(u_n) \in T(z_n)$, similar as in the proof of Theorem 17, one concludes that

$$\begin{aligned} | \Gamma\varphi_y^{T+h} | (x) &\geq \limsup_{n\to\infty} \frac{1}{\kappa + n^{-1}} - \lambda \\ &= \kappa^{-1} - \lambda. \end{aligned}$$

The proof is completed.

4. CONCLUSIONS

This artical suggests the models of star regularity on an any subset of product metric spaces as well as established the equivalence of star regular concepts: star openness, star metrically regular and star pseudo-Lipschitz in the literature. Regarding the star Milyutin regularity, we have proved that the stability of Milyutin regularity under small Lipschitz perturbation also attains when the assumption of star Milyutin regularity is imposed on the original set-valued mapping.

https://doi.org/10.52111/qnjs.2024.18306

Acknowledgements

I would like to warmly thank two referees for their constructive comments and valuable suggestions that allowed me to clarify the original version. I am also gratefully indebted to Assoc. Prof. Dr. Habil. Huynh Van Ngai and his collaborators from Quy Nhơn University for the useful discussions.

REFERENCES

1. A. V. Arutyunov, E. R. Avakov, S. E. Zhukovskiy. Stability theorem for estimating the distance to a set of coincidence points, *SIAM Journal on Optimization*, **2015**, *25*(2), 807–828.
2. H. Gfrerer. On directional metric pseudo-(sub)regularity of multifunctions and optimality conditions for degenerated mathematical programs, *Set-Valued and Variational Analysis*, **2013**, *21*, 151–176.
3. H. Frankowska, M. Quincampoix. Holder metric regularity of set-valued maps, *Mathematical Programming*, **2012**, *32*(1-2), 333–354.
4. B. S. Mordukhovich, W. Ouyang. Higher-order metric subregularity and its application, *Journal of Global Optimization*, **2015**, *63*, 777–795.
5. J. P. Penot. *Calculus without derivatives*, Springer Graduate Texts in Mathematics, New York, 2014.
6. A.D. Ioffe. Regularity on fixed sets, *SIAM Journal on Optimization*, **2011**, *21*(4), 1345–1370.
7. A.D. Ioffe. Nonlinear regularity models, *Mathematical Programming*, **2013**, *139*(1), 223–242.
8. H. V. Ngai, N. H. Tron, M. Théra. Implicit multifunction theorems in complete metric spaces, *Mathematical Programming*, **2013**, *139*(1), 301– 326.
9. M. Ivanov, N. Zlateva. On characterizations of metric regularity of multi-valued maps, *Journal of Convex Analysis*, **2020**, *27*(1), 381–388.
10. N. H. Tron, D. N. Han, H. V. Ngai. Nonlinear metric regularity on a fixed set, *Optimization*, **2023**, *72*(6), 1515–1548.
11. A.L. Dontchev, R. T. Rockafellar. *Implicit functions and solution mappings, a view from variational analysis*, Springer, New York, 2009.
12. A.D. Ioffe. *Variational analysis of regular mappings: theory and applications*, Springer Monographs in Mathematics, Switzerland, 2017.
13. E. D. Giorgi, A. Marino, M. Tosques. Problemi di evoluzione in spazi metrici e curve di massima pendenza (Evolution problems in metric spaces and curves of maximal slope), *Atti della Accademia Nazionale dei Lincei*, **1980**, *68*, 180–187.
14. H. V. Ngai, M. Théra. Directional Hölder metric regularity, *Journal of Optimization Theory and Applications*, **2016**, *171*, 785–819.
15. D. Azé. A survey on error bounds for lower semicontinuous functions, *ESAIM: Proceedings*, **2003**, *13*, 1–17.
16. D. Azé, J. N. Corvellec. Characterizations of error bounds for lower semicontinuous functions on metric spaces, *Control, Optimisation and Calculus of Variations*, **2004**, *10*(3), 409– 425.
17. N. D. Cuong, A. Y. Kruger. Transversality properties: primal sufficient conditions, *Set-Valued and Variational Analysis*, **2021**, *29*(2), 221–256.
18. A. D. Ioffe. Metric regularity and subdifferential calculus, *Rusian Mathematical Surveys*, **2000**, *55*, 501–558.

TẠP CHÍ KHOA HỌC
TRƯỜNG ĐẠI HỌC QUY NHƠN

Một phép biến đổi của hàm khối xác suất cho một lớp các biến ngẫu nhiên rời rạc

Lê Thanh Bính*

Khoa Toán và Thống kê, Trường Đại học Quy Nhơn, Việt Nam

Ngày nhận bài: 18/02/2024; Ngày sửa bài: 03/05/2024
Ngày nhận đăng: 04/05/2024; Ngày xuất bản: 28/06/2024

TÓM TẮT

Chúng tôi xét một biến ngẫu nhiên rời rạc X chỉ nhận các giá trị nguyên không âm. Ký hiệu miền giá trị của X và hàm khối xác suất của X lần lượt bởi $\mathcal{R}_X$ và $p_X(x)$. Mục đích của bài báo này nhằm đưa ra một phương pháp biến đổi được dùng để biến đổi hàm $p_X(x)$ thành một hàm khối xác suất của một biến ngẫu nhiên rời rạc $\tilde{X}$ với miền giá trị là $\mathcal{R}_{\tilde{X}} = \{k \in \mathbb{N} : k \geq \min \mathcal{R}_X\}$. Chúng tôi tìm thấy một biểu diễn cho hàm đặc trưng của $\tilde{X}$ theo hàm đặc trưng của X. Ngoài ra, tính bảo toàn phân phối của phép biến đổi được chỉ ra trong một số trường hợp cụ thể.

Từ khóa: *Hàm khối xác suất, biến ngẫu nhiên rời rạc, phép biến đổi, hàm đặc trưng.*

**Tác giả liên hệ chính.*
Email: lethanhbinh@qnu.edu.vn

https://doi.org/10.52111/qnjs.2024.18307

QUY NHON UNIVERSITY
JOURNAL OF SCIENCE

A transformation of probability mass functions for a class of discrete random variables

Le Thanh Binh*

Department of Mathematics and Statistics, Quy Nhon University, Vietnam

Received: 18/02/2024; Revised: 03/05/2024

Accepted: 04/05/2024; Published: 28/06/2024

ABSTRACT

Let us consider a discrete random variable X that takes only non-negative integer values. Let $\mathcal{R}_X$ and $p_X(x)$ denote the range of X and the probability mass function of X, respectively. The aim of this paper is to provide a transformation method used to transform $p_X(x)$ into a probability mass function of a discrete random variable $\tilde{X}$ whose range is $\mathcal{R}_{\tilde{X}} = \{k \in \mathbb{N} : k \geq \min \mathcal{R}_X\}$. We obtain a representation of the characteristic function of $\tilde{X}$ in terms of the characteristic function of X. Moreover, the distribution-preserving property of the transformation is shown in some specific cases.

Keywords: *Probability mass function, discrete random variable, transformation, characteristic function.*

1. INTRODUCTION

In probability theory, a probability distribution is the mathematical function that gives the probabilities of occurrence of different possible outcomes for a random experiment. It is a mathematical description of a random phenomenon in terms of its sample space and the probabilities of events (subsets of the sample space).[1,2] The sample space, often denoted by Ω, is the set of all possible outcomes of a random experiment being observed.

In order to classify probability distributions, we need to define discrete and continuous random variables. A random variable is a function whose domain is a sample space Ω and whose range (i.e., the set of values that it can obtain) is a subset of the real numbers, $\mathbb{R}$. In other words, a random variable assigns real numbers to the outcomes in its sample space. Random variables which take on values from a discrete set of numbers (i.e., whose range is either *finite* or *countably infinite*) are called *discrete random variable*.[3] Otherwise, a random variable is called *continuous* if it ranges over a continuous set of numbers that contains all real numbers between two limits.[3] In other words, a continuous random variable is one that takes an uncountably infinite number of possible values. For instance, a random variable that represents the time between two successive arrivals to a queueing system, or that represents the temperature in a nuclear reactor, is an example of a continuous random variable.[3] It is evident that all random variables defined on a discrete sample space are discrete. However, random variables defined on a continuous sample space may be either discrete or continuous.

**Corresponding author.*
Email: lethanhbinh@qnu.edu.vn

https://doi.org/10.52111/qnjs.2024.18307

Probability distributions can be categorized into two main types: discrete and continuous. Discrete distributions deal with the probabilities of specific values for discrete random variables, while continuous distributions handle the probabilities of various values for continuous random variables. Examples of discrete distributions include the *Binomial*, *Poisson*, and *Negative Binomial* distributions. We will introduce these distributions and several other discrete distributions in more detail in Section 3. For continuous distributions, the most popular example is the *normal distribution*. This is also referred to as the *Gaussian distribution*. Some important continuous distributions are often used to build models and to test hypotheses about random variables, such as the student's t-distribution, the *chi-squared distribution* and the *F-distribution*.

The key difference between a discrete probability distribution and a continuous probability distribution is that in a discrete distribution we are able to compute the probability that a random variable can take on a particular value, therefore the probabilities of individual values can be tabulated. Discrete random variables, or discrete distributions, can be completely characterized by their *probability mass functions*. The probability mass function (frequently abbreviated to *pmf*) for a discrete random variable X, gives the probability that the value obtained by X on the outcome of a probability experiment is equal to x ($x \in \mathbb{R}$).[3] In the present paper, we denote it by $p_X(.)$. The formal definition of the probability mass function for a discrete random variable is given in Section 2. Sometimes the term *discrete density function* is used in place of probability mass function. Since a continuous random variable takes an uncountably infinite number of possible values, the probability that it is exactly equal to any one of the infinite possible values is zero. For this reason, the method mentioned above to describe a discrete random variable will not work in the case of a continuous random variable, and then we have to consider the probability of a continuous random variable taking values in an interval. Continuous random variables, or continuous distributions, can be completely characterized by their *probability density functions* (frequently abbreviated to *pdf*). Because the purpose of this study is to concentrate only on discrete distributions, in the article we will ignore the definitions or concepts associated with continuous random variables, and we refer the reader to [1,2,4] for more details.

The starting point of this paper was to study the Binomial distribution (denoted by Binom(n, p)). This distribution has two parameters: the number of trials , $n \in \mathbb{N}^*$, and the probability of success for a single trial, $p \in (0, 1)$. The outcome from a random variable X obeying the Binomial distribution will always be a nonnegative integer with an upper bound at n. By the rules of probability, we can attain that the probability of the event $\{X = k\}$ (i.e., the probability of k successes in n trials) is equal to $\binom{n}{k}p^k(1-p)^{n-k}$. By definition, the quantity $\binom{n}{k}p^k(1-p)^{n-k}$ is the value of the probability mass function of X at k, namely $p_X(k)$. Then, by chance and by intuition, we have found the following equality:

$$\sum_{k=0}^{n}\sum_{i=0}^{k}(np-i)\binom{n}{i}p^i(1-p)^{n-i} = npq,$$

which can be shortly rewritten as

$$\sum_{k=0}^{n}\sum_{i=0}^{k}(\mu-i)p_X(i) = \sigma^2, \qquad (1)$$

where $\mu = np$ and $\sigma^2 = npq$.

At first glance, equality (1) was nothing special. However, it is worth noticing that the quantities $\mu = np$ and $\sigma^2 = npq$ are the *mean* and *variance* of the Binomial random variable X, respectively. Furthermore, the set $\{0; 1; ...; n\}$ is the range of X (denoted by $\mathcal{R}_X$). The definitions of the mean and variance of a discrete random variable are given in Section 2. Then, a question naturally arose in our mind: *Whether equality* (1) *holds true for an arbitrary discrete random variable X whose range is a subset of the set of natural numbers, if its mean and variance are finite, or not*? Motivated by this question, we have shown that equality (1) remains true for nonnegative integer-valued random variables satisfying a certain condition. This result is presented in Lemma 3.2. Combining Lemma 3.2 and Lemma 3.1, we then obtain the first main theorem (Theorem 3.2), which

gives a way to transform a probability mass function of a nonnegative integer-valued random variable to that of another nonnegative integer-valued random variable. From this result, we achieve the remaining important results as shown in Section 3. Up to the present, there are only a few results on transformations associated with probability mass functions. For instance, the *pignistic transformation* and the *plausibility transformation* are introduced in the research[5]. We briefly recall that these two transformations provide the ways to transform a *basic probability assignment* function to a probability mass function. Notice that a basic probability assignment function (called also mass function) is not a probability mass function. For more detail, see[5].

The rest of the paper is organized as follows. Section 2 revisits key definitions and properties including probability mass function, mean, variance, and characteristic function. Section 3 presents our primary findings. Finally, Section 4 concludes with remarks summarizing the significance of our research outcomes. This systematic approach aids in understanding the framework and contributions of our study.

2. PRELIMINARIES

2.1. Probability mass function, mean and variance

From the point of view of understanding the behavior of a discrete random variable, the important thing is to know the probabilities that the random variable takes each value in its range. Such probabilities are described with a *probability mass function*.

Definition 2.1. [4] Let X be a discrete random variable. The *probability mass function* of X, denoted by $p_X(.)$, is defined as

$$p_X(x) = P(X = x) > 0 \quad \text{if } x \in \mathcal{R}_X,$$
$$p_X(x) = 0 \quad \text{if } x \notin \mathcal{R}_X,$$

where $\mathcal{R}_X$ is the range of X.

Obviously, the range of $p_X(.)$ is a subset of the interval $[0, 1]$. Furthermore, by the rules of probability, one can get that the function values add to 1.0 when summed over all possible values of the random variable X. This means that $\sum_{x\in\mathcal{R}_X} p_X(x) = 1$.

Definition 2.2. [4] Let X be a discrete random variable with $\mathcal{R}_X = \{x_k\}_{k\geq 0}$. The *expectation* or the *mean* of the random variable X, denoted by $\mathbb{E}X$, is the number

$$\mathbb{E}X = \sum_{x\in\mathcal{R}_X} xp_X(x) = \sum_{k=0}^{\infty} x_k p_X(x_k), \quad (2)$$

which is defined when $\sum_{k=0}^{\infty} |x_k| p_X(x_k) < \infty$. If the later series diverges, the mean is not defined.

In the case where the mean is defined, its value does not depend on the order of summation. Essentially, the mean $\mathbb{E}X$ denotes a weighted average of the elements in $\mathcal{R}_X$, where the probabilities act as the weights in the discrete setting.

Definition 2.3. Let X be a discrete random variable with $\mathcal{R}_X = \{x_k\}_{k\geq 0}$, and let $\lambda > 0$ be a positive real number (not necessarily integer). The *moment of order* λ of X is defined as

$$\alpha_\lambda = \mathbb{E}X^\lambda = \sum_{k=0}^{\infty} (x_k)^\lambda p_X(x_k).$$

Definition 2.4. [4] Suppose that the mean and the moment of order 2 of the discrete random variable X are finite. The *variance* of X, denoted by $\mathrm{Var}X$, is the quantity

$$\mathrm{Var}X = \mathbb{E}(X - \mathbb{E}X)^2 = \sum_{k=0}^{\infty} (x_k - \mathbb{E}X)^2 p_X(x_k).$$

The variance characterizes the amount of variation of the random variable from its mean. The following property is commonly useful to compute the variance.

$$\mathrm{Var}X = \mathbb{E}X^2 - (\mathbb{E}X)^2.$$

The expectation and variance of a random variable are two of the foremost notions in probability theory. For basic properties of expectation and variance, we refer the reader to the studies.[1,4,6]

2.2. Characteristic function

In probability theory and mathematical statistics, characteristic functions always play an outstanding role by providing a comprehensive way to describe

https://doi.org/10.52111/qnjs.2024.18307

and analyze probability distributions. They are particularly powerful due to their unique properties and applications in various statistical methodologies.

Definition 2.5. [7] The *characteristic function* of a discrete random variable X is defined as

$$\varphi_X(t) = \mathbb{E}(e^{itX}) = \sum_{k=0}^{\infty} e^{itx_k} p_X(x_k), \qquad (3)$$

where t is any real number and $i = \sqrt{-1}$.

Since $|e^{itx}|$ is a bounded and continuous function for all finite real t and x, the characteristic function always exists. We recall that any characteristic function $\varphi_X(t)$ satisfies the following conditions (see the research[7] Theorem 1.1.1):

1. $\varphi_X(t)$ is uniformly continuous;
2. $\varphi_X(0) = \lim_{t\to 0} \varphi_X(t) = 1$;
3. $|\varphi_X(t)| \leq 1$ for all real numbers t.
4. $\varphi_X(-t) = \overline{\varphi_X(t)}$, where the horizontal bar denotes the complex conjugate.

In addition, if the moment of order n exists (where n is a positive integer) then $\varphi_X(t)$ is n times differentiable for all t, and it is related to the $n-th$ derivative of the characteristic function by the formula[7]

$$\alpha_n = (-i)^n \varphi_X^{(n)}(0). \qquad (4)$$

So, the existence of some moments of a random variable ensures the existence of the corresponding derivatives of the characteristic function. We next introduce the following important result (referred to as the uniqueness theorem), which shows that a probability distribution is uniquely determined by its characteristic function.

Proposition 2.1 (Theorem 1.1.2)**.** [7] *Two probability distributions are identical if and only if their characteristic functions are identical.*

For more details on properties of characteristic functions, interested readers could be refer to[7] and the references therein. Thanks to characteristic functions, we arrive at some interesting results as shown in Subsection 3.3.

3. MAIN RESULTS

Let X be a discrete random variable with the range $\mathcal{R}_X \subseteq \mathbb{N}$ (the set $\mathcal{R}_X$ is either finite or countably infinite). Throughout the forthcoming, we always assume that the mean and variance of X exist, and are denoted by μ and σ^2 ($\sigma > 0$) respectively.

3.1. Formulation of transformation

Lemma 3.1. *Let k be a nonnegative integer. If $\mathcal{R}_X$ is countably infinite, we then get*

$$\sum_{i=0}^{k} (\mu - i) p_X(i) > 0 \Leftrightarrow k \geq \min \mathcal{R}_X.$$

If $\mathcal{R}_X$ is finite with $|\mathcal{R}_X|$ greater than 1, we have

$$\sum_{i=0}^{k} (\mu - i) p_X(i) > 0 \Leftrightarrow \min \mathcal{R}_X \leq k \leq \max \mathcal{R}_X - 1.$$

Proof. If $\mathcal{R}_X$ is countably infinite, we have that

$$\sum_{i=0}^{k} (\mu - i) p_X(i) \geq (\mu - \min \mathcal{R}_X) p_X(\min \mathcal{R}_X) > 0$$

if $\min \mathcal{R}_X \leq k \leq \mu$ (since $\mu > \min \mathcal{R}_X$).

For $k > \mu$, setting $a(i) = (\mu - i) p_X(i)$, we obtain

$$\begin{aligned} \sum_{i=0}^{k} (\mu - i) p_X(i) &= \sum_{i=0}^{[\mu]} a(i) + \sum_{i=[\mu]+1}^{k} a(i) \\ &> \sum_{i=0}^{[\mu]} a(i) + \sum_{i=[\mu]+1}^{\infty} a(i) \\ &= \sum_{i=0}^{\infty} a(i) = \mu - \mu = 0, \end{aligned}$$

where $[.]$ denotes the floor function. Obviously, $\sum_{i=0}^{k} (\mu - i) p_X(i) = 0$ if $k < \min \mathcal{R}_X$.

If $\mathcal{R}_X$ is a finite set (with $|\mathcal{R}_X| > 1$), due to $\sum_{i=0}^{\max \mathcal{R}_X} (\mu - i) p_X(i) = 0$, we only need to consider k such that $\min \mathcal{R}_X \leq k \leq \max \mathcal{R}_X - 1$. □

Lemma 3.2. *Assume that*

$$\lim_{n\to\infty} n \sum_{i=0}^{n} (\mu - i) p_X(i) = 0. \qquad (5)$$

Then, setting $m = \min \mathcal{R}_X$, we have

$$\sum_{k=m}^{\infty} \sum_{i=m}^{k} (\mu - i) p_X(i) = \sigma^2. \qquad (6)$$

In the case that $\mathcal{R}_X$ is finite, equality (6) *becomes*

$$\sum_{k=m}^{M-1}\sum_{i=m}^{k}(\mu-i)p_X(i)=\sigma^2, \tag{7}$$

where $M := \max \mathcal{R}_X$.

Proof. For each positive integer $n \geq m$, we have

$$\begin{aligned}
&\sum_{k=m}^{n}\sum_{i=m}^{k}(\mu-i)p_X(i)\\
&=\sum_{k=0}^{n}\sum_{i=0}^{k}(\mu-i)p_X(i) \quad (p_X(i)=0 \text{ if } i\notin\mathcal{R}_X)\\
&=\sum_{i=0}^{n}(n+1-i)(\mu-i)p_X(i)\\
&=\sum_{i=0}^{n}[(i-\mu)^2+n(\mu-i)+(1-\mu)(\mu-i)]p_X(i)\\
&=\sum_{i=0}^{n}(i-\mu)^2p_X(i)+n\sum_{i=0}^{n}(\mu-i)p_X(i)\\
&\qquad+(1-\mu)\sum_{i=0}^{n}(\mu-i)p_X(i). \quad (8)
\end{aligned}$$

It is noteworthy that, by the definitions of μ and σ^2,

$$\sum_{i=0}^{\infty}(i-\mu)^2p_X(i)=\sigma^2;\sum_{i=0}^{\infty}(\mu-i)p_X(i)=0. \tag{9}$$

Equality (6) readily follows from (5), (8) and (9).

If R_X is a finite set, by the definition of μ one can easily see that $\sum_{i=m}^{n}(\mu-i)p_X(i)=0$ for every $n \geq M$. Therefore, condition (5) is always true and we obtain (7). □

Remark 3.1. Lemma 3.2 yields another formula for the variance of a discrete random variable X if its range is a subset of the set of natural numbers, provided that (5) is satisfied. Furthermore, from the proof of Lemma 3.2, we notice that (5) is a necessary and sufficient condition for the validity of (6).

Combining Lemma 3.1 with Lemma 3.2, we immediately attain the first main theorem.

Theorem 3.2. *Assume that* (5) *holds and set* $m = \min \mathcal{R}_X$, $M = \max \mathcal{R}_X$. *Then, there exists a discrete random variable* $\tilde{X}$ *such that*

$$\mathcal{R}_{\tilde{X}}=\begin{cases}\{k\in\mathbb{N}: m\leq k\} & \text{if } \mathcal{R}_X \text{ is infinite;}\\ \{k\in\mathbb{N}: m\leq k<M\} & \text{if } \mathcal{R}_X \text{ is finite;}\end{cases}$$

and its probability mass function is given by

$$p_{\tilde{X}}(k)=P(\tilde{X}=k)=\frac{1}{\sigma^2}\sum_{i=m}^{k}(\mu-i)p_X(i), \tag{10}$$

for all $k \in \mathcal{R}_{\tilde{X}}$.

Proof. According to Lemmas 3.1 and 3.2, we have

$$p_{\tilde{X}}(k)>0\ (\forall k\in\mathcal{R}_{\tilde{X}}) \quad \text{and} \quad \sum_{k=m}^{\infty}p_{\tilde{X}}(k)=1,$$

which imply the statement of Theorem 3.2. □

Remark 3.3. In other words, Theorem 3.2 or formula (10) textcolorredprovide a probability transformation which transforms the probability mass function $p_X(.)$ to another probability mass function, $p_{\tilde{X}}(.)$. Also, one can see that the range of $\tilde{X}$ is always a set containing consecutive nonnegative intergers, and has the same minimum value as the one of the initial random variable, $\mathcal{R}_X$.

Let us now consider the following example to more understand the use of the transformation.

Example 3.4. Let X be the random variable with the probability distribution described as follows:

X	0	4	6	8
$p_X(x)$	$\frac{1}{8}$	$\frac{1}{8}$	$\frac{1}{4}$	$\frac{1}{2}$

By direct calculation, using (10) we get

$$\begin{aligned}
&\mu=6;\sigma^2=7;\\
&p_{\tilde{X}}(0)=p_{\tilde{X}}(1)=p_{\tilde{X}}(2)=p_{\tilde{X}}(3)=\frac{3}{28};\\
&p_{\tilde{X}}(4)=p_{\tilde{X}}(5)=\frac{1}{7};\\
&p_{\tilde{X}}(6)=p_{\tilde{X}}(7)=\frac{1}{7}.
\end{aligned}$$

Clearly, $\sum_{k=0}^{7}p_{\tilde{X}}(k)=1$ and the corresponding probability distribution of $\tilde{X}$ is given as

$\tilde{X}$	0	1	2	3	4	5	6	7
$p_{\tilde{X}}(k)$	$\frac{3}{28}$	$\frac{3}{28}$	$\frac{3}{28}$	$\frac{3}{28}$	$\frac{1}{7}$	$\frac{1}{7}$	$\frac{1}{7}$	$\frac{1}{7}$

https://doi.org/10.52111/qnjs.2024.18307

The next example was intended as an attempt to extend the claim of Theorem 3.2 to the case that X takes (positive) noninteger values. However, we obtain that the claim is no longer true.

Example 3.5. Let X be the random variable with the probability distribution given as

X	0	$\frac{1}{2}$	1	$\frac{3}{2}$	2
$p_X(x)$	$\frac{1}{8}$	$\frac{2}{8}$	$\frac{1}{8}$	$\frac{1}{8}$	$\frac{3}{8}$

From (10), we get

$$\mu = \frac{19}{16};\ \sigma^2 = \frac{143}{256};$$
$$p_{\tilde{X}}(0) = \frac{38}{143};$$
$$p_{\tilde{X}}(1) = \frac{88}{143}.$$

We obtain

$$p_{\tilde{X}}(0) + p_{\tilde{X}}(1) = \frac{126}{143} \neq 1.$$

Hence, equality (6) does not hold.

3.2. The characteristic function $\varphi_{\tilde{X}}(.)$

As mentioned in Section 1, it will be very useful to obtain an expression for the characteristic function of $\tilde{X}$. By Proposition 2.1, the fact that every distribution is uniquely determined by its characteristic function allows us to be able to determine the distribution type of $\tilde{X}$, without having to find the mass probability function $p_{\tilde{X}}(.)$.

Theorem 3.6. *With the settings of Theorem 3.2, the characteristic function $\varphi_{\tilde{X}}(.)$ of the random variable $\tilde{X}$ is given by*

$$\varphi_{\tilde{X}}(t) = \frac{\mu\varphi_X(t) + i\varphi'_X(t)}{\sigma^2(1 - e^{it})}, \forall t \in \mathbb{R}, \tag{11}$$

where, as before, μ, σ^2 and $\varphi_X(.)$ are respectively the mean, variance and characteristic function of the random variable X.

Proof. For simplicity of notations, throughout the proof, p_k and $\tilde{p}_k$ stand for $p_X(k)$ and $p_{\tilde{X}}(k)$, respectively. From (10) and by grouping the terms appropriately, we attain

$$\begin{aligned}
S_n(t) &:= \sum_{k=0}^{n} e^{itk}\tilde{p}_k \\
&= \frac{1}{\sigma^2}\sum_{k=0}^{n}\left[e^{itk}\sum_{j=0}^{k}(\mu - j)p_j\right] \\
&= \frac{1}{\sigma^2}(\mu - 0)p_0\sum_{k=0}^{n}e^{itk} + \frac{1}{\sigma^2}(\mu - 1)p_1\sum_{k=1}^{n}e^{itk} \\
&\quad + \frac{1}{\sigma^2}(\mu - 2)p_2\sum_{k=2}^{n}e^{itk} + ... + \frac{1}{\sigma^2}(\mu - n)p_n e^{itn} \\
&= \frac{1}{\sigma^2}\sum_{j=0}^{n}\left[(\mu - j)p_j\sum_{k=j}^{n}e^{itk}\right] \\
&= \frac{1}{\sigma^2}\left(S_{1,n}(t) - S_{2,n}(t)\right), \qquad (12)
\end{aligned}$$

where

$$S_{1,n}(t) := \sum_{j=0}^{n}\left[(\mu - j)p_j\sum_{k=0}^{n}e^{itk}\right]; \tag{13a}$$

$$S_{2,n}(t) := \sum_{j=1}^{n}\left[(\mu - j)p_j\sum_{k=0}^{j-1}e^{itk}\right]. \tag{13b}$$

On the other hand, by definition,

$$\varphi_{\tilde{X}}(t) = \lim_{n\to\infty} S_n(t), \tag{14}$$

we are thus left with the task of determining the limits of $S_{1,n}(t)$ and $S_{2,n}(t)$ as n tends to ∞.

To find the limit of $S_{1,n}(t)$ defined as (13a), it is worth pointing out that

$$\begin{aligned}
0 < |S_{1,n}(t)| &= \left|\sum_{k=0}^{n}e^{itk}\right|\left|\sum_{j=0}^{n}(\mu - j)p_j\right| \\
&\leq \left|n\sum_{j=0}^{n}(\mu - j)p_j\right|.
\end{aligned}$$

From (5) and the Squeeze Theorem, it immediately follows that

$$\lim_{n\to\infty} S_{1,n}(t) = 0. \tag{15}$$

In order to arrive at the remaining limit, we first rewrite $S_{n,2}(t)$, given by (13b), as follows

$$S_{2,n}(t) = \frac{1}{1-e^{it}}\sum_{j=1}^{n}(\mu-j)p_j(1-e^{itj})$$
$$= \frac{1}{1-e^{it}}\sum_{j=0}^{n}(\mu-j)p_j(1-e^{itj})$$
$$= \frac{1}{1-e^{it}}\Big[\sum_{j=0}^{n}(\mu-j)p_j - \mu\sum_{j=0}^{n}p_je^{itj} + \sum_{j=0}^{n}jp_je^{itj}\Big]. \quad (16)$$

Letting n tend to ∞ in the both sides of (16), we get

$$\lim_{n\to\infty} S_{2,n}(t) = \frac{1}{1-e^{it}}\Big[-\mu\varphi_X(t)+\frac{\varphi'_X(t)}{i}\Big], \quad (17)$$

owing to the following simple equalities,

$$\sum_{j=0}^{\infty}(\mu-j)p_j = 0;$$
$$\sum_{j=0}^{\infty}p_je^{itj} = \varphi_X(t); \quad \sum_{j=0}^{\infty}jp_je^{itj} = \frac{1}{i}\varphi'_X(t).$$

From (12), (14), (15) and (17), the proof of Theorem 3.6 is completed. □

3.3. Distribution-preserving property

The work of this section contains descriptions of some different well-known discrete distributions used in probability. By the method of characteristic functions, our aim is to verify whether the random variables X and $\tilde{X}$ are able to belong to the same family of distributions (in other words, whether the distribution family of X can be preserved by the formulated transformation) for each considered case.

- **Binomial distribution**

Binomial distributions correspond to random variables that count the number of successes among n independent trials having the same probability of success. Such trials are called Bernoulli trials. The probabilistic model of Bernoulli trials is applicable in many situations, where it is reasonable to assume independence and constant success probability.

Definition 3.1. [6,8] A random variable X is said to have a *Binomial distribution* with parameters n and p (where $n \in \mathbb{N}^*$, $0 < p < 1$) if

$$P(X=k) = \binom{n}{k}p^k(1-p)^{n-k}, \quad (18)$$

for all $k = 0, 1, ..., n$. We write $X \sim \mathrm{B}(n,p)$.

If $X \sim \mathrm{B}(n,p)$, the mean and variance are[6]

$$\mu = np, \ \ \sigma^2 = np(1-p), \quad (19)$$

and the characteristic function is given by[7]

$$\varphi_X(t) = (1-p+pe^{it})^n. \quad (20)$$

From (19), (20) and (11), we have

$$\varphi_{\tilde{X}}(t) = (1-p+pe^{it})^{n-1}, \quad (21)$$

which immediately implies that

$$\tilde{X} \sim \mathrm{B}(n-1,p),$$

for all $n \geq 2$.

- **Poisson distribution**

Poisson distributions are applied when the random variables under consideration count the number of events occurring in a specified time period or a spatial area, and the observed processes satisfy the primary conditions of time (or space) homogeneity, independent increments, and no memory of the past.

Definition 3.2. [6,8] A random variable X is said to have a *Poisson distribution* with unique parameter $\lambda > 0$ if

$$P(X=k) = \frac{e^{-\lambda}\lambda^k}{k!}, \quad k = 0,1,2,... \quad (22)$$

We then write $X \sim Pois(\lambda)$.

The mean, variance and characteristic function of the Poisson distribution are[7]

$$\mu = \sigma^2 = \lambda, \quad (23)$$
$$\varphi_X(t) = \exp[\lambda(e^{it}-1)]. \quad (24)$$

First of all, let us prove that assumption (5) is satisfied. Indeed, by (22) and (23), we get

$$\sum_{k=0}^{n}(\mu-k)p_X(k)$$
$$= \sum_{k=0}^{n}(\lambda-k)\frac{e^{-\lambda}\lambda^k}{k!}$$
$$= e^{-\lambda}\Big[\sum_{k=0}^{n}\frac{\lambda^{k+1}}{k!} - \sum_{k=1}^{n}\frac{\lambda^k}{(k-1)!}\Big]$$

https://doi.org/10.52111/qnjs.2024.18307

$$= e^{-\lambda}\Big[\sum_{k=0}^{n}\frac{\lambda^{k+1}}{k!} - \sum_{k=0}^{n-1}\frac{\lambda^{k+1}}{k!}\Big]$$

$$= e^{-\lambda}\frac{\lambda^{n+1}}{n!}.$$

As a result, assumption (5) is equivalent to

$$\frac{\lambda^n}{n!} \longrightarrow 0 \text{ as } n \to \infty,$$

which is true for all $\lambda > 0$. So, (5) is valid. By Theorem 3.6, (23) and (24), it is straightforward to find the expression for $\varphi_{\tilde{X}}$,

$$\varphi_{\tilde{X}}(t) = \exp[\lambda(e^{it} - 1)] = \varphi_X(t).$$

Thus, we have

$$\tilde{X} \sim \text{ Pois}(\lambda).$$

• Negative binomial distribution

The Negative Binomial distribution is a discrete probability distribution that models the number of failures in a sequence of independent and identically distributed Bernoulli trials before a specified number of successes occurs. In a sequence of independent Bernoulli trials, each trial has two potential outcomes called "success" and "failure". In each trial the probability of success is p $(0 < p < 1)$ and of failure is $1 - p$. One observes this sequence until a number r of successes occurs, where r is a fixed integer.

Definition 3.3. [6,8] Let the random variable X denote the number of observed failures before the r^{th} success occurs. Then

$$P(X = k) = \binom{k + r - 1}{k}(1 - p)^k p^r, \qquad (25)$$

for all $k = 0, 1, 2, ...$

In this case, the random variable X is said to have the *Negative Binomial distribution* with parameters r and p. We denote by $X \sim \text{NB}(r, p)$.

If $X \sim \text{NB}(r, p)$, then

$$\mu = \frac{r(1 - p)}{p}, \sigma^2 = \frac{r(1 - p)}{p^2}, \qquad (26)$$

and its characteristic function is given as [7]

$$\varphi_X(t) = \left(\frac{p}{1 - (1 - p)e^{it}}\right)^r, \ t \in \mathbb{R}. \qquad (27)$$

From (25) and (26), we first remark that

$$\sum_{k=0}^{n}(\mu - k)p_X(k)$$

$$= \sum_{k=0}^{n}\Big(\frac{rq}{p} - k\Big)C_{k+r-1}^{k}q^k p^r \qquad (q := 1 - p)$$

$$= rqp^{r-1} + rp^{r-1}\sum_{k=1}^{n}\Big(C_{k+r-1}^{k}q^{k+1} - C_{k+r-1}^{k-1}q^k p\Big)$$

$$= rqp^{r-1} + rp^{r-1}\Big[\sum_{k=1}^{n}\Big(C_{k+r-1}^{k} + C_{k+r-1}^{k-1}\Big)q^{k+1} - \sum_{k=1}^{n}C_{k+r-1}^{k-1}q^k\Big]$$

$$= rqp^{r-1} + rp^{r-1}\Big[\sum_{k=1}^{n}C_{k+r}^{k}q^{k+1} - \sum_{k=0}^{n-1}C_{k+r}^{k}q^{k+1}\Big]$$

$$= rp^{r-1}C_{n+r}^{n}q^{n+1}.$$

Due to $0 < q < 1$, it is easy to check that

$$nC_{n+r}^{n}q^{n+1} = \frac{n(n+1)...(n+r)}{r!}q^{n+1} \longrightarrow 0$$

as $n \to \infty$. In other words, (5) holds true.

Accordingly, by Theorem 3.6, we attain the characteristic function of $\tilde{X}$ defined by

$$\varphi_{\tilde{X}}(t) = \left(\frac{p}{1 - (1 - p)e^{it}}\right)^{r+1},$$

which concludes that $\tilde{X} \sim \text{NB}(r + 1, p)$.

• Geometric distribution

Consider independent trials such that a certain event may happen at any given trial with probability p. The trials continue until the event occurs for the first time. The number, X, of trials performed before the event occurs has a geometric distribution. [6]

Definition 3.4. [6] A random variable X is said to have a *geometric distribution* with parameter p, where $0 < p < 1$, if its probability mass function is defined by

$$P(X = k) = (1 - p)^k p, \qquad (28)$$

for all $k = 0, 1, 2, ...$ We then write $X \sim \text{Geo}(p)$.

From (28), it is easy to see that the geometric distribution is the special case of the negative binomial with $r = 1$, namely,

$$X \sim \text{Geo}(p) \Leftrightarrow X \sim \text{NG}(1, p).$$

As a consequence, we get that $\tilde{X} \sim \text{NB}(2, r)$ if $X \sim \text{Geo}(p)$.

• Hypergeometric distribution

The hypergeometric distribution is a discrete probability distribution that models the probability of obtaining a specific number of successes in a sample drawn without replacement from a finite population containing two distinct types of elements[6,8] (i.e., a finite population whose elements can be classified into two categories one which possesses a certain characteristic and another which does not possess that characteristic). For instance, suppose an urn contains K white balls and $(N - K)$ black balls. From this, n balls are drawn without replacement. The probability that the sample of size n contains k white balls and $(n-k)$ black balls can be obtained by hypergeometric distribution.

The hypergeometric distribution is characterized by the following parameters:

- N: The total population size.
- K: The number of elements of Type 1 in the population.
- n: The number of draws without replacement (the sample size).

Definition 3.5. Let N, K and n be integers such that $N \geq 1$, $0 \leq K \leq N$, and $1 \leq n \leq N$. A random variable X is said to have a *hypergeometric distribution* with parameters (N, K, n), written as $X \sim \text{HG}(N, K, n)$, if the corresponding probability mass function is given by

$$P(X = k) = \frac{\binom{K}{k}\binom{N-K}{n-k}}{\binom{N}{n}}, \tag{29}$$

where $k \in \mathbb{Z}$ and

$$\max(0, n + K - N) \leq k \leq \min(n, K).$$

If $X \sim \text{HG}(N, K, n)$, the mean and variance are

$$\mu = n\frac{K}{N}\ ,\ \sigma^2 = n\frac{K(N-K)(N-n)}{N^2(N-1)}, \tag{30}$$

and its characteristic function is given by[7]

$$\varphi_X(t) = \frac{\binom{N-K}{n}{}_2F_1[-n, -K; N-K-n+1; e^{it}]}{\binom{N}{n}}. \tag{31}$$

where

$${}_2F_1[a, b; c; z] = 1 + \frac{ab}{c}\frac{z}{1!} + \frac{a(a+1)b(b+1)}{c(c+1)}\frac{z^2}{2!} + \cdots \tag{32}$$

is the *Gaussian hypergeometric function*.[6]

By virtue of the fact that

$$\frac{\partial {}_2F_1[a, b; c; z]}{\partial z} = \frac{ab}{c}{}_2F_1[a+1, b+1; c+1; z],$$

we then attain

$$\varphi'_X(t) = ie^{it}\frac{nK\binom{N-K}{n}{}_2F_1[\alpha, \beta; \gamma; e^{it}]}{(N-K-n+1)\binom{N}{n}}, \tag{33}$$

where $\alpha := -n + 1, \beta := -K + 1$, and $\gamma := N - K - n + 2$. Unfortunately, at first we couldn't find the explicit expression for $\varphi_{\tilde{X}}(t)$ by means of formula (11) in Theorem 3.6. Therefore, it is difficult for us to determine the appropriate distribution of the random variable $\tilde{X}$.

However, according to the above results and Theorem 3.2, we have had a reasonable belief that the random variable $\tilde{X}$ should follow a hypergeometric distribution and, futhermore, its support set must be $\{k \in \mathbb{Z} : \max(0, n + K - N) \leq k \leq \min(n-1, K-1)\}$. For this reason, we aim at proving that

$$\tilde{X} \sim \text{HG}(N - 2, K - 1, n - 1), \tag{34}$$

provided that $N \geq 3$, $K \geq 1$ and $n \geq 2$.

To do this, we first note that (34) is equivalent to

$$\varphi_{\tilde{X}}(t) = \frac{\binom{\tilde{N}-\tilde{K}}{\tilde{n}}{}_2F_1[-\tilde{n}, -\tilde{K}; \tilde{N}-\tilde{K}-\tilde{n}+1; e^{it}]}{\binom{\tilde{N}}{\tilde{n}}}, \tag{35}$$

where $\tilde{N} := N - 2$, $\tilde{K} := K - 1$ and $\tilde{n} := n - 1$. With the aid of the algebraic computation software

https://doi.org/10.52111/qnjs.2024.18307

(MAPLE), we could easily verify that the following identity

$$\varphi_{\tilde{X}}(t) - \frac{\mu\varphi_X(t) + i\varphi'_X(t)}{\sigma^2(1-e^{it})} \equiv 0 \ (\forall t \in \mathbb{R}),$$

holds true if μ, σ^2, $\varphi_X(t)$, $\varphi'_X(t)$, and $\varphi_{\tilde{X}}(t)$ are given by (30), (31), (33) and (35), respectively. Hence, assertion (34) is true.

• Logarithmic series distribution

The logarithmic series distribution (also known as the the log-series distribution) is a discrete probability distribution derived from the Maclaurin series expansion:

$$\ln(1-p) = -p - \frac{p^2}{2} - \frac{p^3}{3} - \cdots = \sum_{k=1}^{\infty} \frac{-p^k}{k}, \quad (36)$$

where $0 < p < 1$. From this, we get

$$\sum_{k=1}^{\infty} \frac{-p^k}{k\ln(1-p)} = 1.$$

So, it is easy to see that

$$f(k) = \frac{-p^k}{k\ln(1-p)}, \ k = 1, 2, ...,$$

defines a probability mass function on the set of positive integers.

Definition 3.6. [6] A random variable X is said to have a *logarithmic series distribution* with parameter p, where $0 < p < 1$, if its probability mass function is given as

$$P(X = k) = -\frac{p^k}{k\ln(1-p)}, k = 1, 2, 3, ... \quad (37)$$

We then write $X \sim \text{LogSeries}(p)$.

The logarithmic series distribution is sometimes used to model the number of items of a product purchased by a buyer in a specified interval.

If $X \sim \text{LogSeries}(p)$, the mean and variance are given as

$$\mu = -\frac{p}{(1-p)\ln(1-p)}, \quad (38a)$$

$$\sigma^2 = -\frac{p^2 + p\ln(1-p)}{(1-p)^2(\ln(1-p))^2}. \quad (38b)$$

Besides, its characteristic function is as follows[7]

$$\varphi_X(t) = \frac{\ln(1-pe^{it})}{\ln(1-p)}. \quad (39)$$

Let us now show that assumption (5) is satisfied when $X \sim \text{LogSeries}(p)$. For any positive integer n, according to (37) and (38a), we derive

$$\begin{aligned}
&n\sum_{k=1}^{n}(\mu - k)p_X(k) \\
&= A(p)n\sum_{k=1}^{n} p^k \left((1-p)\ln(1-p) + \frac{p}{k}\right) \\
&= A(p)n\left(\ln(1-p)\sum_{k=1}^{n}(p^k - p^{k+1}) + p\sum_{k=1}^{n}\frac{p^k}{k}\right) \\
&= A(p)n\left(\ln(1-p)(p - p^{n+1}) + p\sum_{k=1}^{n}\frac{p^k}{k}\right) \\
&= A(p)\left(-np^{n+1}\ln(1-p) + pnB_n(p)\right), \quad (40)
\end{aligned}$$

where

$$A(p) := \frac{1}{(1-p)(\ln(1-p))^2}, \quad (41a)$$

$$B_n(p) := \ln(1-p) + \sum_{k=1}^{n}\frac{p^k}{k}. \quad (41b)$$

Owing to $\lim_{n\to\infty} np^{n+1} = 0$ for all $p \in (0, 1)$, it follows easily from (40) that assumption (5) holds true if and only if

$$\lim_{n\to\infty} nB_n(p) = 0. \quad (42)$$

To verify (42), it is worth noting that $B_n(p)$ defined as (41b) is exactly equal to the Lagrange remainder of order n (usually denoted by $R_n(.)$) for the Maclaurin series in equation (36). Using the Lagrange remainder formula[9] applied for the function $f(x) = \ln(1+x)$ at $x = -p$, for each n, we then attain

$$\begin{aligned}
B_n(p) &= \frac{(-1)^n(-p)^{n+1}}{(1+\xi_n)^{n+1}(n+1)} \\
&= \frac{-1}{n+1}\left(\frac{p}{1+\xi_n}\right)^{n+1}, \quad (43)
\end{aligned}$$

where ξ_n is some number (depending on n) between $-p$ and 0. Thus, owing to (43), limit (42) is equivalent to

$$\lim_{n\to\infty}\left(\frac{p}{1+\xi_n}\right)^{n+1}=0, \tag{44}$$

which evidently depends on the limit of $\frac{p}{1+\xi_n}$ as n tends to ∞. More specifically, noticing $0<1-p<1+\xi_n$ and setting $c:=\lim_{n\to\infty}\frac{p}{1+\xi_n}$, if $c\in[0,1)$ then (44) is true. If $c=1$, the right hand side of (44) has the indeterminate form 1^∞, and hence we haven't been able to draw an exact conclusion on (44).

Moreover, from the following estimate

$$0<\frac{p}{1+\xi_n}\le\frac{p}{1-p}\ \ (\forall n\in\mathbb{N}^*),$$

we easily achieve that (44) holds true for all $p\in(0,1/2)$. However, we haven't yet verified the validity of (44) (equivalently, that of (42)) in the case $p\in[1/2,1)$. We want to emphasize here that the claims of Lemma 3.2, Theorem 3.2 and Theorem 3.6 are no longer true if (44) does not hold.

Let $p\in(0,1/2)$. By virtue of Theorem 3.6, and from (38a), (38b), we get the characteristic function of $\tilde{X}$ given as

$$\varphi_{\tilde{X}}(t)=\frac{q\left((1-pe^{it})\ln(1-pe^{it})-e^{it}q\ln q\right)}{(\ln q+p)(1-e^{it})(1-pe^{it})}, \tag{45}$$

where $q:=1-p$. We haven't determined the probability distribution family corresponding to the characteristic function defined by (45).

Remark 3.7. By using L'Hospital's rule, we get that $\lim_{t\to0}\varphi_{\tilde{X}}(t)=0$ for all $p\in(0,1)$ (not only for $p\in(0,1/2)$), where $\varphi_{\tilde{X}}(t)$ is given as (45). This means that a basic property of characteristic functions (as presented in Section 2) is satisfied for all values of p. In addition, with the aid of MAPLE, we have checked by direct calculation that (42) (hence, so is assumption (5)) remains true for many values of p in $[0.5,1)$ (such as 0.5, 0.6, 0.65, 0.7, and up to $p=0.78$). Therefore, we can reasonably predict that if $X\sim\text{LogSeries}(p)$, Theorems 3.2 and 3.6 is then true for every $p\in(0,1)$. We have been trying to Prove this.

4. CONCLUSION

In the present study, we propose a novel transformation of probability mass functions associated with nonnegative interger-valued discrete random variables. We also demonstrate that our proposed transformation preserves some well-known families of distributions, such as Poisson distribution, Negative Binomial distribution and Hypergeometric distribution. In the future, we intend to extend our research in two directions. The first one is to continue determining the distribution of the resulting random variable ($\tilde{X}$) when the initial random variable (X) has another discrete distrbution, in addition to the distributions listed in Section 3. This work aims to further verify the distribution-preserving property of the transformation. Besides, we would like to discover its useful applications in various fields. The second direction, and the more difficult, is to construct an analogous transformation of probability density functions in the case of continuous random variables. One of the most important aims of probability theory is to find transformations which can preserve an initial probability distribution in some sense. Consequently, such transformations have attracted a great deal of attention.

Acknowledgment

This study is conducted within the framework of science and technology projects at institutional level of Quy Nhon University under the project code T2023.792.02.

REFERENCES

1. R. B. Ash. *Basic probability theory* (*2nd edition*), Dover, New York, 2008.
2. M. Evans, J. S. Rosenthal. *Probability and statistics: the science of uncertainty*, W. H. Freeman and Co., New York, 2010.
3. W. J. Stewart. *Probability, markov chains, queues, and simulation* (*1st edition*), Princeton University Press, New Jersey, 2009.
4. A. D. Gupta. *Fundamentals of probability: a first course*, Springer, New York, 2010.

5. R. P. Srivastava, T. J. Mock. *Belief functions in business decisions (studies in fuzziness and soft computing)*, Springer, Berlin Heidelberg, 2002.

6. N. L. Johnson, A. W. Kemp, S. Kotz. *Univariate discrete distributions* (*3rd edition*), Wiley, New Jersey, 2005.

7. N. G. Ushakov. *Selected topics in characteristic functions*, De Gruyter, Berlin, 2011.

8. Y. G. Sinai. *Probability theory: an introductory course*, Springer, Berlin Heidelberg, 1992.

9. D. Bock, D. Donovan, S. O. Hockett. *Barron's AP calculus* (*14th edition*), Barron's Educational Series, New York, 2017.

https://doi.org/10.52111/qnjs.2024.18307

TẠP CHÍ KHOA HỌC
TRƯỜNG ĐẠI HỌC QUY NHƠN

Nghiên cứu cường độ chống cắt không thoát nước của đất sét mềm khu dân cư Lò Vôi, phường 1, thành phố Tuy Hòa, tỉnh Phú Yên bằng thí nghiệm nén một trục nở hông và thí nghiệm cắt phẳng

Nguyễn Thị Khánh Ngân*

Khoa Kỹ thuật và Công nghệ, Trường Đại học Quy Nhơn, Việt Nam

Ngày nhận bài: 03/10/2023; Ngày sửa bài: 21/05/2024;
Ngày nhận đăng: 28/05/2024; Ngày xuất bản:28/06/2024

TÓM TẮT

Sức kháng cắt không thoát nước của đất sét yếu là thông số quan trọng để thiết kế nền đắp, móng nông và móng cọc. Sức kháng cắt không thoát nước của đất được xác định từ thí nghiệm trong phòng (ví dụ: nén ba trục, cắt đơn giản, nén mộ trục nở hông) và các thí nghiệm tại hiện trường (ví dụ: thí nghiệm CPT, thí nghiệm cắt cánh). Trong nghiên cứu này tác giả sử dụng mẫu đất sét nguyên dạng có đường kính 90 mm thu được tại khu dân cư Lò Vôi, phường 1, thành phố Tuy Hòa, tỉnh Phú Yên. Mục đích chính của nghiên cứu này là dùng thí nghiệm nén một trục nở hông và thí nghiệm cắt trực tiếp để khảo sát giá trị cường độ sức chống cắt của loại đất sét yếu phân bố phổ biến địa chất tại khu vực này. Sau đó, các giá trị cường độ cắt không thoát nước (S_u) từ thí nghiệm nén một trục nở hông được so sánh với các giá trị ứng suất cắt (τ) từ thí nghiệm cắt phẳng. Kết quả cho thấy sức chống cắt không thoát nước của mẫu thu được từ thí nghiệm nén một trục nở hông và thí nghiệm cắt trực tiếp đều có kết quả nhỏ hơn 25 kN/m^2 và phần trăm chênh lệch thu được cả hai phương pháp thí nghiệm này là khoảng 1.2%. Từ đó đánh giá được mẫu đất sét tại khu dân cư Lò Vôi, phường 1, thành phố Tuy Hòa, tỉnh Phú Yên là loại đất sét yếu và rất yếu. Vì vậy, khi xây dựng công trình trên nền đất sét này với bề dày phân bố tương đối lớn thì cần tiến hành xử lý đất yếu.

Keywords: *Đất sét yếu, sức kháng cắt không thoát nước, thí nghiệm nén một trục nở hông, thí nghiệm cắt trực tiếp.*

**Tác giả liên hệ chính.*
Email: nguyenthikhanhngan@qnu.edu.vn

QUY NHON UNIVERSITY
JOURNAL OF SCIENCE

Research of undrained shear strength of soft clay in the Lo Voi residential area, ward 1, Tuy Hoa city, Phu Yen province by unconfined compressive strength and direct simple shear test

Nguyen Thi Khanh Ngan*

Department of Engineering and Technology, Quy Nhon Univesity, Vietnam

Received: 03/10/2023; Revised: 21/05/2024;
Accepted: 28/05/2024; Published:28/06/2024

ABSTRACT

The undrained shear strength of soft clays is an important parameter for designing embankments, shallow foundations, and pile foundations. The undrained shear strength of soil is determined from laboratory tests (i.e., triaxial test, direct shear test, unconfined compressive test) and field tests (i.e., CPT tests, vane shear test). In this study, the author used intact clay samples with a 90 mm diameter collected in the Lo Voi residential area, ward 1, Tuy Hoa city, Phu Yen province. The main purpose of this study is to use the unconfined compressive test and direct shear test to investigate the shear strength value of samples. Then, the values of undrained shear strength (S_u) from the unconfined compressive strength test were compared with the values of shear stress (τ) from the simple shear test. The results show that the undrained shear strength of the samples obtained from the unconfined compressive test and the direct shear test are both less than 25 kN/m^2 and the percentage difference is obtained from both testing methods about 1.2%. The soft clays in the survey area are classified as soft and very soft. Therefore, buildings are built on this clay foundation with a relatively large distribution thickness, so it is necessary to treat the soft soil.

Keywords: *Soft clays, undrained shear strength, unconfined compressive strength, direct simple shear tests.*

1. INTRODUCTION

In recent years, the Central Coast region has been considered one of the regions with a relatively strong tourism economic development rate, especially Phu Yen province where dense population, political, economic, and cultural centers gather. Therefore, localities are making efforts to renovate and upgrade transport infrastructure, connecting road systems, railways, airways, houses, offices, apartments, etc. However, the geological characteristics of this area are quite complex and quite new. In this geological area, there is almost a young sedimentary soft layer, which is widely and deeply distributed along the coastal route extending to Binh Dinh province. This greatly affects work such as geological surveys, underground design, and underground construction methods. Most geological engineers of laboratories in the region encounter many difficulties in conducting

**Corresponding author.*
Email:nguyenthikhanhngan@qnu.edu.vn

https://doi.org/10.52111/qnjs.2024.18308

sampling and laboratory testing to determine physical and mechanical criteria, deformation characteristics, and shear strength of soft clays.[1,2]

This paper presents a full geotechnical characterization, and engineering properties of the soft site in the Lo Voi residential area, ward 1, Tuy Hoa city, Phu Yen province, which is located in north Phu Yen province as can be seen in Figure 1.

The scope of the topographic survey in the expected survey area is as follows: The North borders vacant land and current residential status; the South borders Tran Quang Khai street and Ong Chu bridge; the East borders Nguyen Tat Thanh street; the West borders Chua river.

Lo Voi residential area project is a synchronous technical infrastructure construction project including a western landslide prevention embankment, leveling the ground, road system, rainwater drainage system, sewerage system, plumbing system and fire protection system, power supply and lighting system.

The construction engineer used the undrained shear strength to calculate the bearing capacity of the foundation, the thickness of the embankment layer, and the embankment stages in the basic design phase of leveling work for the project. Therefore, the undrained shear strength of the soft clays was determined by laboratory tests (e.g., triaxial test, direct shear test, unconfined compressive test).

Figure 1. Map of Lo Voi residential area, ward 1, Tuy Hoa city, Phu Yen province.

2. METHODOLOGY

2.1. Unconfined compressive test (ASTM D2166)

This test method covers the determination of the unconfined compressive strength of cohesive soil in the undisturbed, remolded, or compacted condition, using strain-controlled application of the axial load.[1,2]

In this test method, unconfined compressive strength (q_u) is taken as the maximum load attained per unit area or the load per unit area at 15 % axial strain, whichever is secured first during the performance of a test. Shear strength (s_u) - for unconfined compressive strength test specimens, the shear strength is calculated to be

1⁄2 of the compressive stress at failure[2,3] and is expressed as[1]

$$S_u = \frac{q_u}{2} (1)$$

Where s_u is Shear strength and q_u is the compressive stress at failure.

In this study, the compression device used the Triplex II advanced as Figure 2.

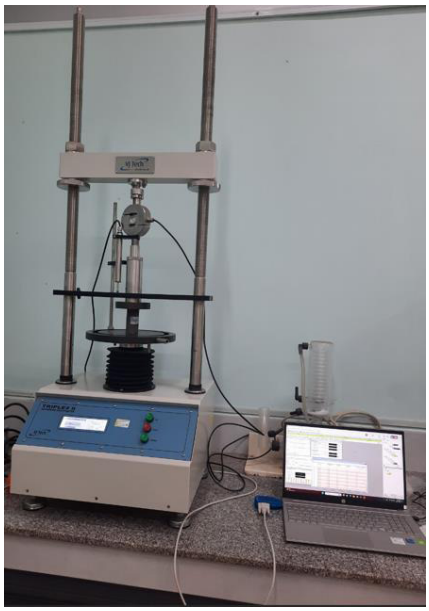

Figure 2. The Triplex II advanced.

2.2. The direct simple shear test

The direct simple shear test which is an experiment in geotechnical engineering determines the shear strength of clays. In this test, the shear strength is evaluated using the Mohr-Coulomb failure criteria and is given by $s = c + \sigma \tan(\varphi)$ (2)

Where c is cohesion, σ is the normal stress, and ϕ is the angle of internal friction of the soil.[1]

In this theory, failure along a plane in a material occurs by a critical combination of normal and shear stresses. Consider the stress at points a, b, and c as shown in Figure 3. The shear failure along that plane will not appear as point A but it occurs if the stresses plot as point B. The stress plotting as point C cannot exist because a shear failure had happened before this condition was reached.

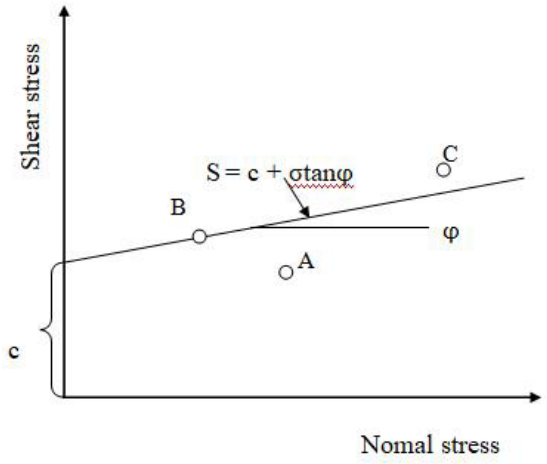

Figure 3. The failure criteria of Mohr-Coulomb.

The shear device uses strain controlled direct shear apparatus (two speed) which is made in China as illustrated in Figure 4. The product parameters of the equipment are stated in the Table 1.

Table 1. The product parameters of the strain controlled direct shear apparatus (two speed).

Vertical load	400kPa, 300kPa, 200kPa, 100kPa, 50kPa, 25kPa
Horizontal load	1.2kN
Lever ratio	1:12
Specimen size	30cm^2
Power supply	220VAC 50Hz

Figure 4. The two-speed soil shearing machine.

The experimental method is based on standard TCVN 4199:2012.[1,2]

https://doi.org/10.52111/qnjs.2024.18308

2.3. Test specimens

Testing was conducted on six reconstituted clay specimens with high plasticity. Onsoy clay samples were retrieved from a depth of 2-6 m in a test pit in Lo Voi residential area, ward 1, Tuy Hoa city, Phu Yen province. The samples in the unconfined compressive test were 48 mm in diameter and 70 mm in height. The samples in the direct simple shear test were 60 mm in diameter and 20 mm in height.[4,5] The characterizations of the soft clay samples are listed in Table 1 and the results of geotechnical characterization are plotted in Table 2 and Table 3.

Table 2. The Specifications of the specimens.

Sample	Deep (m)	Described test sample	Test	Diameter (cm)	Height (cm)
1	1.8-2	Soft, gray, sandy lean clay, low plasticity.	Unconfined compressive test (ASTM D2166)	48	76
2	3.8-4	Soft, gray, lean clay, high plasticity, Pasty state.	Unconfined compressive test (ASTM D2166)	48	76
3	5.8-6	Soft, gray, lean clay, high plasticity, Pasty state.	Unconfined compressive test (ASTM D2166)	48	76
4	1.8-2	Soft, gray, sandy lean clay, low plasticity.	Direct simple shear test (TCVN 8868:2011)	60	20
5	3.8-4	Soft, gray, lean clay, high plasticity, Pasty state.	Direct simple shear test (TCVN 8868:2011)	60	20
6	5.8-6	Soft, gray, lean clay, high plasticity, Pasty state.	Direct simple shear test (TCVN 8868:2011)	60	20

Table 3. Geotechnical characterization of soft clays in Lo Voi residential area, ward 1, Tuy Hoa city, Phu Yen province.

Simple	Deep	γ	γ_d	w	w_L	w_P	I_P	I_L	e_0
	m	kN/m^3	kN/m^3	%	%	%			
1	1.8-2	16.09	9.81	63.98	60.6	28.5	32.1	1.11	1.696
2	3.8-4	16.1	9.6	68	54.3	33.6	20.7	1.67	1.828
3	5.8-6	17.2	11.1	54.63	55.1	34.1	21	0.98	1.445

3. RESULTS AND DISCUSSION

The samples in the direct shear test had an unequal distribution of stress over the shear surface. Because the impact load on the sample is the axial load but the shear failure plane is cut in the horizontal direction. This result is partly due to the equipment's unstable load increase speed. This type of stress distribution results in progressive failure. The failure plane predetermined by the shear box of the testing equipment as shown in Figure 5.[1,4-6]

In this unconfined compressive test, axial stress on the specimen is gradually increased until the specimen fails. The shear stress is distributed over the specimens. The failure plane appeared with a random tilt angle from the center to the outer edge of the specimen as shown in Figure 6. This means pure shear only exists at the center of the specimen.

The values of undrained shear strength of soft clays in the Lo Voi residential area, ward 1, Tuy Hoa city, Phu Yen province from the

unconfined compressive test are smaller than the direct simple shear test. The value difference ranges from 1.19% to 1.2%.

As can be seen in Figure 5, the value of the undrained shear strength from the unconfined compression test varies from 4.6 kN/m^2 to 20.45 kN/m^2 and the value of the undrained shear strength from the direct shear test varies from 5.5 kN/m^2 to 24.3 kN/m^2 as shown in Figure 5.

The shear strength of soft clays increases gradually with depth in the same soil layer as shown in Figure 6. [1,6-7]

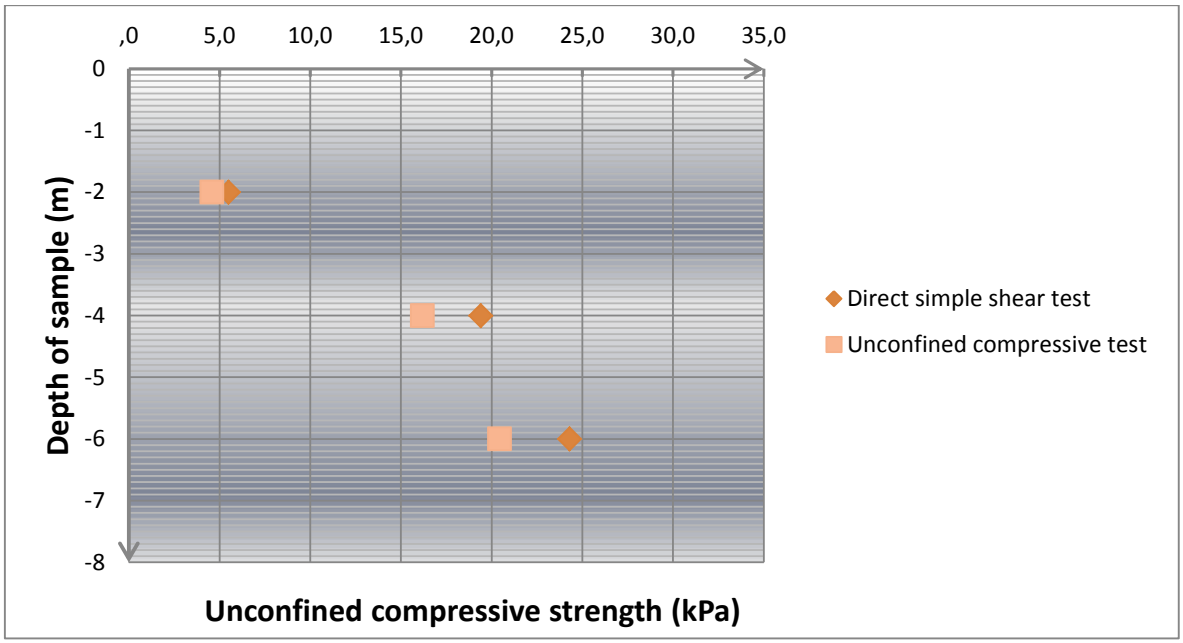

Figure 5. The values of undrained shear strength of soft clays in Lo Voi residential area, ward 1, Tuy Hoa city, Phu Yen province from unconfined compressive test and direct simple test.

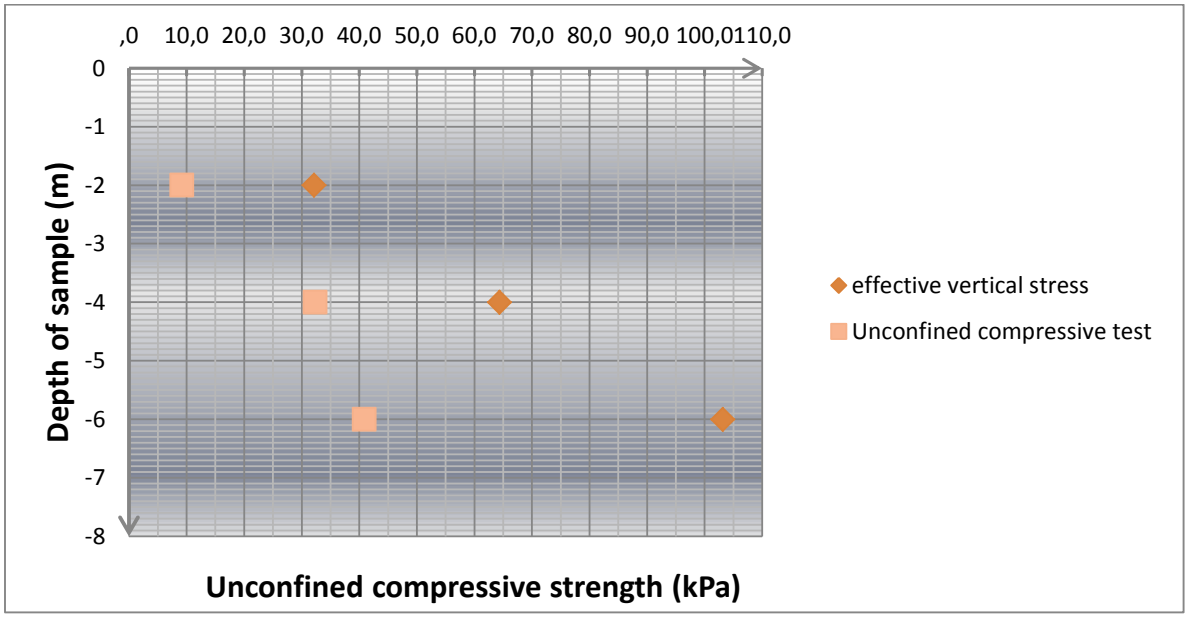

Figure 6. The values of undrained shear strength of soft clays in Lo Voi residential area, ward 1, Tuy Hoa city, Phu Yen province from unconfined compressive test and effective vertical stress of soil.

https://doi.org/10.52111/qnjs.2024.18308

4. CONCLUSIONS

In conclusion, the undrained shear strengths of 123 soft clay samples were determined from three method tests inclusion: triaxial test (UU), direct shear test, and vane shear test. These values were given results of less than 20 kN/m^2.

In this study, the value of the unconfined compression strength q_u of very soft clays and soft clays with similar characteristics as in the study ranges from 20.45 kN/m^2 to 24.3 kN/m^2 for both the unconfined compressive test and direct shear test.

In addition, the undrained shear strengths of clay samples at depths from 2 m to 5 m were determined from the triaxial test (UU), and a value is given of 15.3 kN/m^2.

The undrained shear strength of soft clay was determined by the unconfined compression test shows that it is more suitable for the actual working conditions of the ground than the direct shear test and gives approximately to the published results before.

Designers should use the unconfined compression test instead of the direct simple shear test to determine the undrained shear strength of soft clays for large projects.

However, actual experiments show that the accuracy of the results test depends largely on the level of damage to the soil sample due to the process of sampling, transporting, preserving, and cutting the sample. In particular, for very soft clays, laboratory testing is not always convenient because it is not possible to get intact samples.

Acknowledgment

This research is conducted within the framework of science and technology projects at institutional level of Quy Nhon University under the project code T2023.803.13.

REFERENCES

1. B. M. Das. *Advanced soil mechanics (5th edition),* Taylor & Francis Group, London New York, 2019.
2. A. S. Gundersen, R. C. Hansen, T. Lunne, J. S. L'Heureu, S. O. Strandvik. Characterization and engineering properties of the NGTS Onsoy soft clay site, *AIMS Geosciences*, **2019**, *5*(3), 665-703.
3. T. Tsuchida. Evaluation of undrained shear strength of soft clay with consideration of sample quality, *Soils and Foundations*, **2000**, *40*(3), 29-42.
4. R. Larsson. *Basic behavior of Scandinavian soft clays*, *Rapport No 4*, Swedish Geotekniska Instiut, Linkoping, 1977.
5. N. T. P. Khue. Some results of unconfined compressive strength testing of soil by trixial compression equipment, *The University of Danang Journal of Science and Technology*, **2020**, *18*(1), 17-22.
6. B. Huang, S. Cai, J. Li, K. Wu, W. Yang. Undrained strength of clay determined from simple shear test, *Frontiers in Earth Science*, **2023**, 1-13.
7. N. T. N. Yen, N. T. P. Khue. Characteristics of deformation - consolidation and shear strength of some types of clay soil distributed in Da Nang city, *The University of Danang Journal of Science and Technology,* **2016**, *7*(104), 67-71.

TẠP CHÍ KHOA HỌC
TRƯỜNG ĐẠI HỌC QUY NHƠN

Tìm nghiệm liouville của phương trình vi phân đại số cấp một bằng phép đổi biến

Nguyễn Trí Đạt*

Khoa Cơ bản, Trường Đại học Giao thông vận tải Thành phố Hồ Chí Minh, Việt Nam

Ngày nhận bài: 31/03/2024; Ngày sửa bài: 26/05/2024
Ngày nhận đăng: 28/05/2024; Ngày xuất bản: 28/06/2024

TÓM TẮT

Chúng tôi trình bày một phương pháp tìm nghiệm liouville của phương trình vi phân đại số cấp một bằng phép đổi biến. Cụ thể, một phương trình vi phân đại số cấp một với hệ số thuộc vào một mở rộng liouville được biến đổi thành một phương trình vi phân với hệ số thuộc vào trường vi phân hữu tỷ bằng phép đổi biến trên trường cơ sở. Thêm nữa, sử dụng phép đổi biến giữa các hàm số, phương trình vi phân đại số cấp một với hệ số trên trường vi phân hữu tỷ có thể được biến đổi về dạng phương trình đơn giản hơn phù hợp với các thuật toán đã biết. Một số ví dụ được trình bày để minh họa phương pháp đã đưa ra.

Từ khóa: *Phương trình vi phân đại số, nghiệm liouville, phép đổi biến.*

**Tác giả liên hệ chính.*
Email: tridat.nguyen@ut.edu.vn

QUY NHON UNIVERSITY
JOURNAL OF SCIENCE

Finding liouvillian solutions of first-order algebraic ordinary differential equations by change of variables

Nguyen Tri Dat*

Faculty of Basic Science, Ho Chi Minh City University of Transport, Vietnam

Received: 31/03/2024; Revised: 26/05/2024
Accepted: 28/05/2024; Published: 28/06/2024

ABSTRACT

We present an approach for finding liouvillian solutions of first-order algebraic ordinary differential equations (AODEs) by means of change of variables. In particular, a first-order AODE with liouvillian coefficients can be transformed into an AODE over rational fields by the change of indeterminate over the ground fields. In addition, by the change of functions, the last AODE can be converted into the one which is suitable for known algorithms. Some examples are given to illustrate the method.

Keywords: *Algebraic ordinary differential equation, liouvillian solution, change of variables.*

1. INTRODUCTION

The ideas of using geometric properties which satisfy the differential constraint into the problem of solving differential equations are well-known. There are notable works for finding rational general solutions which are based on rational parametrizations of algebraic curves of genus zero.[1–3] Recently, by this technical method, we have presented an algorithm for determining liouvillian solutions of first-order AODEs of genus zero.

In this paper, we give an approach for solving first-order AODEs which is based on the change of variables. This continues the ideas considered in the previous works.[◇,4–5] In more details, we aim to transform certain first-order AODEs into sub-types with respect to the two cases of change of variables, that are the change of the functions and the change of the indeterminate over the ground fields. From these considerations, first-order AODEs with liouvillian coefficients can be converted into the AODEs over $\mathbb{C}(z)$ (Section 4). Moreover, such an AODE over $\mathbb{C}(z)$ can be transformed into an autonomous AODE or a rational one (Section 3) where known algorithms can be applied.[6–7]

2. PRELIMINARIES

We present some necessary definitions which are well known in literature.[8–10]

Definition 2.1. Let k be an algebraic field of characteristic zero. A *derivation* of the field k, denote by $'$, is an operation of k such that $\forall a, b \in k$, the followings hold.

$$(a+b)' = a' + b', \qquad (ab)' = a'b + ab'.$$

A field k equipped with a derivation $'$ is called a *differential field*. An element $a \in k$ is called a *constant* if $a' = 0$. A field extension E of k is called a *differential field extension* of k if and only if the derivation of E restricted to k coincides with the derivation of k.

Definition 2.2. Let E be a differential field extension of k and let $'$ denote the derivation on E. $t \in E$ is called *primitive* over k if $t' \in k$. $t \in E \setminus 0$ is called *hyperexponential* over k if $t'/t \in k$. $t \in E$ is called *liouvillian* over k if t is either algebraic, or primitive or hyperexponential over k. E is a *liouvillian extension* of k if $E = k(t_1, t_2, \ldots, t_n)$, and there is a tower of differential fields $k = k_0 \subseteq k_1 \subseteq \cdots \subseteq k_n = E$ such that for each $i \in \{1, \ldots, n\}$, $k_i = k_{i-1}(t_i)$ and t_i is liouvillian over k_{i-1}.

**Corresponding author.*
Email: tridat.nguyen@ut.edu.vn

https://doi.org/10.52111/qnjs.2024.18309

Definition 2.3. Let $F(y,w) \in k[y,w]$ be an irreducible polynomial in two variables and K be the algebraic closure of k. Then we define an *affine algebraic curve* over k by the set

$$\mathbb{L} := \left\{(a,b) \in \mathbb{A}^2(K) \mid F(a,b) = 0\right\}.$$

The polynomial $F(y,w)$ is called the *defining polynomial* of $\mathbb{L}$. We may write $F(y,w) = 0$ to indicate an algebraic curve $\mathbb{L}$.

Definition 2.4. Let k be a differential field with a derivation $'$ and let $F \in k[y,w]$. A first-order algebraic ordinary differential equation (AODE) is a differential equation of the form

$$F(Y,Y') = 0. \tag{1}$$

Then, the equation $F(y,w) = 0$ is called the *corresponding algebraic curve* of the first-order AODE (1).

By abuse of notations, when we refer to an AODE (1), we mean $k = \mathbb{C}(z)$ with $' = \dfrac{d}{dz}$ whose field of constants is $\mathbb{C}$ and $z' = 1$.

Definition 2.5. ξ is called a solution of the AODE (1) if $F(\xi,\xi') = 0$. If such ξ belongs to a liouvillian extension E of k then we call it a *liouvillian solution*. A solution ξ is called a *liouvillian general solution* if it does not vanish the separant $S_F = \dfrac{\partial F}{\partial Y'}$.

Remark 2.1. A general solution ξ defined by the way in Definition 2.5 first introduced in the work by Hubert,[11] and it is tantamount to the classical one defined in the book of Ritt.[8] Moreover, ξ is called a *singular solution* if it fails to annul S_F. It is well known that an AODE (1) has only finite singular solutions, hence, the paper's method is only applicable for finding liouvillian general solutions since it generates infinitely many solutions.

3. THE CHANGE OF VARIABLES $u = \psi(Y)$

We show how a geometric transformation induces a differential one. Let

$$G(u,u') = 0 \tag{2}$$

be a first-order AODE and $G(u,v) = 0$ be its algebraic corresponding curve over $\mathbb{C}(z)$. As above, let $F(y,w) = 0$ be the corresponding algebraic curve of the AODE (1). Assume that there is a transformation of the form

$$u = \psi(y,w), v = \gamma(y,w) \tag{3}$$

such that

$$G(u,v) = G(\psi(y,w),\gamma(y,w)) = F(y,w) = 0.$$

Then the transformation (3) induces a differential transformation between such two AODEs

$$u = \psi(Y,Y'), u' = \gamma(Y,Y') = \psi'(Y,Y'). \tag{4}$$

Lemma 3.1. *The transformation* (4) *must be of the form*

$$u = \psi(Y), u' = \psi'(Y). \tag{5}$$

Proof. In fact, if the first component of the transformation (4) contains the term Y' then the second component must include Y'' which is a contradiction if we compare with (3). □

Remark 3.1. The transformation (5) is based on the change $u = \psi(Y)$ and it can be started with any rational function $\psi(Y) \in \mathbb{C}(Y)$. However, just simple cases are considered in practical application. Recently, the change of variables $u = Y^n$ has been studied in the work by Dat and Chau. This consideration induces the one called a *power transformation*. Such a transformation may lead to a change of the genus of algebraic curves, by that, it can be applied for solving first-order AODEs whose genera are positive.

In the rest of this section, we consider a transformation induced by a rational function u of the form

$$u = M(Y) = \frac{\alpha Y + \beta}{\gamma Y + \delta},$$

where $\alpha,\beta,\gamma,\delta \in \overline{\mathbb{C}(z)}$, $\alpha\delta - \beta\gamma \neq 0$. A *Möbius transformation* is a transformation of the form

$$u = \frac{\alpha Y + \beta}{\gamma Y + \delta}, u' = \left(\frac{\alpha Y + \beta}{\gamma Y + \delta}\right)'. \tag{6}$$

The inverse substitution of (6) is

$$Y = \frac{\delta u - \beta}{-\gamma u + \alpha}, Y' = \left(\frac{\delta u - \beta}{-\gamma u + \alpha}\right)'. \tag{7}$$

In this part, we follow the work by Ngo and Ha for the details of Möbius transformations.[4] They have been studied for finding algebraic and rational solutions.[4,12] Hence, there is no

need to elaborate about them. Our contribution is to show that Möbius transformations are also applicable for determining liouvillian solutions. First, there is an expression for u'

$$\begin{aligned}\frac{\partial M(Y)}{\partial Y} =&\frac{\alpha\delta-\beta\gamma}{(\gamma Y+\delta)^2},\\ \frac{\partial M(Y)}{\partial z} =&\frac{(\alpha'\gamma-\gamma'\alpha)Y^2++\beta'\delta-\delta'\beta}{(\gamma Y+\delta)^2}\\ &+\frac{(\alpha'\delta-\alpha\delta'+\beta'\gamma-\gamma'\beta)Y}{(\gamma Y+\delta)^2},\end{aligned} \tag{8}$$

$$\begin{aligned}u'=\frac{du}{dz} =&\frac{d(M(Y))}{dz}\\ =&\frac{\partial M(Y)}{\partial Y}Y'+\frac{\partial M(Y)}{\partial z}.\end{aligned}$$

Definition 3.1. Let

$$F(Y,Y')=\sum a_{ij}Y^iY'^j$$

be an irreducible polynomial over $\mathbb{C}(z)$. Then we define the *differential total degree* of F by

$$\mu(F)=\max\{i+2j \mid 0\neq a_{ij}\in\mathbb{C}(z)\}.$$

Putting (6) into an AODE (2) and using (8), we obtain

$$\begin{aligned}G(u,u') =&G\left(\frac{\alpha Y+\beta}{\gamma Y+\delta},\left(\frac{\alpha Y+\beta}{\gamma Y+\delta}\right)'\right)\\ =&\left(\frac{\alpha\delta-\beta\gamma}{\gamma Y+\delta}\right)^{\mu(G)}F(Y,Y')=0.\end{aligned} \tag{9}$$

In the reverse, from the formulas (7) and (9), we have

$$\begin{aligned}&(\alpha-\gamma u)^{\mu(F)}F\left(\frac{\delta u-\beta}{-\gamma u+\alpha},\left(\frac{\delta u-\beta}{-\gamma u+\alpha}\right)'\right)\\ &=G(u,u')=0.\end{aligned} \tag{10}$$

Moreover, in (9) and (10), $\mu(G)=\mu(F)$.[5]

Definition 3.2. Let $F(Y,Y')=0$ (1) and $G(u,u')=0$ (2) be two first-order AODEs. We say F is *equivalent* to G if there is a Möbius transformation (6) such that the formula (10) is satisfied.

Möbius transformations preserve the genus among the corresponding algebraic curves since they are birational. Moreover, They give an equivalence relation among first-order AODEs and preserve the property of having algebraic solutions of the equivalence class.[4] Next, we will prove that Möbius transformations also preserve the property of having a liouvillian solution of the equivalence class.

Theorem 3.1. *Assume that F is equivalent to G. Then F has a liouvillian solution if and only if so does G. In the affirmative case, the correspondence of such solution is one to one.*

Proof. The case of having an algebraic general solution has been proved by Theorem 2.2.[4] From formula (10) and since

$$(-c\xi+a)^{\mu(F)}\neq 0,$$

we find that an AODE $G=0$ has a liouvillian transcendental solution ξ if and only if

$$M^{-1}(\xi)=\frac{\delta\xi-\beta}{-\gamma\xi+\alpha}$$

is a transcendental solution $F=0$. Finally, by formula (6), the correspondence of liouvillian solutions between F and G is one to one. □

Möbius transformation is used to check whether a first-order AODE is equivalent to an autonomous one.[4] If this is the case, then there is an algorithm for finding an algebraic general solution.[7] From that, an algebraic solution of the original AODE can be returned. Based on Theorem 3.1, we aim to apply Möbius transformations for determining liouvillian solutions. The following example, see Section 3, illustrates our idea.

Example 3.1. Consider first-order AODE

$$\begin{aligned}F(Y,Y') =&-z^3Y^3+z^2Y'^2-2z^2Y^2\\ &+2zYY'-zY+Y^2=0.\end{aligned} \tag{11}$$

Putting $Y=\dfrac{u-1}{z}$ into the AODE (11) and using formula (10), we obtain

$$\begin{aligned}&z^4F\left(\frac{u-1}{z},(\frac{u-1}{z})'\right)=\\ &G(u,u')=u'^2-u^3+u^2=0.\end{aligned} \tag{12}$$

By Algorithm 4.1,[6] a liouvillian solution of the AODE (12) is

$$(\exp i(z+c)+1)^2u-2\exp i(z+c)=0,\quad i^2=-1.$$

Therefore, a liouvillian general solution of the AODE (11) is

$$(\exp i(z+c)+1)^2(zY+1)-2\exp i(z+c)=0.$$

https://doi.org/10.52111/qnjs.2024.18309

4. THE CHANGE OF VARIABLES $z = \varphi(x)$

This section studies some cases of differential transformations induced by change of variables over the ground fields. Let $k = \mathbb{C}(x)$ with $' = \dfrac{d}{dx}$ and let E be a liouvillian extension of k. Consider the differential equation

$$\tilde{F}(y, y') = 0, \tag{13}$$

where y is a function of x and $\tilde{F} \in E[y, w]$, i.e. a first-order AODE with the coefficients in a liouvillian extension E of $\mathbb{C}(x)$. For briefly, we call it an AODE with *liouvillian coefficients* (see Definition 2.4).

The issue of considering a differential equation with coefficients in an extension field is quite naturally. A general investigation for determining liouvillian solutions of a linear differential equation with liouvillian coefficients can be found in Singer.[13] In this section, our purpose is to consider some simple cases which convert an AODE (13) into an AODE (1) by means of change of variables $z = \varphi(x)$.

Definition 4.1. (Definition 2.7)[14] Let E be a liouvillian extension over $\mathbb{C}(x)$ and $z \in E \setminus \mathbb{C}$, then z is called a *rational liouvillian element* over $\mathbb{C}$ if $\dfrac{dz}{dx} \in \mathbb{C}(z)$.

Example 4.1. The element $z = \sqrt{x} + \sqrt{x+1}$ is a rational liouvillian element over $\mathbb{C}$ since z is algebraic over $\mathbb{C}(x)$ and

$$\frac{dz}{dx} = \frac{1}{2\sqrt{x}} + \frac{1}{2\sqrt{x+1}} \in \mathbb{C}(\sqrt{x} + \sqrt{x+1}).$$

Since Algorithm 1 is independent of the particular form of the indeterminate z, then z can be seen as a rational liouvillian element over $\mathbb{C}$. Hence, this algorithm can be extended to the case of solving first-order AODEs (13) by a change of variable. Assume that there is a change of variable

$$z = \varphi(x), \tag{14}$$

such that it turns an AODE (13) into (1), i.e.

$$\tilde{F}(y, y') = F(Y, Y') = 0.$$

If this occurs and $Y(z)$ is a liouvillian solution of the AODE (1), then

$$y(x) = Y \circ \varphi(x)$$

is a liouvillian solution of the AODE (13).

Remark 4.1. We remind the two differential fields $\left(\mathbb{C}(z), \dfrac{d}{dz}\right)$ and $\left(\mathbb{C}(x), \dfrac{d}{dx}\right)$ with their derivatives y' and Y' whose defined as follows

$$y' = \frac{dy}{dx}, \; Y' = \frac{dY}{dz}.$$

By the chain rule, a relation between y' and Y' is expressed as

$$y' = \frac{dy}{dx} = \frac{d(Y \circ \varphi)}{dx} = \frac{dY}{d\varphi}\frac{d\varphi}{dx} = \frac{dY}{dz}\frac{dz}{dx} = Y'\frac{dz}{dx}.$$

The above expression may be applied to detect a candidate change of variables (14).

4.1. The AODEs with transcendental coefficients

In the case of transcendental coefficients, we refer the readers to some standard works for reference.[9,13] Unfortunately, there is no a full algorithm to find the change of variable for this case, and we are going to deal with it in the future. Here, we just present some examples to illustrate the change of variables (14) in the affirmative cases.

Example 4.2. (I·463)[15] Consider first-order AODE

$$yy'^2 - \exp(2x) = 0. \tag{15}$$

The coefficients of the AODE (15) are in $\mathbb{C}(\exp x)$. By setting $z = \varphi(x) = \exp x$, then (15) is converted into an AODE (1)

$$z^2(YY'^2 - 1) = 0.$$

After dividing z^2, we obtain an autonomous AODE (I·462)[15]

$$YY'^2 - 1 = 0, \tag{16}$$

which has a liouvillian general solution

$$Y = \sqrt[3]{\frac{9}{4}(z+c)^2}.$$

Therefore, a liouvillian general solution of the AODE (15) is

$$y = Y \circ \varphi = \sqrt[3]{\frac{9}{4}(\exp x + c)^2}.$$

https://doi.org/10.52111/qnjs.2024.18309

Example 4.3. (I·387)[15] Consider first-order AODE

$$y'^2 + (y' - y)\exp x = 0. \tag{17}$$

By setting $z = \varphi(x) = \exp x$, the AODE (17) is converted into an AODE

$$Y'^2 z^2 + Y' z^2 - Yz = 0 \tag{18}$$

which has a proper parametrization

$$\mathcal{P}(t) = (t^2 z + tz, t).$$

By using Algorithm 1, the associated ODE respect to $\mathcal{P}(t)$ is

$$t' = -\frac{t^2}{z(2t+1)}$$

which has only a general solution ensured by Risch,[16]

$$\ln(t^2 z) - \frac{1}{t} = c.$$

Due to the work by Rosenlicht,[17] this solution is not liouvillian. Therefore, the AODE (17) has no liouvillian general solution.

4.2. The AODEs with radical coefficients

In the case of solving an AODE with radical coefficients, Algorithm 3.5 by Caravantes et al. can be relied.[5] Assume that there is a change of variables

$$x = r(z) \in \mathbb{C}(z),$$

then it leads to the existence of the inverse substitution (14)

$$z = \varphi(x).$$

Since z is algebraic over $\mathbb{C}(x)$ and

$$\frac{dz}{dx} = (\frac{dr}{dz})^{-1} \in \mathbb{C}(z),$$

then z is a rational liouvillian element over $\mathbb{C}$. The following example illustrates the ideas.

Example 4.4. Consider the first-order AODE

$$\begin{aligned}\tilde{F}(y, y') = &- x\sqrt{x}y^3 + 4x^2 y'^2 - 2xy^2 \\ &+ 4xyy' - \sqrt{x}y + y^2 = 0\end{aligned} \tag{19}$$

By Algorithm 3.5,[5] there is a change of variables $z = \varphi(x) = \sqrt{x}$, which transforms the AODE (19) into (11)

$$\begin{aligned}F(Y, Y') = &- z^3 Y^3 + z^2 Y'^2 - 2z^2 Y^2 \\ &+ 2zYY' - zY + Y^2 = 0.\end{aligned}$$

From Example 3.1, then (19) has a liouvillian general solution

$$\begin{aligned}&(\exp i(\sqrt{x} + c) + 1)^2(\sqrt{x}y + 1) \\ &\quad -2\exp i(\sqrt{x} + c) = 0.\end{aligned}$$

Remark 4.2. There are more examples of transforming first-order AODEs with radical coefficients into the AODEs (1).[5] Since all of the AODEs (1) obtained here are of genus zero, then they are suitable for Algorithm 1.

5. CONCLUSION

In this paper, we have investigated some ways to convert a first-order AODE into the one where known-algorithms exist. In details, first-order AODEs with liouvillian coefficients can be transformed into first-order AODEs (1) in Section 4. Moreover, an AODE (1) may be converted into an autonomous one by Möbius transformation in Section 3. In addition, if the AODEs (1) are of positive genera, the power transformations (respect to $u = Y^n$) may be considered. A full algorithm for determining liouvillian solutions of first-order AODEs will challenge us in the future.

Acknowledgment

This research is conducted with in the frame work of science an technology projects at institutional level of Ho Chi Minh City University of Transport under the project code KH2307.

REFERENCES

1. R. Feng, X. S. Gao. *Rational general solutions of algebraic ordinary differential equations,* Proceedings of the 2004 International Symposium on Symbolic and Algebraic Computation, Santander, 2004.
2. L. X. C. Ngo, F. Winkler. Rational general solutions of first order non-autonomous parametrizable odes, *Journal of Symbolic Computation*, **2010**, *45*, 1426–1441.

https://doi.org/10.52111/qnjs.2024.18309

3. N. T. Vo, G. Grasegger, F. Winkler. Deciding the existence of rational general solutions for first-order algebraic odes, *Journal of Symbolic Computation*, **2018**, *87*, 127–139.

4. L. X. C. Ngo, T. T. Ha. Möbius transformations on algebraic odes of order one and algebraic general solutions of the autonomous equivalence classes, *Journal of Computational and Applied Mathematics*, **2020**, *380*, 112999.

5. J. Caravantes, J. R. Sendra, D. Sevilla, C. Villarino. Transforming ODEs and PDEs from radical coefficients to rational coefficients, *Mediterranean Journal of Mathematics*, **2021**, *18*, 96.

6. T. D. Nguyen, L. X. C. Ngo. Liouvillian solutions of algebraic ordinary differential equations of order one of genus zero, *Journal of Systems Science and Complexity*, **2023**, *36*(2), 884–893.

7. J. M. Aroca, J. Cano, R. Feng, X. S. Gao. *Algebraic general solutions of algebraic ordinary differential equations*, Proceedings of the 2005 International Symposium on Symbolic and Algebraic Computation, Beijing, 2005.

8. J. F. Ritt. *Differential algebra*, American Mathematical Society, 1950.

9. M. Bronstein. *Symbolic integration I: transcendental functions, algorithms and computation in mathematics (2nd edition)*, Springer-Verlag, Berlin Heidelberg, 2004.

10. J. R. Sendra, F. Winkler, S. P. Díaz. *Rational algebraic curves - a computer algebra approach*, Springer-Verlag, Berlin Heidelberg, 2008.

11. E. Hubert. *The general solution of an ordinary differential equation*, Proceedings of the 1996 International Symposium on Symbolic and Algebraic Computation, Zurich, 1996.

12. L. X. C. Ngo, J. R. Sendra, F. Winkler. Birational transformations preserving rational solutions of algebraic ordinary differential equations, *Journal of Computational and Applied Mathematics*, **2015**, *286*, 114–127.

13. M. F. Singer. Liouvillian solutions of linear differential equations with liouvillian coefficients, *Journal of Symbolic Computation*, **1991**, *11*, 251–273.

14. T. D. Nguyen, L. X. C. Ngo. Rational liouvillian solutions of algebraic ordinary differential equations of order one, *Acta Mathematica Vietnamica*, **2021**, *46*(4), 689–700.

15. E. Kamke. *Differentialgleichungen: lösungsmethoden und lösungen I. gewöhnliche differentialgleichungen*, B. G. Teubner, Stuttgart, 1977.

16. R. H. Risch. The problem of integration in finite terms, *Transactions of the American Mathematical Society*, **1969**, *139*, 167–189.

17. M. Rosenlicht. On the explicit solvability of certain transcendental equations, *Publications Mathématiques de l'Institut des Hautes Scientifiques*, **1969**, *36*, 15–22.

https://doi.org/10.52111/qnjs.2024.18309

TẠP CHÍ KHOA HỌC
TRƯỜNG ĐẠI HỌC QUY NHƠN

Nghiên cứu đánh giá ảnh hưởng của các thông số kết cấu đến chất lượng phun nhiên liệu trên động cơ Diesel Kubota D1703-M-DI

Nguyễn Quốc Hoàng*, Dương Trọng Chung

Bộ môn Kỹ thuật ô tô, Trường Đại học Quy Nhơn, Việt Nam

Ngày nhận bài: 27/11/2023; Ngày sửa bài: 21/02/2024;
Ngày nhận đăng: 08/03/2024; Ngày xuất bản: 28/06/2024

TÓM TẮT

Trên cơ sở nghiên cứu lý thuyết quá trình cung cấp nhiên liệu, quá trình hình thành hỗn hợp trong động cơ Diesel, cơ sở lý thuyết tính toán trong phần mềm Hydsim, kết hợp với quá trình khảo sát, đo đạc và phân tích đặc điểm kết cấu hệ thống cung cấp nhiên liệu trên động cơ Diesel Kubota D1703-M-DI nhóm tác giả đã ứng dụng phần mềm Hydsim để mô phỏng quá trình cung cấp nhiên liệu động cơ Diesel Kubota D1703-M-DI với điều kiện mô phỏng ở tải định mức, tải trung bình, không tải và có sự thay đổi giá trị các thông số kết cấu: biên dạng cam, tỉ số D/h_1, đường kính lỗ phun, chiều dài lỗ phun, độ cứng lò xo vòi phun,... Dựa trên kết quả mô phỏng thu được, nhóm tác giả đã phân tích, đánh giá kết quả mô phỏng và đưa ra các kết luận liên quan về ảnh hưởng của các thông số kết cấu đến chất lượng phun nhiên liệu trên động cơ Diesel Kubota D1703-M-DI, từ đó đưa ra các đề xuất cải tiến về mặt thông số kết cấu phù hợp hơn. Việc làm này có ý nghĩa quan trọng trong việc giảm tiêu hao nhiên liệu, giảm tiếng ồn, giảm hàm lượng các chất ô nhiễm trong khí xả động cơ.

Từ khóa: *Mô phỏng, hệ thống cung cấp nhiên liệu động cơ Diesel, máy cày Kubota L3804VN, bơm cao áp tập trung, vòi phun cao áp.*

**Tác giả liên hệ chính.*
Email: nguyenquochoang@qnu.edu.vn

QUY NHON UNIVERSITY
JOURNAL OF SCIENCE

Research to evaluate the influence of structural parameters on fuel injection quality on Kubota D1703-M-DI Diesel engine

Nguyen Quoc Hoang*, Duong Trong Chung

Department of Automotive Engineering, Quy Nhon University, Vietnam.

Received: 27/11/2023; Revised: 21/02/2024;
Accepted: 08/03/2024; Published: 28/06/2024

ABSTRACT

Based on theoretical research of the fuel supply process, mixture formation process in Diesel engines, the theoretical basis of calculation in Hydsim software, combined with the process of surveying, measuring, and analyzing structural characteristics of the fuel supply system on the Kubota D1703-M-DI Diesel engine, the authors have applied Hydsim software to simulate the fuel supply process of the Kubota D1703-M-DI Diesel engine under simulated conditions at rated load, average load and no load and with changes in the values of structural parameters: cam profile, D/h_i ratio, nozzle diameter, nozzle length, nozzle spring stiffness spray, etc. Based on the simulation results obtained, the authors analyzed and evaluated the results and made relevant conclusions about the influence of structural parameters on the quality of fuel injection in the Kubota D1703-M-DI Diesel engine, thereby providing suggestions for more suitable structural parameters. This is important in reducing fuel consumption, noise, and the content of pollutants in engine exhaust.

Keywords: *Simulation, Diesel engine fuel supply system, Kubota L3804VN tractor, centralized high-pressure pump, high-pressure injector.*

1. INTRODUCTION

In the period of industrialization and modernization of the country, especially in the current mechanization of rural agriculture, internal combustion engines, in general, and Diesel engines, in particular, are indispensable. Diesel engines are widely used today, and they have advantages such as large capacity, high efficiency, and cheaper fuel costs than gasoline. In particular, small-sized Diesel engines, with a power range of 5 ÷ 40 HP (Horsepower), are highly economical and meet the needs of users, so they are increasingly approaching rural life and construction sites built and used as the primary power source for services such as plows, cultivators, harrows, water pumps, harvesters, etc.; milling machine, rice screening machine, etc.; agricultural vehicles, motorboats, etc.; small capacity concrete mixer; air compressors with small and medium capacity, etc.

The number and scale of our country's engine manufacturers still need to be improved. They mainly produce small single-cylinder diesel engines for agriculture and construction. Due to product price conditions, these engines mostly use old-style fuel supply systems (high-pressure

*Corresponding author.
Email: nguyenquochoang@qnu.edu.vn

https://doi.org/10.52111/qnjs.2024.18310

mechanical pumps) to ensure competitiveness with engines produced in other countries.

Among them, we must mention engines with capacity from 5 to 25 HP from Vikyno company, with characteristics of low fuel consumption, durable use, and production process requiring high precision, such as VIKYNO RV-70, RV-105, RV-125, RV-195, KND5B, D9. These products are used on agricultural machinery such as plows, generators, milling machines, water pumps, etc., and are machines that serve the construction industry favored by domestic and foreign consumers. Most of these products are transferred production technologies under copyright from KUBOTA (Japan) with an increasing rate of details localization, from 40% in 1992 to 70 - 80% in 2004 and currently about 90%.

However, these engines have a small working capacity range, are noisy, and do not meet consumer needs. The problem is that it is necessary to quickly research and produce multi-cylinder engines with a broader power range and higher efficiency and economy.

To meet consumer needs, agricultural machinery companies have imported many products, such as tractors, combine harvesters, etc., from brands such as KUBOTA, YANGMA, MITSUBISI, ISUZU, etc. This product has a 3, and 4-cylinder Diesel engine with a 20 ÷ 40 horsepower capacity. In addition, during engine operation at high load and high speed, the fuel injection process is poor, producing much black smoke due to falling, burning on the expansion line, and consuming much fuel. When running at idle speed, the engine design is unstable, causing environmental pollution and reducing the engine's economy. One of the reasons is the poor quality of the fuel injection process.

The problem is that it is necessary to improve or research new designs of engines in general and fuel systems of these types of engines, in particular, to suit the conditions of use in our country, bringing the highest economic benefit for users. But calculating, designing, manufacturing, renovating, installing new things, and doing experiments are complicated and take much time. Therefore, researching and exploiting the application of information technology software in calculating design, simulating engines in general, and the process of supplying fuel to internal combustion engines, in particular, will help significantly shorten the time for designing, testing, and optimizing the fuel supply process of the engine fuel system. This will significantly reduce design, manufacturing, and testing costs, thereby reducing product costs.[1]

Currently, in the world, there appears a lot of information technology software related to simulating engines in general and hydrodynamic processes, in particular, such as KIVA software is used to calculate and simulate the thermodynamic process of the engine); PROMO software (German) is used to calculate the thermodynamics of the engine's working process based on CFD (computational Fluit Dynamics) computational fluid dynamics theory; The software BOOST, FIRE, HYDSIM, EXCITE, GLIDE, TYCON, BRICKS from AVL (Austria) are very powerful toolkits in calculating and simulating kinetic, dynamic, thermodynamic processes, hydrodynamics, etc. of structures and systems in internal combustion engines; AUTOMATION STUDIO software is used to estimate and simulate hydraulic and pneumatic systems; Festo's FluidSIM 5.0 software is used to calculate and simulate hydraulic and pneumatic systems; Fluent software is software capable of modeling cylinder engines, ballistics, turbine engines and equipment, and multiphase systems; etc. This software can be used for in-depth research on engine work cycles and can design models, test theoretical models, etc. In Vietnam, this software has just been used in recent years, so it is currently in the research stage. In addition to those specialised software, there are some very commonly used software such as MATLAB SIMULINK software. The software

https://doi.org/10.52111/qnjs.2024.18310

can handle most mathematical operations based on the available command set; moreover, it can simulate systems in mechanics and electronics.

In short, each software has its advantages in a specific area. In particular, Hydsim software is software in the AVL Workspace software suite of the Republic of Austria, an in-depth software for calculating and simulating the fuel supply process of Diesel engines. In addition, Hydsim software is also suitable for calculating and simulating the fuel supply process for gasoline engines and engines using other alternative fuels such as alcohol, biogas, LPG, etc. The software has been widely applied in developed countries and modern automobile companies such as Audi, Fiat, etc. Several officials, lecturers, students, and research and application students use the software in Vietnam.

Therefore, the authors applied Hydsim software to simulate the fuel supply process of the Kubota D1703-M-DI Diesel engine based on simulation conditions with rated load, average load, and no load and with a change in the value of structural parameters.[2,3] Based on the simulation results obtained, the authors will analyze and evaluate the simulation results and draw relevant conclusions about the influence of structural parameters on the quality of fuel injection on the Kubota Diesel engine D1703-M-DI. From there, proposals for improvements in more appropriate structural parameters are made. This is important in reducing fuel consumption, noise, and the content of pollutants in engine exhaust gases.[1,4]

2. ANALYSIS OF STRUCTURAL CHARACTERISTICS AND CONSTRUCTION OF A SIMULATION MODEL OF THE FUEL SUPPLY SYSTEM OF KUBOTA DIESEL ENGINE D1703-M-DI

2.1. Analyze structural features

2.1.1. Kubota Diesel Engine D1703-M-DI

The Kubota D1703-M-DI engine is a diesel engine with a 4-stroke, 3-cylinder, 1-2-3 firing order, placed vertically, compression ratio of 20:1, displacement of 1.647 liters, and maximum capacity of 22.7 kW power, etc. The engine uses a unified combustion chamber, has a ω-shaped piston top cutout, and injects fuel directly onto the piston top, creating a swirling movement of the gas flow, optimizing the process. Mix the mixture, thus reducing up to 50% of PM particles compared to level 2 of the EPA standard. The MoS_2 plating layer on the valve body and piston reduces noise by 1-2 dBA compared to a conventional engine. It is manufactured by the Japanese company Kubota and is used on tractors, such as L3408VN (Figure 1), in KUBOTA, Japan. The D1703-M-DI engine complies with temporary regulations on EPA (US) tier 4 exhaust standards and EU (European) stage 3A standards passed in 2012 and has been recognized by the European market.

Figure 1. KUBOTA L3408VN tractor.

2.1.2. Kubota D1703-M-DI Diesel engine fuel system

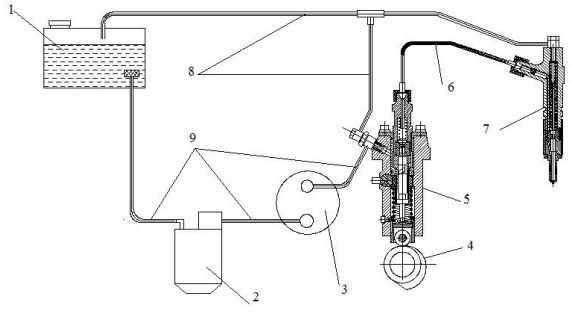

Figure 2. Structure diagram of Kubota D1703-M-DI Diesel engine fuel system. 1. Oil tank, 2. Oil filter, 3. Low-pressure pump, 4. Camshaft, 5. High-pressure pump, 6. High pressure pipe, 7. Injector, 8. Oil return pipe, 9. Supply oil pipe.

Kubota D1703-M-DI Diesel engine uses a Diesel engine fuel system with a 3-cylinder, in-line (5) centralized high-pressure pump of the

https://doi.org/10.52111/qnjs.2024.18310

Bosch “K” Type Mini Pump. Each pump unit supplies fuel for one machine (Figure 3). Fuel is injected directly into the combustion chamber through closed nozzles (7) of the Bosch "P" Type Hole Nozzle type with five spray holes (Figure 11). The oil tank is stamped from a steel plate and has a capacity of 34 liters. Oil filters use a pleated paper-type filter element, which increases filtration efficiency and compact structure. A diaphragm-type low-pressure pump is located on the side of the engine body and is driven by the high-pressure pump camshaft.

The low-pressure pump sucks fuel from the tank through the filter into the pump and then is pumped to the high-pressure pump. Filters filter out dirt mixed in fuel. The high-pressure pump compresses the fuel further into the high-pressure line and then to the nozzle. Fuel is injected into the engine combustion chamber at the end of the compression process. Then, the injected fuel beam is shredded, heated, evaporated, and mixed evenly with air to create a mixture that spontaneously ignites. Excess fuel in the injector and high-pressure pump passes through the return valve to the tank.

a. High-pressure pump

The Kubota D1703-M-DI Diesel engine uses a centralized high-pressure pump with three machines in line and a fuel supply order 1-2-3. The removable camshaft is installed in the engine body. The high-pressure pump consists of 3 pump groups. Each pump group includes a pair of high-pressure pump piston-cylinders. The control of changing the amount of fuel supplied for each cycle is thanks to the oblique groove on the piston, which is controlled to rotate by the rack and pinion mechanism. The unique feature of this type of pump is adjusting the fuel quantity between pump units; we change it by rotating the adjustment tube (6) back or forth.

*** Structure (Figure 3):** This is a high-pressure pump that adjusts the amount of fuel supplied to the cycle with a piston valve, changing the amount of the fuel provided by changing the proper stroke of the piston. The main details of the high-pressure pump are the pair of pistons (15) and cylinders (16). This is a super precise pair requiring very high precision manufacturing. It has been chosen to be installed together, and when replaced, the entire pair must be replaced. The cylinder is inserted into the hole in the adjusting tube body, positioned by the pin on the adjusting tube (6). The space inside the cylinder is connected to the fuel chamber in the pump body by a port and to the high-pressure fuel line when the high-pressure valve is open.

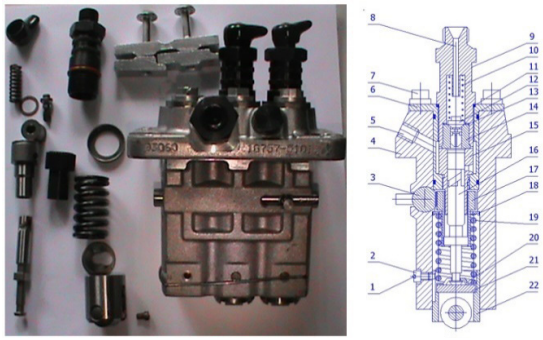

(a) (b)

Figure 3. Structure of high-pressure pump of Kubota D1703-M-DI Diesel engine. (a) Actual image of high-pressure pump, (b) longitudinal section of a pump unit. 1. Locking ring, 2. Locating pin, 3. Pinion rack, 4. High-pressure pump body, 5. Oil inlet line, 6. Adjusting tube, 7. Retainer bolt, 8. Fuel to injector, 9. High-pressure hose connector, 10. High-pressure valve spring, 11. Oil seal, 12. High pressure valve, 13. Copper gasket, 14. High-pressure valve seat, 15. Cylinder, 16. Piston, 17. Pipe teeth, 18. Upper spring stop plate, 19. Piston return spring, 20. Lower spring stop plate, 21. Adjusting pad, 22. Roller head.

The high-pressure pump has another super-precise pair: the high-pressure valve (12) and valve seat (14). The screw (9) is screwed tightly onto the adjusting pipe body (the adjusting pipe is screwed tightly on the pump body) to press the high-pressure valve seat tightly onto the cylinder head (16) so the contact surface between the valve seat (14) and the cylinder (16) consistently tight. Thanks to the high-pressure valve spring (10), the high-pressure valve (12) is pressed tightly against the conical surface of the valve seat, separating the space above the piston of

the pump unit from the high-pressure pipe. The tooth rack (3) and tooth tube (17) are connected to the piston tail, and the amount of fuel injection supplied to the cycle is adjusted.

*** Working principle (Figure 4):**

Fuel suction process: When the cam drives, the high-pressure pump rotates, and the roller rolls on the cam profile. When the rocker roller goes down, thanks to the force of the piston return spring, the high-pressure valve closes thanks to the high-pressure valve spring. At this time, under the influence of the high-pressure pump spring, it will push the piston (1) down, creating a vacuum in the cylinder chamber (5). When the piston opens the port (4), the fuel from the fuel chamber (3) will be loaded into the cylinder chamber until the piston is at its lowest position.

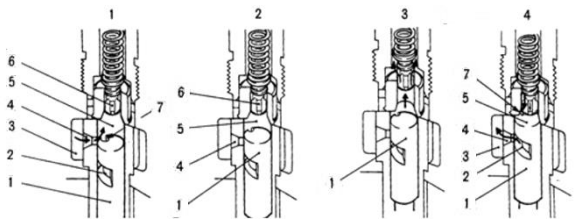

Figure 4. Fuel suction and ejection stroke of the high-pressure pump. 1. High-pressure pump piston, 2. Groove on piston, 3. Fuel compartment, 4. Diaphragm port, 5. Cylinder cavity, 6. High pressure valve, 7. Groove on high-pressure valve.

Fuel pushing process: When the rotating cam pushes up the piston (1), the fuel is initially pushed out through the hole (4). When the piston covers the hole, the pressure fuel supply process begins. In the high-pressure pump, the effect on the high-pressure valve continues to increase until the tension of the high-pressure valve spring and residual pressure on the high-pressure pipe are overcome, the high-pressure valve opens, and fuel enters the high-pressure line to the nozzle. The fuel supply process continues until the piston's inclined groove opens the port (4), ending the fuel supply. Leading to a sudden decrease in fuel pressure in the pump chamber, the high-pressure valve closes tightly on the valve seat (under the Influence of the high-pressure valve spring and fuel pressure on the high-pressure pipe). The fuel injection ends even though the piston continues to move up. Complete a fueling cycle and then repeat the cycle as above. Due to the throttling phenomenon of the port (4) and the compression phenomenon of the fuel, the actual supply start and end times are different from the geometric supply start and end times.

Controlling the amount of fuel supplied: To change the fuel provided to an engine's working cycle, we move the rack, and the gear tube rotates, making the piston rotate. This changes the proper stroke of the pump piston.

*** Structure of main details in high-pressure pump:**

- Ultra-precise piston and cylinder duo:

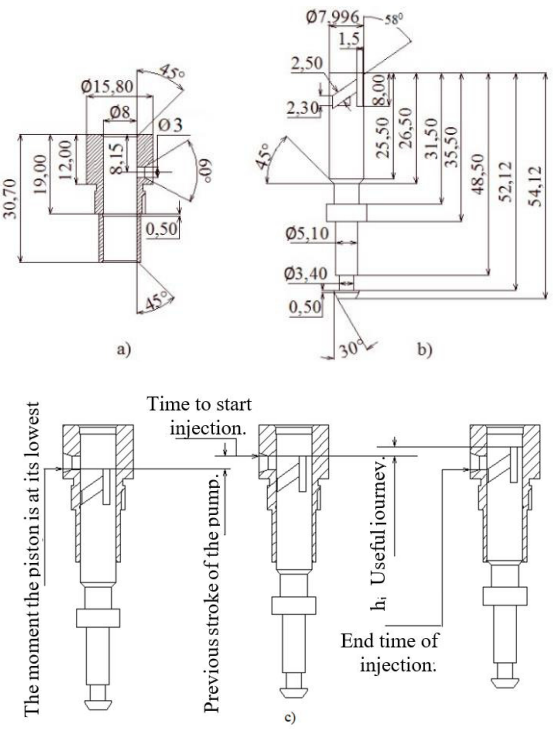

Figure 5. Measurement parameters of the high-pressure pump piston-cylinder duo. (a) Cylinder, (b) piston, (c) Pump working parameters.

High-pressure pump pistons and cylinders have precise geometric shapes and good wear resistance. The manufacturing material is Cr15 steel, which has a stable microstructure and more

https://doi.org/10.52111/qnjs.2024.18310

stable geometric dimensions. The part is heat-treated to meet the requirements of the friction surfaces of the piston and cylinder pair having a hardness not less than 58 HRC, and the end faces having a hardness not less than 55 HRC.

Main parameters of piston and cylinder (Figure 5):

+ The mass of the piston is m_p = 15.7 g.

+ Piston diameter: d_p = 7.996 mm.

+ Suction hole diameter: d_{lh} = 3.0 mm.

+ Spiral groove elevation angle (oblique): α = 32 degrees.

+ Spiral groove width (oblique): b = 2.5 mm.

+ Vertical chamfer width (vertical): b_1 = 1.5 mm.

+ Piston front stroke: h_t = 2.8 mm.

- Piston return spring: responsible for returning the pump piston during the cam lowering stroke. Make sure the roller is always in contact with the cam surface. The parameters of the piston return spring are shown in Figure 6:

+ Mass of piston return spring: m_{lx} = 16.6 g.

+ Number of twist steps: 5 steps.

+ Initial pressure of plunger piston spring: F_0 = 185 N.

+ Hardness: k = 32000 N/m.

+ Damping degree: C = 10 N.s/m.

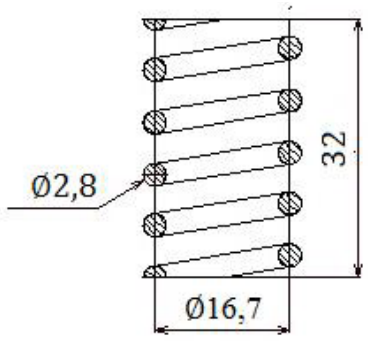

Figure 6. Measurement parameters of piston return spring.

- Roller jack:

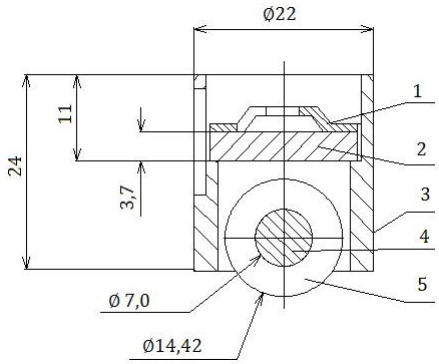

Figure 7. Measurement parameters of the roller handle. 1. Spring stop disc, 2. Adjusting pad, 3. Jack body, 4. Roller shaft, 5. Roller.

Roller jack: This helps reduce friction during contact between the roller and the cam. Thanks to that, the cam can rotate easily, avoiding cam jamming. It has a total mass of 46.5 g (including the spring stop disc and adjusting pad).

- Pair of high-pressure valves and high-pressure valve seats: Each pump unit is equipped with a high-pressure valve cluster, which has the following tasks: Prevent gas from the engine cylinder from entering the high-pressure pump cylinder; Prevent fuel on the high-pressure pipe from flowing back to the high-pressure pump cylinder; Complete the fuel supply process decisively, avoiding the phenomenon of dropped spray.

The high-pressure valve pair is a precision pair made of Cr15 alloy steel. The valve has a hardness after heat treatment of about HRC 56÷62, and the valve seat is HRC 60÷64. The valve and valve seat must be ground together. The tightness of a high-pressure valve is usually checked by using compressed air with a residual pressure of 0.4 ÷0.5 MN/m^2, immersing the valve in a barrel of kerosene; there must be no air bubbles. Main parameters of high-pressure valve assembly (Figure 8):

+ Mass of high-pressure valve spring: m_{lxv} = 1.9 g.

+ Mass of high-pressure valve: m_v = 2.2 g.

https://doi.org/10.52111/qnjs.2024.18310

+ Valve spring hardness: k_{lxv} = 13500 N/m.

+ Valve spring damping degree: C_{lxv} = 5 N.s/m.

+ Valve seat hardness: k_{dv} = 50000000 N/m.

+ Valve seat damping degree: C_{dv} = 50 N.s/m.

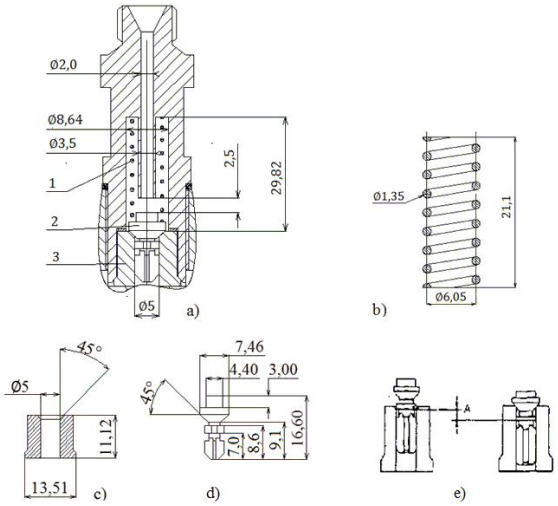

Figure 8. Measurement parameters of the valve duo and high-pressure valve seat. (a) High-pressure valve assembly, (b) high-pressure valve spring, (c) High-pressure valve seat, (d) High-pressure valve, (e) High-pressure valve lift stroke A, 1. High-pressure valve spring, 2. High pressure valve, 3. High-pressure valve seat.

- High-pressure pump camshaft: *The camshaft is cast in one piece and designed with an almost straight beveled cam face.* As the cam lift stroke increases, the piston's movement speed increases, rapidly increasing fuel pressure.

Main parameters:

+ Base circle radius of cam: R = 17.04 mm.

+ Roller radius: r_{roll} = 7.21 mm.

+ Effective width of roller: b_{roll} = 8.5 mm.

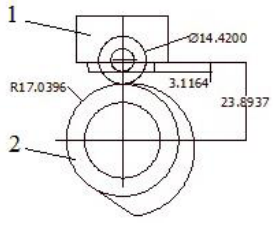

Figure 9. High-pressure pump cam profile of Kubota D1703-M-DI engine. 1. Roller shaft, 2. High-pressure pump camshaft.

b. High-pressure hose

A high-pressure steel pipe with high hardness is used to carry high-pressure fuel from the high-pressure pump to the high-pressure injector.

Figure 10. D1703-M-DI engine high-pressure hose.

Main parameters:

+ Overall length: l = 325 mm.

+ High-pressure oil hole diameter: d = 1.5 mm.

+ High-pressure pipe wall thickness: δ = 1.5 mm.

c. High-pressure nozzle

The Kubota D1703-M-DI engine uses a two-stage nozzle. The nozzle head is arranged with five spray holes with a diameter of about 0.2 mm distributed around with angles about 75 degrees apart to suit the Combustion chamber structure to create the best mixture. This injector will inject more fuel in the 2nd stage as the fuel pressure increases. Using a 2-stage nozzle reduces injection pressure to lift the injector, thereby improving low-speed injection stability and unloading capability. On the other hand, because the initial amount of fuel injection is small, it improves typing and smoothness of motion.

Two springs (No. 8 and No. 12) and a push rod (No. 14 and No. 13) are inside the nozzle. In this two-gap stage, a gap between pin 14 and pin 13 for fuel injection is called initial lift.

The initial lift, the tension of spring No. 8 (stage 1 fuel pressure), and the tension of spring No. 12 (stage 2 fuel pressure) are adjusted by replacing the corresponding adjusting pads. Nominate them.

https://doi.org/10.52111/qnjs.2024.18310

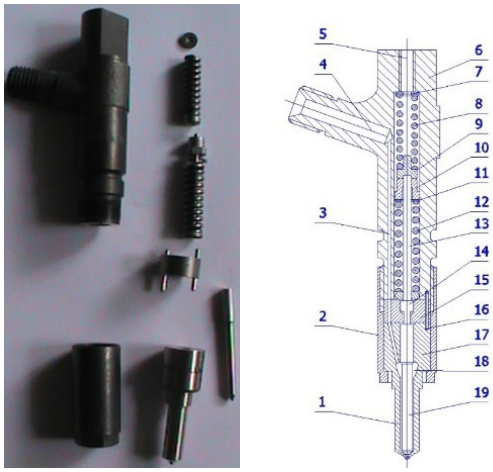

Figure 11. Structure of D1703-M-DI engine nozzle. 1. Injector body, 2. Locking nut, 3. Body longitudinal fuel pipe, 4. High-pressure hose connection, 5. Oil return line connection, 6. Injector body, 7. Adjusting gasket, 8. 1st stage spring, 9. Spring stop plate, 10. Guide tube, 11. Adjusting pad, 12. 2nd stage spring, 13. Push rod, 14. Intermediate connecting pin, 15. Setting base maximum injector lift stroke position, 16. Locating pin, 17. Nozzle body, 18. High-pressure chamber, 19. Injector.

Stage 1 (Figure 12): When the fuel pressure increases due to the operation of the high-pressure pump and reaches about 190 KG/cm^2, it overcomes the tension of spring number 8, pushing the injector upward and causing injection to begin. After pin 14 comes into contact with spring base 12, the lift of the injector only changes once the pressure increases to about 230 KG/cm^2.

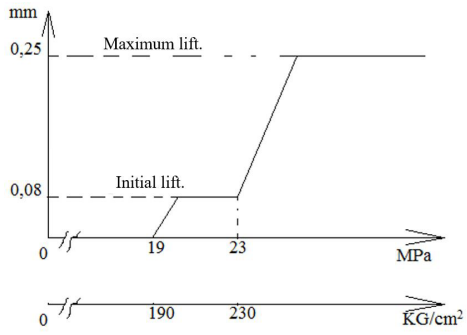

Figure 12. Graph of nozzle operating pressure evolution.

Stage 2 (Figure 12): when the fuel pressure reaches about 230 KG/cm^2, it overcomes the tension of springs No. 8 and No. 12 and lifts the injector higher. Once the injector contacts the spacer (15), the needle lift will not change anymore, even if the fuel pressure increases.

Therefore, when the engine is under a light load, only a tiny amount of fuel is injected at the low lift stage. On the other hand, under heavy load, a small amount of fuel is injected at the initial lift stage, and then large amounts of fuel are injected at a more advanced stage. The main parameters of the nozzle are shown in Figures 13 and 14.

+ Injector mass: $m_{kim} = 2.9$ g.

+ Spray hole length: $l_{hole} = 0,8$ mm.

+ Nozzle cavity diameter at hole: $d = 1,0$ mm.

+ Injector base angle: $\alpha_{seat} = 45^0$.

+ Diameter of injector spring wire 1: $d_{lx1} = 1.86$ mm.

+ Average diameter of injector spring 1: $d_{tb} = 4.52$ mm.

+ Mass of injector spring 1: $m_{lx1} = 3.0$ g.

+ Diameter of injector spring wire 2: $d_{lx2} = 2.05$ mm.

+ Average diameter of injector spring 2: $d_{tb} = 5.25$ mm.

+ Mass of injector spring 2: $m_{lx2} = 4.4$ g.

+ Number of injector spring steps 1,2: 10 steps.

+ Push rod mass: $m_{td} = 1.2$ g.

+ Mass of connecting pin: $m_{cn} = 0.4$ g.

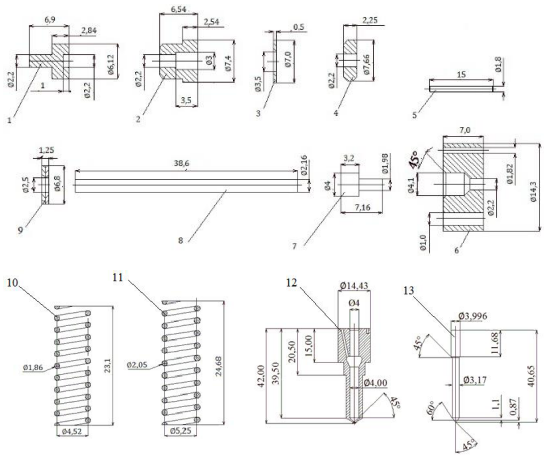

Figure 13. Parameters of the high-pressure nozzle of Diesel engine D1703-M-DI. 1. 1st stage spray spring stopper disc, 2. Guide tube, 3. 2nd stage spray spring adjustment pad, 4. 2nd stage spray spring stopper disc, 5. Locating pin, 6. Fixing base maximum injector lift stroke position, 7. Intermediate connection pin, 8. Push rod, 9. Stage 1 injection spring adjustment pad, 10. Stage 1 injection spring, 11. Stage 2 injection spring, 12. Nozzle body, 13. Injector.

https://doi.org/10.52111/qnjs.2024.18310

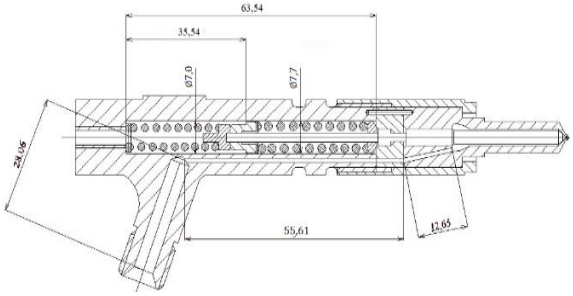

Figure 14. Basic parameters of the nozzle.

d. Combustion chamber shape

The Kubota D1703-M-DI Diesel engine uses a unified combustion chamber and ω-shaped piston top to create an airflow vortex, improving the quality of mixture formation.

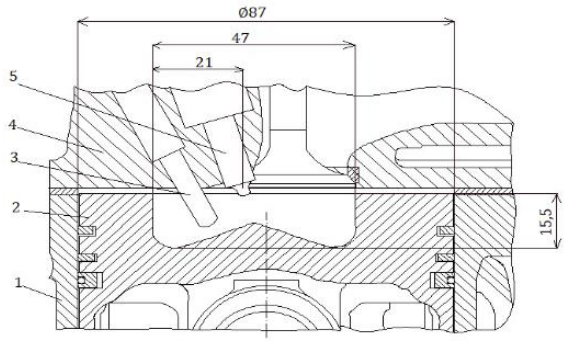

Figure 15. Combustion chamber parameters of Kubota D1703-M-DI Diesel engine. 1. Cylinder, 2. Piston, 3. Dryer shaft, 4. Engine cover, 5. Nozzle.

Conclusion: The quality of fuel injection in a Diesel engine (average fuel particle diameter, spray beam taper angle, and spray beam length) will determine the quality of mixture formation and combustion. Many parameters must be considered to achieve the best fuel injection quality, such as fuel system structural parameters, operating conditions, engine type, fuel properties used, etc. We must research, calculate, and choose to make these parameters optimal.

2.2. Build a model and simulate the fuel supply system of the Kubota D1703-M-DI Diesel engine

2.2.1. Algorithm diagram

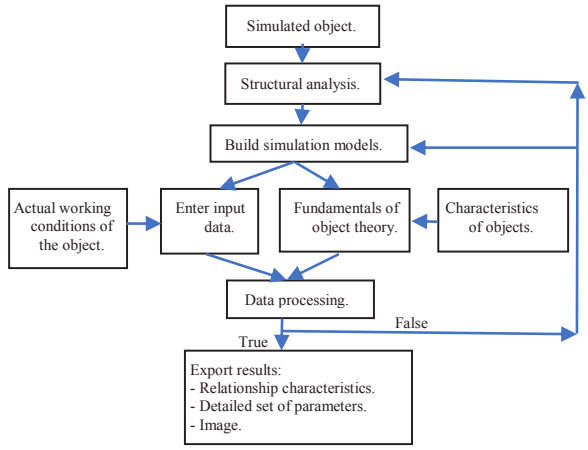

Figure 16. Algorithm diagram of the simulation program.

Based on simulation theory,[4] calculations on Hydsim software, and the structure and actual working conditions of the Kubota D1703-M-DI Diesel engine fuel system, we have created a schematic diagram of the Kubota D1703-M-DI Diesel engine fuel supply system simulation program (Figure 16).

2.2.2. Build simulation models

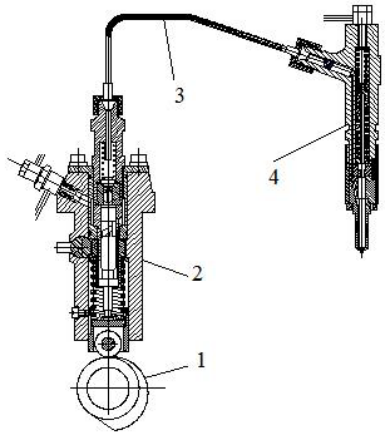

Figure 17. Main assemblies used for simulation. 1. High-pressure pump camshaft, 2. High-pressure pump assembly, 3. High pressure pipe, 4. Injector nozzle.

The detailed assemblies used to simulate the Kubota D1703-M-DI Diesel engine fuel system (Figure 17) structurally combine three main elements: a high-pressure pump, pipes, and a nozzle.

The in-line high-pressure pump consists of 3 pump groups. Because the pump groups

https://doi.org/10.52111/qnjs.2024.18310

have the same structure, the simulation is only performed for one pump group.

The structure of a pump unit includes Cam (4) (convex cam), which rotates thanks to the drive shaft, causing the pump piston to move up and down (piston plunger). The cam (4) has a convex cam lobe, so the plunger piston goes up and down once during its one revolution. The cavity above the plunger piston is the pressure chamber (chamber before the high-pressure valve). Fuel from the low-pressure pump enters the common intake chamber of the high-pressure pump (Pressure margin), then through the fuel inlet (inline inlet/overflow type) and into the high-pressure pump chamber. Here, the plunger piston compresses the fuel, which is pushed through the high-pressure valve (which has a pressure-reducing rim) to the chamber behind the high-pressure valve (this chamber has residual pressure). From here, high-pressure fuel follows the high-pressure pipe to the high-pressure injector (high-pressure oil chamber that lifts the injector). Part of the fuel leaks through the gap between the plunger piston and the cylinder through the port to the fuel tank.

The high-pressure pipeline transports high-pressure fuel from the high-pressure pump to each injector. During the working process, high-pressure pipes expand and contract.

High-pressure fuel from the high-pressure pipe follows the pipeline along the nozzle body to the high-pressure chamber in the nozzle body. When the oil pressure applied to the injector cone surface is enough to overcome the injector spring tension (2 springs), the injector is lifted (2 stages), and high-pressure fuel is injected into the engine combustion chamber through the spray hole on the nozzle head.

When the inclined groove on the pump piston head (metering groove) opens the inlet/pressure chamber in the high pump chamber before the high-pressure valve suddenly decreases, the high-pressure valve closes to reduce the pressure and the return force. The injector closes by pressing the high-pressure valve spring, ending the fuel injection.

From analyzing the structural characteristics of the fuel supply system of the Kubota D1703-M-DI Diesel engine, we select the corresponding elements in Hydsim software to perform the simulation. Once the corresponding elements have been identified, we create a block model of the equipment in the fuel system.

a. Create a high-pressure pump block model

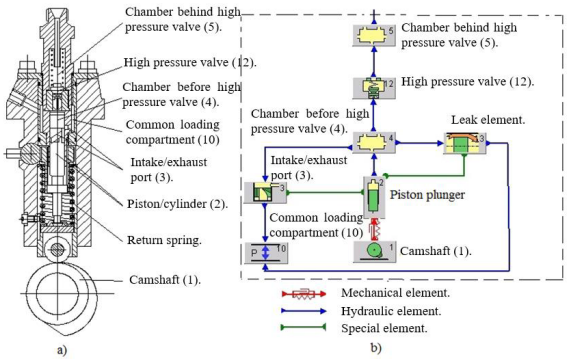

Figure 18. Model of Kubota D1703-M-DI Diesel engine high-pressure pump block. (a) Actual high-pressure pump structure, (b) High-pressure pump block model.

b. Create a high-pressure pipeline block model

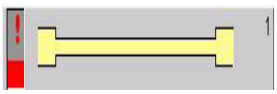

Figure 19. Kubota D1703-M-DI Diesel engine high-pressure pipe block model.

c. Create a nozzle block model

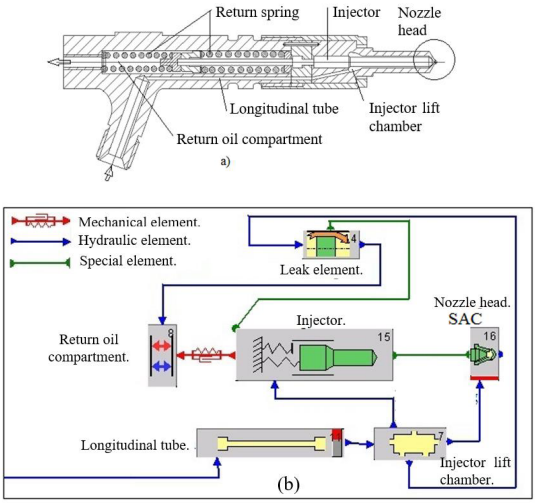

Figure 20. Model of Kubota D1703-M-DI Diesel engine high-pressure injector block. (a) Fundamental structure of high-pressure nozzle, (b) block model of high-pressure nozzle.

d. Create a block model of the combustion chamber

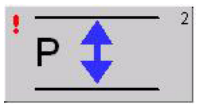

Figure 21. Model of the combustion chamber block of the Kubota D1703-M-DI Diesel engine.

2.2.3. Simulation model of Kubota D1703-M-DI engine fuel system

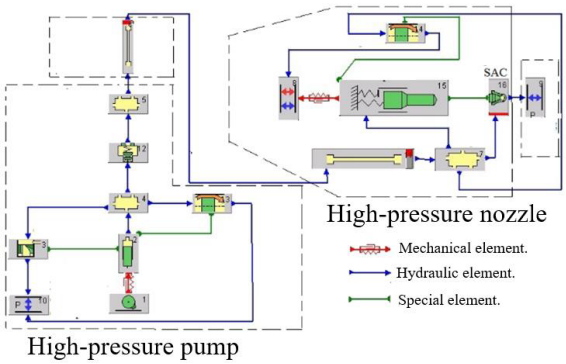

Figure 22. Simulation model of D1703-M-DI Diesel engine fuel system. 1. Camshaft (1), 2. Piston, 3. Intake/exhaust port, 4. Chamber before the high-pressure valve, 5. Chamber behind the high-pressure valve, 6. High pressure pipe, 7. Injector lift chamber, 8. Return oil compartment, 9. Combustion chamber, 10. Joint loading compartment, 11. Longitudinal tube, 12. High-pressure valve, 13,14. Leak element, 15. Injector, 16. Nozzle head SAC.

2.2.4. Analysis of simulation calculation mode of Kubota D1703-M-DI engine fuel supply system

The parameters of the fuel equipment, combustion chamber structure, charging mechanism, and engine rotation are designed with the rated working mode (revolution and rated load) to ensure good atomization and mixture quality. Changing the engine's working mode causes the quality of the mist and mixture to deteriorate, affecting the engine's economy, reliability, and longevity.

a. Rated load mode

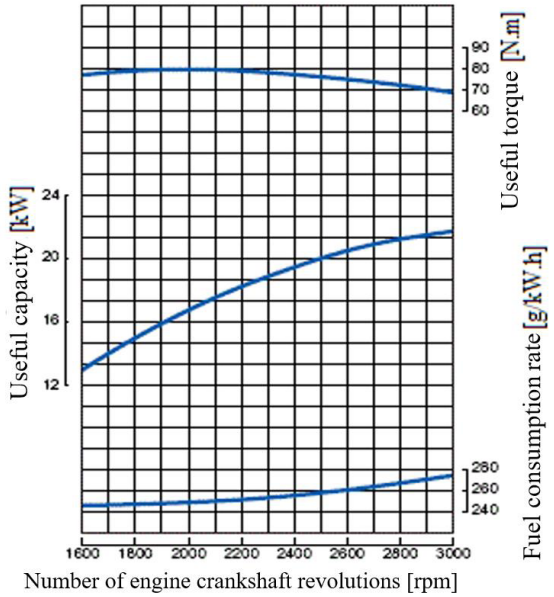

Figure 23. External speed characteristic graph of D1703-M-DI engine.

The characteristic parameter for the rated load mode at the rated number of revolutions and rated load is (h_{imax}: maximum helpful stroke of the high-pressure pump piston). Based on the external speed characteristic graph of the D1703-M-DI engine (Figure 23) and the technical specifications of the D1703-M-DI engine, we can determine that the rated speed of the engine is 2800 rpm, rated power N_e= 22.7 kW. The remaining thing is to determine the h_{imax}. The amount of fuel supplied to a cylinder during a working cycle is calculated according to the following formula:[2-4]

$$V_x = \frac{N_e.g_e.\tau.10^{-3}}{120.n.i.\rho_{nl}} \text{ [mm}^3\text{]} \quad (1)$$

We have: $\tau = 4$; $i = 3$;

The D1703-M-DI engine uses Diesel fuel, so it has $\rho_{nl} = 0.82$ g/cm^3.

Considering the speed of 2800 rpm, look at the graph in Figure 23. We get Ne = 22.7 kW and g_e = 265 g/kW.h.

Substitute numbers into equation (1). We get V_x = 29,111 mm^3.

From there, we can calculate the proper stroke of the pump piston: $h_{imax} \approx 0.85$ mm.

https://doi.org/10.52111/qnjs.2024.18310

b. Idle mode

Idle mode is when the engine operates stably at the lowest speed without external load. The no-load mode corresponds to the minor helpful stroke of the high-pressure pump piston (h_{imin}).

Figure 24. Measuring fuel consumption of Kubota D1703-M-DI engine.

Table 1. Engine fuel consumption without external load.

Accelerator pedal displacement (%)	0	20	40	60	80	100
Amount of fuel consumed in 60 seconds (g)	4	8.5	12	16	27	30.3
Number of crankshaft revolutions (rpm)	1000	1600	2000	2400	2650	2800
Proper stroke of H_{imin} pump piston (mm)	0.08	0.11	0.12	0.13	0.21	0.22

From the results of measuring actual fuel consumption (Figure 24) according to the accelerator pedal stroke from 0% to 100% when the engine is not carrying a load (Table 1), with the electronic weighing device's error being 0.1 g, we can determine the minimum helpful stroke of the high-pressure pump piston corresponding to the no-load mode $h_{imin} \approx 0.08$ mm.

c. Intermediate loading mode

Based on the actual working conditions of the Kubota D1703-M-DI engine on the L3408VN tractor, we see that when the tractor is operating (plowing), the engine almost operates in the area of 80 ÷ 100% of the table travel. Step on the accelerator (the tractor runs in gear 2) at a speed of 1600 ÷ 2000 [rpm]. However, when moving, changing direction, etc, the engine usually runs at an average load of 40 ÷ 70% of the accelerator pedal stroke, with a speed of about 2000 ÷ 2800 rpm. Therefore, determining the valuable stroke in local load modes is very complicated. For simplicity, we select the proper stroke at representative local load modes for general simulation as $h_{itb} = 0.42$ mm.

Conclusion: To see the influence of structural parameters of the fuel system and engine operating mode (speed, load, proper stroke of high-pressure pump) on the quality of the fuel supply process, we choose the simulation mode corresponding to 4 engine crankshaft speed positions: 1600, 2000, 2400, 2800 rpm. We conduct a thin tissue for each simulated speed position corresponding to the three high-pressure pump rack positions: $h_{imax} = 0.85$ mm, $h_{itb} = 0.42$ mm, and h_{imin} (Table 1).

2.2.5. Declare input data for elements

Declare input and output data for elements. I am declaring boundary conditions and properties of Diesel fuel. Run the simulation and export the results.

3. ANALYSIS AND EVALUATION OF THE INFLUENCE OF STRUCTURAL PARAMETERS ON THE QUALITY OF THE FUEL SUPPLY PROCESS OF THE KUBOTA D1703-M-DI ENGINE

3.1. Influence of cam profile

The Kubota D1703-M-DI engine high-pressure pump camshaft is designed with high rigidity and a sudden growth profile (almost straight bevel).

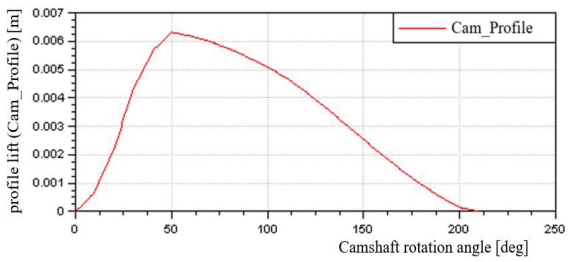

Figure 25. Lift graph of the cam profile.

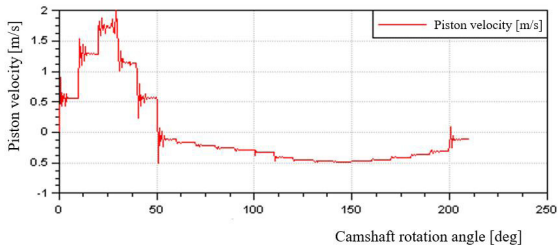

Figure 26. Graph of variation of pump piston displacement speed.

The lift of the cam profile is in the x direction (Figure 25). During the cam lift stroke, the piston is raised at high speed (Figure 26), and the fuel pressure in the pump chamber increases rapidly, leading to high chamber pressure behind the valve. Pressure, high-pressure pipe, and injector lift chamber increase quickly (Figure 27). When this pressure overcomes injector spring tension, the injector lifts fuel into the engine combustion chamber. The process of injecting fuel into the combustion chamber lasts until the inclined groove on the piston opens, and the injection process ends.

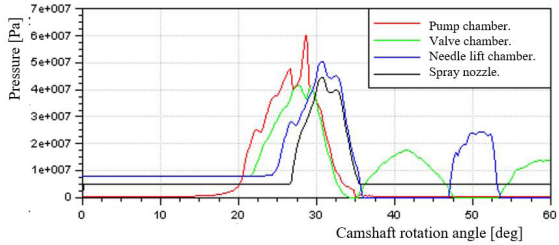

Figure 27. Graph of fuel pressure variation in the fuel system.

Due to the cam profile's sudden growth, the system's fuel pressure increases rapidly. The compression stroke of the piston is turbulence. This turbulence is in the form of a pressure wave that propagates in the fuel line in an elastic medium with the speed of sound; this speed depends on the compressibility and fuel density. The pressure wave reaches the injector later than the fuel supply period. High injection pressure and fuel compressibility not only cause a phase shift in the fuel supply in the pump and nozzle but also cause complex oscillatory motion of the fuel layer in the high-pressure pipeline, thus causing the circulation process to change. The movement of fuel through the injector orifice sometimes has a pulsating character. The source of pressure fluctuation interference is the movement of pistons, injectors, and high-pressure valves. Due to strong fluctuations in fuel pressure, the injector can open repeatedly after closing, causing a spray drop. Fuel injection on the expansion line has poor atomization quality due to low injection pressure. Drop injection increases the combustion period on the expansion path and reduces engine economy.

The fuel injection quality is quite good in the delay and main injection stages due to the high fuel injection pressure. The average fuel particle diameter is small and uniform (Figure 28), and the spray beam taper angle (Figure 29) and the spray beam length (Figure 30) gradually increase. However, in the free-flow phase (fuel supply has stopped), the fuel injection occurs thanks to the high-pressure pipeline's fuel compression energy and elasticity. Hence, the injection pressure gradually decreases, the diameter of the average fuel particle increases, and the spray beam taper angle and the spray beam length decrease progressively.[2-5]

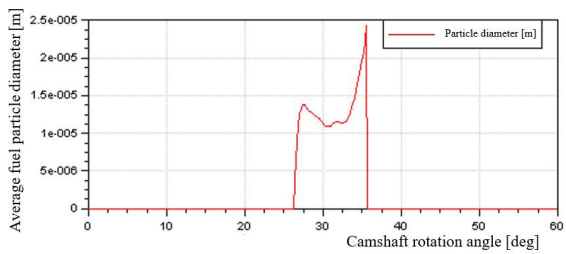

Figure 28. Graph of average fuel particle diameter variation.

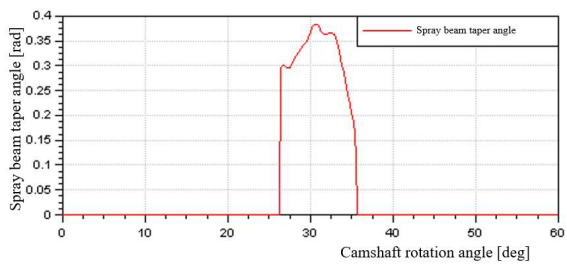

Figure 29. Graph of fuel injection beam cone angle variation.

https://doi.org/10.52111/qnjs.2024.18310

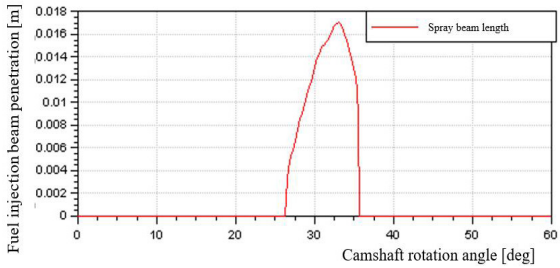

Figure 30. Graph of fuel injection beam length variation.

In general, the quality of fuel injection at the beginning and end of injection is not good, negatively affecting the quality of mixture formation and combustion, reducing engine economy, and causing environmental pollution. The quality of fuel injection is relatively good at about 30 ÷ 33^0 camshaft rotation angle (average fuel particle diameter is small, and even spray beam taper angle is significant, and beam length is large enough. [2-5]

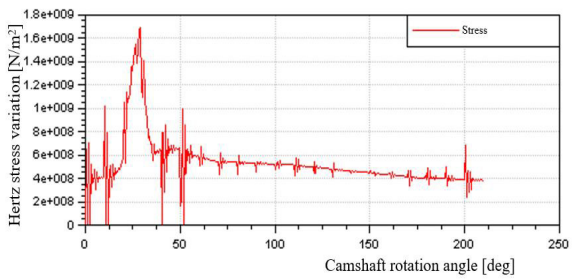

Figure 31. Hertz stress variation graph.

Value and variation of contact stress between roller file and convex cam during the working process (Figure 31). The most significant stress at the position where the plunger piston goes up compresses the fuel with the highest pressure at about 28-29^0 camshaft rotation angle (GQTC). Then the stress decreases rapidly corresponding to the moment the inclined groove on the piston head opens the exhaust port; the fuel pressure in the pump chamber suddenly decreases along with the elasticity of the high-pressure pump spring, causing the stress to fluctuate strongly, then The stress gradually decreases when only the elastic force of the spring remains, causing the cam lowering stroke. [2-5]

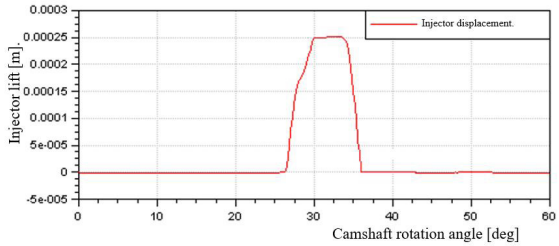

Figure 32. Graph of injector lift variation.

Due to the sudden lift of the cam, the pressure in the injector lift chamber increases rapidly. The hydraulic force acting on the needle is vast, overcoming the tension of both injector springs, so the injector is lifted to inject fuel into the engine combustion chamber. When fuel begins to be injected into the combustion chamber, the pressure in the injector lift chamber decreases slightly. Then, it continues to increase, causing a slow increase in the injector lift stroke.

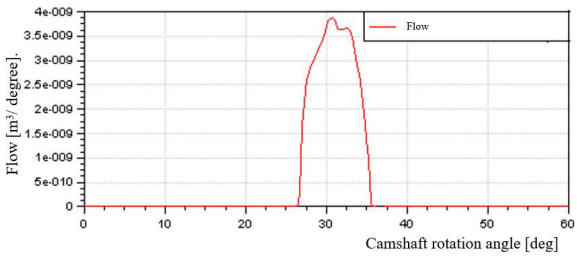

Figure 33. Graph of fuel injection flow variation.

The amount of fuel supplied in one working cycle of a pumping unit corresponding to the rated mode is about 26 mm^3 (Figure 34). Due to low injection pressure, the flow is small at the beginning and end of the injection process. The most enormous injection flow is about 3.8 mm^3/degree (Figure 33). The injection time is about 0.00119 s.

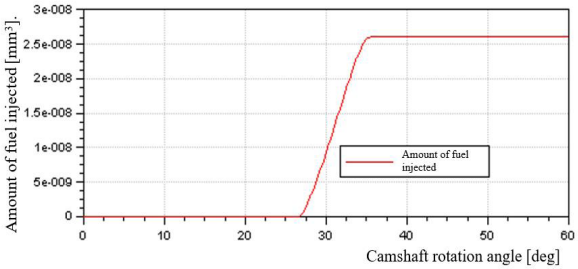

Figure 34. Graph of fuel injection volume variation in one cycle.

3.2. Influence of D/h_i ratio

To study the influence of the ratio between piston diameter and proper stroke (D/h_i) on fuel injection quality under the same conditions. Corresponding to the same amount of fuel supplied for one engine cycle at rated load mode is 29.11 mm^3. We choose the piston diameters to be 8, 7.5, 7, 6.5, and 6 mm. We can calculate the maximum beneficial journey: 0.85, 0.96, 1.11, 1.28, 1.50 mm.

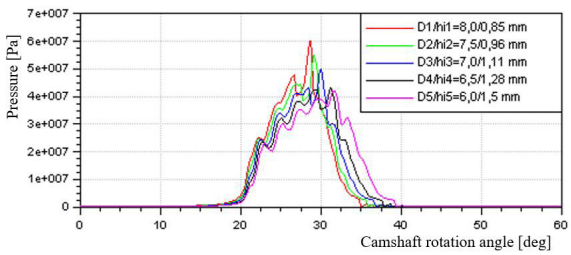

Figure 35. Influence of D/h_i ratio on pump chamber fuel pressure.

Simulation results show that the more minor the piston diameter, the larger the piston's helpful stroke, the lower the pressure in the system, and the larger the fluctuations (Figure 35). However, the pressure pulse at the end of the injection process has a gradually decreasing amplitude (Figure 36), meaning that the spray drop phenomenon is slowly overcome. As the pressure in the injector lift chamber decreases, the hydraulic force acting on the injector also decreases (Figure 37), so the injector lift gradually decreases (Figure 38). Therefore, the fuel circulation cross-section through the injector base also decreases (Figure 39). As a result, the fuel flow through the nozzle decreases (Figure 40), prolongs the fuel injection completion time, and negatively affects the mixture formation and combustion process. [2-5]

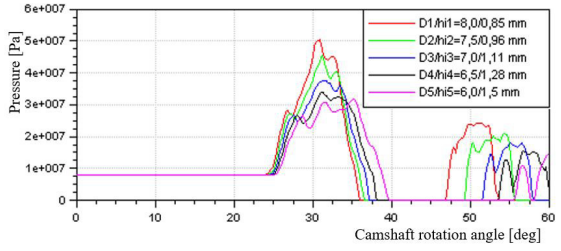

Figure 36. Influence of D/h_i ratio on injector lift chamber pressure.

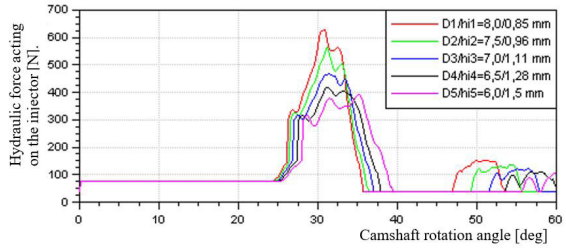

Figure 37. Influence of D/h_i ratio on the hydraulic force acting on the injector.

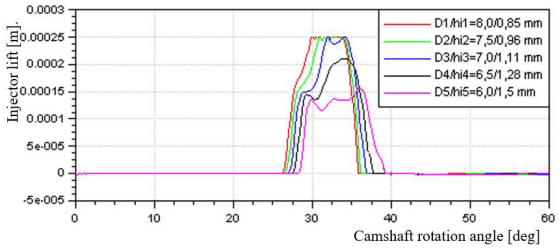

Figure 38. Influence of D/h_i ratio on injector lift.

As the piston diameter becomes smaller, the proper stroke of the piston becomes larger. We can see that the injection start time is gradually delayed, the average particle diameter gradually increases (Figure 41), the spray beam taper angle decreases (Figure 42), and the direction of the spray beam decreases (Figure 42). The spray beam length gradually decreases (Figure 43), and the injection end time is slowly delayed. The average fuel particle diameter gradually decreases, the spray beam taper angle decreases (Figure 42), and the spray beam length gradually increases (Figure 43).

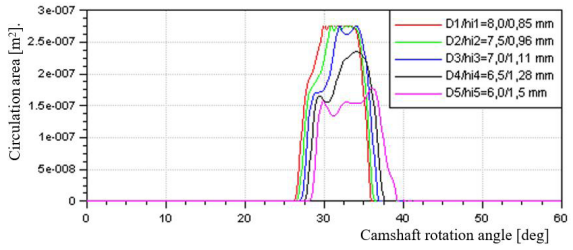

Figure 39. Influence of D/h_i ratio on the flow cross-section to the injector.

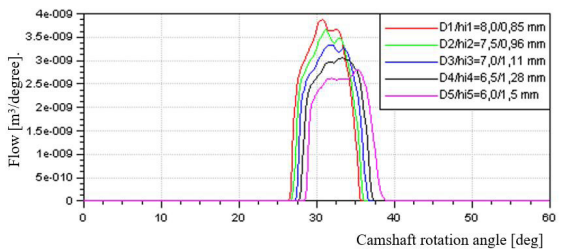

Figure 40. Influence of D/h_i ratio on fuel injection flow.

https://doi.org/10.52111/qnjs.2024.18310

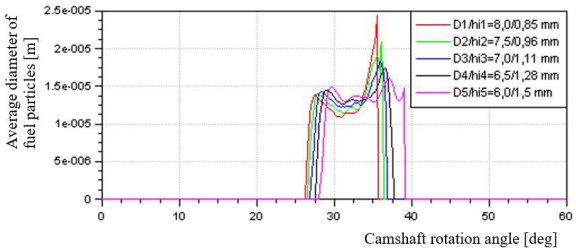

Figure 41. Influence of D/h_i ratio on average fuel particle diameter.

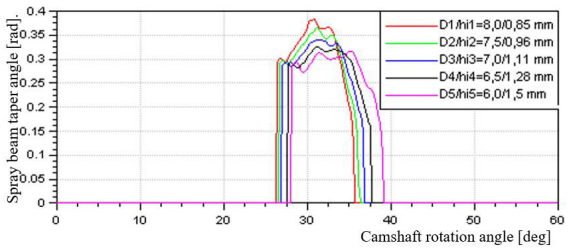

Figure 42. Influence of D/h_i ratio on fuel injection beam taper angle.

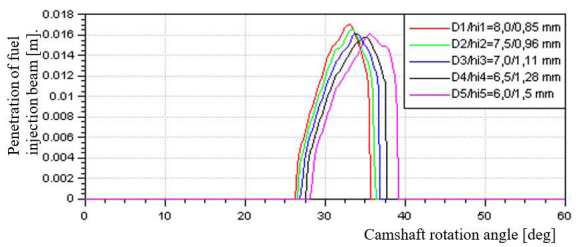

Figure 43. Influence of D/h_i ratio on fuel injection beam length.

Conclusion: When changing the D/h_i ratio, we see a massive change in the system's fuel injection quality. With the same amount of fuel supplied to a cycle, the more we reduce the piston diameter, the more helpful stroke the pump piston will have, so the injection time will be longer. Due to the decrease in piston diameter, the instantaneous compressed fuel flow through the high-pressure valve decreases, and the pressure in the system decreases. The force lifting the injector decreases, the fuel flow through the injector decreases, and the fuel flow leaking through the injector decreases. The average fuel particle diameter is generally small and uniform throughout the injection process. The spray beam taper angle and spray length are reduced but not significantly.

3.3. Influence of nozzle diameter

When other conditions are equal, we change the nozzle hole diameter by 0.18, 0.22, 0.25 mm, and 0.30 mm and simulate rated load mode. Consider the impact on fuel injection quality compared to when the nozzle hole diameter is 0.20 mm. The results show that when the nozzle hole diameter is smaller (0.18 mm), the fuel flow through the nozzle is more minimum (Figure 47), and the spray beam quality is uneven. In the delay and main injection stages, the average fuel particle diameter is the smallest (0.1÷0.13) μm. Still, in the free injection stage at the end of the injection process, the average fuel particle diameter is 0.38 μm (Figure 44), the spray beam taper angle (Figure 45) and the spray beam length are too small (Figure 46), and when spraying starts at the nozzle mouth, mist often condenses into mist, and at the end of the spraying process. There is a phenomenon of spray drop due to pressure pulsation in the system. Adversely affects the quality of the mixture formation and combustion process, reduces engine economy, and causes environmental pollution. [2-5]

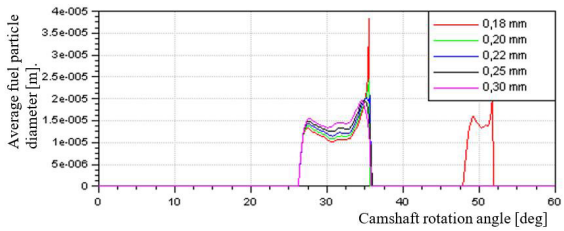

Figure 44. Influence of nozzle diameter on average fuel particle diameter.

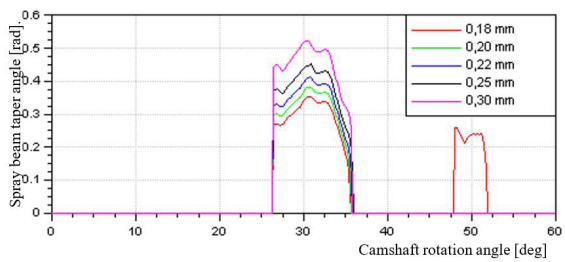

Figure 45. Influence of nozzle diameter on fuel injection beam taper angle.

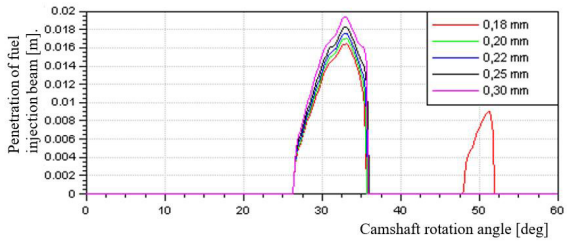

Figure 46. Influence of nozzle diameter on fuel injection beam length.

As the nozzle hole diameter grows, the fuel flow through the nozzle increases (Figure 47), so the fuel injection pressure gradually decreases (Figure 48). This results in the average fuel particle diameter increasing progressively (Figure 44), the spray beam taper angle gradually increasing (Figure 45), the spray beam length increasing progressively (Figure 46), and the average final fuel particle diameter being too high. The spraying process gradually decreases. At the same time, it overcomes the phenomenon of creating pressure pulses in the system, avoiding the phenomenon of spray drops. However, the diameter of the nozzle hole must be manageable, leading to the average diameter of the fuel particles being too large, rough, complex to tear apart, and evaporation slow, leading to poor mixture formation quality. [2-5]

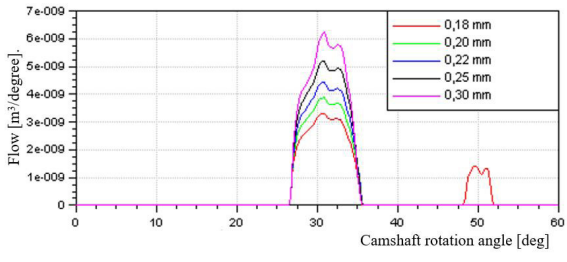

Figure 47. Influence of nozzle diameter on fuel injection flow.

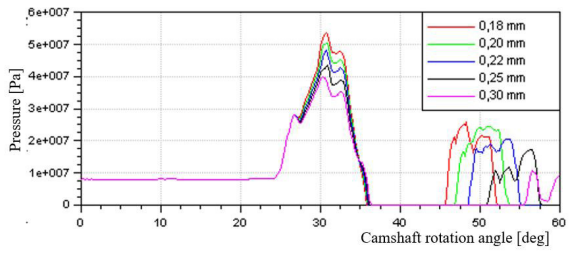

Figure 48. Influence of injection hole diameter on injector lift chamber pressure.

Conclusion: When increasing the nozzle diameter from 0.20 mm to 0.22, 0.25, and 0.30 mm, the spray circulation area will increase, the amount of fuel injected will increase, and the fuel flow will increase significantly. Therefore, the oil pressure in the injector lift chamber decreases, increasing the average fuel particle diameter, spray taper angle, and spray length (poor tearing level). In this case, we see a decrease in fuel flow leaking through the injector.

When the nozzle diameter is reduced from 0.20 mm to 0.18 mm, the spray circulation cross-section will be reduced, and the amount of fuel injected and the fuel injection flow will decrease. Therefore, the oil pressure in the injector lift chamber increases, and the injector opens large, decreasing the average fuel particle diameter, spray taper angle, and spray length (due to too strong tearing). In this case, we see an increase in fuel leaking through the injector. However, in this case, pressure pulses appear, causing spray drops that negatively affect the quality of the mixture formation process. [2-5]

3.4. Influence of nozzle length

Increasing the nozzle length from 0.8 mm to 1.0 mm decreases the spray cone angle and vice versa. Reducing the nozzle length from 0.8 mm to 0.6 mm decreases the beam taper angle and the spray increases.

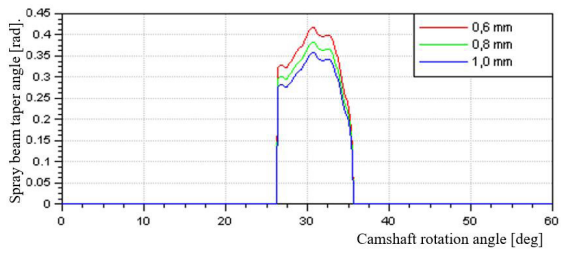

Figure 49. Influence of nozzle length on spray beam taper angle.

https://doi.org/10.52111/qnjs.2024.18310

3.5. Influence of nozzle spring stiffness

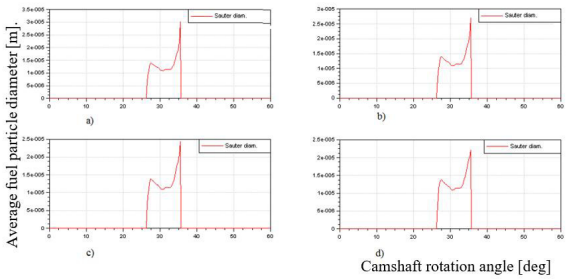

Figure 50. Influence of injector spring stiffness on average fuel particle diameter. (a) k_1=200000 N/m and k_2=300000 N/m, (b) k_1=225000 N/m and k_2=325000 N/m, (c) k_1=250000 N/m and k_2=350000 N/m, (d) k_1=275000 N/m and k_2=375000 N/m.

It remains constant when the stiffness of the two injector springs is changed with other conditions. We can see that the greater the injector spring stiffness, the better the fuel injection quality the smaller and more uniform the average diameter of fuel particles at the end of the injection process. However, the hardness of the two injector springs must be manageable, which will affect the injector lift and fuel circulation cross-section through the injector base. [2-5]

4. CONCLUSIONS

Through the process of researching and applying HydSim software to simulate, analyze, and evaluate the influence of structural parameters on the quality of the fuel supply process of the D1703-M-DI engine, we see that Hydsim is a software used to simulate and calculate the fuel system is quite powerful. The simulation parameters achieved are close to the actual parameters of the engine, and the simulation results accurately reflect the influence of structural parameters, operating conditions, and combustion chamber pressure on fuel injection quality.

During the implementation of the project, with many runs and tests, the desired analytical results were achieved. In general, the quality of the fuel injection beam is satisfactory. Still, there are some limitations, such as at high speeds and large loads, the average diameter of fuel particles at the end of the extensive injection process, there is a phenomenon of spray drop; the fuel injection beam taper angle is small, the spray penetration is slight (L/S<1.05). To improve fuel injection quality, we can proceed by:

- Because the cam profile is not reasonable, the pressure in the system increases suddenly and fluctuates strongly. When the engine operates at high speed and high load at the end of the injection process, because the pressure in the system is still significant and fluctuates strongly, the injector does not close tightly, leading to the injection falling.

- The diameter and helpful stroke of the pump piston are not suitable. Combined with the sudden growth of the cam profile and high operating speed, the time for fuel injection into the combustion chamber needs to be longer. The free flow injection period is extended. The pressure drops sharply, so the average diameter of fuel particles at this stage is extensive, negatively affecting the quality of mixture formation and combustion. According to the simulation results of Section 3.2, the best spray quality is selected with a piston diameter of 7 mm and a piston stroke of 1.11 mm.

- The nozzle hole diameter is small, so when the engine operates at high speed and load, the injector opens repeatedly, causing spray to drop or spray on the expansion line. The simulation results in Section 3.3 show that the best spray hole diameter is from 0.22 ÷ 0.25 mm.

- The length of the spray hole only affects the spray beam taper angle. Due to the considerable design nozzle length, the spray beam taper angle is slight, and the ability to fill the combustion chamber space could be improved. Therefore, the mixing quality could be better. The larger the spray beam, the better. According to the simulation results of Section 3.4, we need to reduce the spray hole length to 0.6 mm.

- The injector hardness is not suitable and small, causing the injector to close slowly and not decisively, leading to dropped injection, spraying on the expansion path, and the average size of fuel particles at the end of the injection process is significant. According to the simulation results in Section 3.5, it is necessary to increase the injector hardness (k_1 = 275000 N/m and k_2 = 375000 N/m).

In addition, other structural parameters of the fuel system, such as pump spring stiffness, high-pressure pipe length, the viscosity of fuel used, etc., and the influence of operating parameters such as speed, the degree of the high-pressure pump camshaft, the proper stroke of the high-pressure pump (h_i), and the compressed air pressure in the combustion chamber at the time of fuel injection also need to be thoroughly studied as a whole. From there, we propose solutions to improve this engine fuel system to become more complete and more suitable for operating conditions in our country.

Acknowledgment

This study is conducted within the framework of science and technology projects at Quy Nhon University's institutional level under project code T2023.808.18.

REFERENCES

1. V. N. Tuoc. *Computer modeling and simulation,* Education Publishing House, Hanoi, 2001.
2. N. T. Tien. *Calculation structure of internal combustion engines, volumes 1, 2, 3,* Education Publishing House, Hanoi, 1996.
3. L. V. Luong. *Diesel engine theory,* Education Publishing House, Hanoi, 2001.
4. B. V. Ga, V. T. Bong, P. X. Mai, T. V. Nam, T. T. H. Tung. *Cars and environmental pollution,* Education Publishing House, Hanoi, 1999.
5. K. Mollenhauer, H. Tschoeke. *Handbook of diesel engine,* Springer, Verlag Berlin Heidelberg, 2010.

https://doi.org/10.52111/qnjs.2024.18310

TẬP 18, SỐ 3, THÁNG 6 - 2024
ISSN: 1859-0357 E-ISSN: 2815-6242

MỤC LỤC